Modeling and Analysis of Ground Loop Cooling for Thermo-Electric Power Generation

By

Sharath Kumar Reddy Challa

MS, Mechanical Engineering, 2017

Submitted to the graduate degree program in Mechanical Engineering and the Graduate Faculty of the University of Kansas in partial fulfillment of the requirements for the degree of Master of Science.

Thesis Advisor Chair: Dr. Ronald L. Dougherty

Committee Member: Dr. Sara E. Wilson

Committee Member: Dr. Brian A. Rock

Date Defended: June 1st, 2017

The Thesis Committee for Sharath Kumar Reddy Challa certifies
that this is the approved version of the following thesis:

Modeling and Analysis of Ground Loop Cooling for Thermo-Electric Power Generation

Chair: Dr. Ronald L. Dougherty

Date Approved:

Abstract

The focus of this thesis is to model a ground loop cooling system to substitute for typical cooling systems of a thermal power plant. Steam power plants generate heat from fuel (e.g., coal, natural gas, and nuclear) which is used to convert water to steam and which, in turn, expands through turbines to turn generators which produce electricity. After passing through the turbine, the mixture of low pressure steam and water must be cooled to become all liquid water in order to be reused. Cooling towers play a crucial role in the removal of waste heat for thermal power generation. This waste heat is commonly rejected to lakes, rivers or air with the help of cooling towers and condensers. Although these methods are efficient, they are no longer considered the best choices due to consumption of large amounts water, water scarcity in certain geographical locations, and environmental effects where power plants are needed.

For the ground loop cooling technique, the warm cooling water coming out of the condenser is sent into the earth through a number of closed loop tubes in vertical bore holes. The heat is then transferred from the warm cooling water to the earth, and the cooling water's exit temperature [from the closed loop tubes] is reduced from that of the inlet. This 'cooled' cooling water is then used to condense the mixture of low pressure steam and water in the power plant's condenser. Therefore, in modeling a ground loop cooling system to substitute for a wet or dry cooling system, so as to maintain the cycle efficiency of the plant, it is necessary to determine the number of bore holes required and the spacing that has to be provided between the bore holes in order to reach the needed bore hole exit water temperature.

To model the ground loop cooling system, ANSYS-CFX, a computational fluid dynamics (CFD) software tool, was used to evaluate different results (e.g., bore hole exit water temperature and temperature distribution in the surrounding earth). This software can simulate a wide range of fluid flow problems with good accuracy and allows defining a conjugate heat transfer problem with different input parameters. The results are determined for different values of various input parameters such as thermal conductivity of the earth, water mass flow rate, and depth of the bore holes, operational time, and inner diameter of the tubes in the bore holes.

All of the results, including the number of bore holes required, spacing that has to be provided between the bore holes, and the cost to install a ground loop cooling system, are estimated for a

1000 MW thermal power plant operating at full load with a cycle thermal efficiency of 40%. It was determined that, in order to maintain the cycle thermal efficiency of the power plant for an earth thermal conductivity of 5 W/m-K and bore hole depth of 150 m, 84230 bore holes would be needed for a total installation cost of 5,206.24 million USD. In addition, it was determined that, when reducing the depth of the bore holes from 150 m to 100 m (while keeping earth thermal conductivity at 5 W/m-K), the installation cost of the ground loop cooling systems decreased by 81.43 million USD. Comparable wet cooling tower installation costs are currently 39 million USD. Considering these huge ground source cooling costs, future studies must be done.

Since the total cost of the project is hugely dependent on the number of bore holes required and their diameter, future studies should be aimed at decreasing the number and diameter of bore holes required for the project. It costs less to drill a bore hole of smaller diameter. For instance, it costs approximately 1/3 to drill a 0.16 m diameter bore hole as compared to a 0.6 m diameter bore hole. Therefore, the installation cost can be reduced by changing the inner diameter of the tubes and decreasing the spacing between the U-tubes. Although, this would increase the number of bore holes required, since the mass flow rate through each bore hole decreases, the effect of decreasing the bore hole diameter on the installation cost can be examined. Since the cost of the project increases by 81.43 million USD when the depth of the bore hole is increased from 100 m to 150 m (at an earth thermal conductivity of 5 W/m-K), studies can also be done to determine the cost sensitivity of the project to bore hole depth. All results of the study and future recommendations are presented in an easy-to-use systematic form so that estimates for individual cases may be made.

Acknowledgments

I would like to thank Dr. Ronald L. Dougherty, my advisor, for providing all the help and guidance to overcome the difficulties in this project, and being so patient and supportive.

I would like to thank Dr. Sara E. Wilson and Dr. Brian A. Rock for their time and contributions by being part of my committee.

I would also like to express my thanks to John Robert Stark and Richard Heskett (Technical Sales Manager, CETCO Drilling Products), for their invaluable suggestions and assistance, especially when the project got more complicated. Finally, I would like to thank my wonderful family for their support and patience.

TABLE OF CONTENTS

LIST OF FIGURES

LIST OF APPENDICES FIGURES

LIST OF TABLES

LIST OF APPENDICES TABLES

Nomenclature

A	=	Function used in solving the closed-form solution (Eq. (3-6)) (m-K/s)
A_c	=	Cross-sectional area of the tube (m^2)
B_{Num}	=	Number of bore holes (no units)
$B_{Spacing}$	=	Radial spacing to be provided between the bore holes (m)
C_p	=	Heat capacity at constant pressure of earth (J/kg-K)
$C_{p\ (water)}$	=	Heat capacity at constant pressure of water (J/kg-K)
d	=	Depth along the bore hole (m)
D_i	=	Inner diameter of the earth domain (m)
D_o	=	Outer diameter of the earth domain (m)
DT_e	=	Difference between two earth temperatures obtained from two different solution methods or different time steps or different radii (K)
e	=	Roughness of the tube surface at the water-tube interface (m)
I	=	Turbulence intensity of water domain (no units)
J_o	=	Zeroth order Bessel function of first kind (no units)
k	=	Thermal conductivity (W/m-K)
$K_o(\beta_m, r)$	=	Normalized eigenfunction of the closed form solution (1/m)
L	=	Total depth of the bore hole (m)
m	=	m^{th} eigenvalue of transcendental Eq. (3-10) (no units)
$\dot{m}$	=	Mass flow rate of the cooling water through each tube (kg/s)
$\dot{M}$	=	Total mass flow rate of the cooling water from the condenser of a power plant (kg/s)
N	=	Normalization integral of the eigenfunction (m^2)
$\dot{Q}_r$	=	Heat rejection rate (MW)
r	=	Radius (m)
r_i	=	Inner radius of the earth domain (m)
r_j	=	Radius at the j^{th} point in Finite Difference solution (m)
r_{j+1}	=	Radius at ($j+1^{th}$) point in Finite Difference solution (m)
r_o	=	Outer radius of the earth domain (m)
$r_{unchanged}$	=	Radius at the which the initial temperature of the earth domain remains unchanged (m)
R_o	=	Eigenfunction of the closed form solution (no units)
t	=	Total time of the simulation (s)
T_c	=	Cold reservoir temperature (K)
T_e	=	Temperature of the earth (K)
$T_{e\ (ANSYS\text{-}CFX)}$	=	Temperature of the earth calculated using ANSYS-CFX (K)

$T_{e\ (closed\ form,\ D_i\ =\ 0.1\ m)}$	=	Temperature of the earth calculated using closed form solution when D_i = 0.1 m (K)
$T_{e\ (closed\ form,\ D_i\ =\ 0.2\ m)}$	=	Temperature of the earth calculated using closed form solution when D_i = 0.2 m (K)
$T_{e\ (closed\ form\ solution)}$	=	Temperature of the earth calculated using closed form solution (K)
$T_{e\ (Finite\ Difference\ method)}$	=	Temperature of the earth calculated using Finite Difference method (K)
$T_{e\ (Finite\ Difference\ method,\ \Delta\tau\ =\ 600\ s)}$	=	Temperature of the earth calculated using Finite Difference method with $\Delta\tau$ = 600 s (K)
$T_{e\ (Finite\ Difference\ method,\ \Delta\tau\ =\ 18000\ s)}$	=	Temperature of the earth calculated using Finite Difference method with $\Delta\tau$ = 18000 s (K)
$T_{e,\ m}(r,\ \tau)$	=	m^{th} component of the earth temperature summation of Eq. (3-5) and Eq. (B-3) (K)
T_{exit}	=	Area averaged bore hole exit water temperature (K)
T_h	=	Hot reservoir temperature (K)
T_i	=	Temperature at the earth domain's inner radius, r_i (K)
T_{ie}	=	Initial temperature of earth domain (K)
T_{in}	=	Inlet temperature of the cooling water (K)
T_j	=	Temperature at j^{th} radius point in Finite Difference solution (K)
T_m	=	Mean earth temperature (^{o}F)
T_o	=	Temperature at the earth domain's outer radius, r_o (K)
T_{op}	=	Opening temperature at the outlet boundary (K)
T_w	=	Area averaged water temperature at any depth along the bore hole (K)
T_τ	=	Temperature at τ^{th} time point in Finite Difference solution (K)
$T_{\tau+\Delta\tau}$	=	Temperature at $(\tau+\Delta\tau)^{th}$ time point in Finite Difference solution (K)
V_{in}	=	Water velocity at the inlet of water domain (m/s)
Y_o	=	Zeroth order Bessel function of second kind (no units)

Greek

α	=	Thermal diffusivity (m^2/s)
β_m	=	Eigenvalues (positive roots of transcendental Eq. (3-10)) (1/m)
Δr	=	Radius step for Finite Difference solution (m)
ΔT_e	=	Earth temperature (T_e) – 285 K (K)
$\Delta T_{e,\ m}(r,\ \tau)$	=	Difference between two consecutive terms of Eq. (B-3) (K)
$\Delta\tau$	=	Time step for Finite Difference solution and simulations with ANSYS-CFX (s)
η	=	Cycle thermal efficiency of power plant (no units)
ρ	=	Density of the earth (kg/m^3)
ρ_w	=	Density of water (kg/m^3)

τ	=	Time at which results are determined (s)
τ'	=	Time variable for integration (s)

Abbreviations

ACC	=	Air-Cooled Condenser
CFD	=	Computational Fluid Dynamics
CPU	=	Central Processing Unit
GB	=	Gigabyte
GHz	=	Gigahertz
GSHP	=	Ground Source Heat Pump
GUI	=	Graphical User Interface
RAM	=	Random Access Memory
USD	=	United States Dollars

CHAPTER 1

OVERVIEW OF THESIS

1.1 Introduction

In electric power generation, alternative cooling methods, such as geothermal cooling techniques, have received much attention in recent years due to the need for cooling without consuming water. Because of the rapid population growth, urbanization and improving living standards of people worldwide, there is an exponential increase in demand for electric power [1]. The demand for cooling in steam power plants has also increased because of increased demand for electric power generation. In the United States, 90% of the electricity comes from thermoelectric power plants, and about 90% of those thermoelectric power plants use wet cooling systems [2].

Since wet cooling towers reject 70% to 80% of their heat load by evaporation, they require very large amounts of makeup water, about 600 L/min for every 70,000 L/min of circulation flow, for a 10 ^{o}C drop in the temperature from inlet to exit [2]. So, considering the scarcity of fresh water and rising demand for drinking water, there is a need to find ways to decrease the amount of water usage in cooling the working fluid of a power plant [3]. One of the possible methods of dry cooling is to use the earth as a sink for rejected heat. This is also termed earth coupled cooling or geothermal cooling. Using the earth as a heat sink will reduce the consumption of water in thermal power plants.

1.2 Objectives

The aim of this thesis is to model a ground loop cooling system as a substitute for wet cooling of a power plant. To model a ground loop cooling system, warm cooling water coming out of the condenser is sent through number of closed loop vertical bore holes to reduce the cooling water temperature. Cooling water temperature at the exit of the loop depends on the mass flow rate of the cooling water through each loop and thermal conductivity, density, and heat capacity of the earth. The number bore holes required is determined by the mass flow rate of water through each bore hole that can achieve the exit temperatures needed to maintain the cycle thermal efficiency of the power plant. Also, the spacing between the bore holes should be large enough, so that each bore hole's thermal performance is not affected by any other bore hole. Provided in this thesis are the numbers of tubes and bore holes required to meet a power plant's cooling needs as a function of different parameters such as water flow rate, tube diameter, bore hole depth, tubing length, bore hole spacing, operation time and thermal conductivity of earth.

1.2.1 Specific Objectives

- Provide background information on requirements of cooling systems, and discuss once-through, recirculating, dry, hybrid, and ground loop cooling systems for a power plant. Also, examine the importance and tradeoffs of dry cooling techniques compared to wet cooling techniques.
- Solve mathematical models for heat transfer in the cylindrical coordinate system in order to determine the spacing that has to be provided between the bore holes so that each bore hole's performance is not thermally affected by adjacent bore holes.
- Using ANSYS-CFX, model temperature distributions in the earth domain at different times.
- Using ANSYS-CFX, solve for the bore hole exit water temperatures for different mass flow rates, tube diameters, bore hole depths, spacing between bore holes, operation times, and thermal conductivities of the earth in order to determine the number of bore holes [per net power output of a power plant] required to substitute for wet cooling systems.

1.2.2 Methodology

- <u>Literature review:</u> Research has been done to collect information related to the project from previous journal papers, books, and ground source loop installers, etc.; and relevant information has been used for the work described herein.
- <u>Modeling:</u> One-dimensional transient heat transfer problems in the cylindrical coordinate system are solved using both a closed form solution and the Finite Difference method in order to determine the spacing that has to be provided between the bore holes. Also, different models for bore holes have been designed using SolidWorks and simulated using ANSYS-CFX in order to determine the temperature distributions in the earth at different depths, radii and times. Bore hole exit water temperatures have also been found for different bore hole depths, tubing diameters, inlet water velocities (or flow rates), earth thermal conductivities, and operation times.
- <u>Analyze the results</u>: The results are analyzed to determine the optimum bore hole depth, and the number of bore holes and tubes required per net power output of a power plant.

CHAPTER 2
BACKGROUND INFORMATION

2.1 Overview

Electric power and water are two highly essential and interdependent resources on which humans depends. As the population has increased over the years, the demand for electric power and water has had exponential growth [1]. In 2010, the electric power industry was the largest water user in the U.S., using 609,451 L/day, which accounted for 38% of the total freshwater withdrawals and about 91% of saline water withdrawals. Therefore, power plants are hugely dependent upon reliable water supplies [4].

A typical steam power plant operates in a cycle, as broadly shown in Fig. 1.

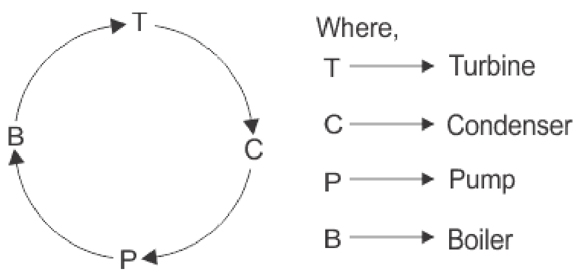

Figure 1. Diagram showing a very generalized thermal power plant cycle (reproduced from Ref. 5).

Steam power plants generate heat from fuel (e.g., coal, natural gas, and nuclear) which is used to convert water to steam and which, in turn, expands through turbines to turn generators in order to produce electricity (see Figs. 1 and 2) [5]. As shown in Fig. 2, after passing through the turbine, the low pressure steam and water mixture must be cooled in the condenser in order to be pumped back to the boiler for reuse. The Rankine cycle is the typical thermodynamic cycle on which the thermal power plants work.

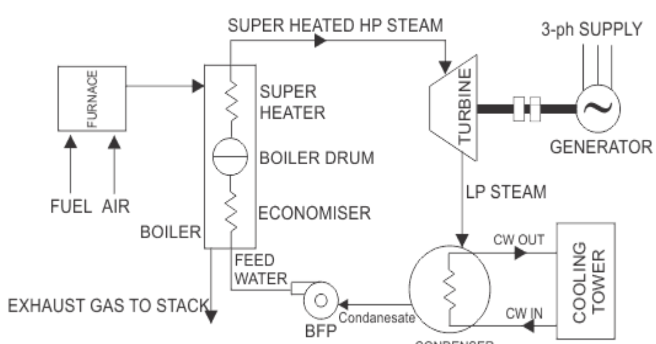

Figure 2. Diagram of typical thermal power plant showing different flow paths (reproduced from Ref. 5).

Virtually all of the water that is lost or used in electric power generation is evaporated in the process of condensing the hot steam and water mixture coming out of the turbine for reuse. As of 2012, approximately 90% of the electric power that was produced in the U.S. used the steam cycle as its primary process for power generation; and plants that required cooling water accounted for 60% of the U.S. electric generating capacity or a little more than 70% of all electricity generated [2].

The cycle efficiency of a typical thermal power plant, which uses the steam cycle as its primary process for power generation, is [6].

$$\eta = 1- \frac{T_c}{T_h} \tag{2-1}$$

Therefore, for better efficiency of a thermal power plant, T_c should be kept as low as possible. Different cooling techniques are used to achieve these low values for T_c, and the amount of water that is consumed depends on the method of cooling.

There are different methods of cooling which are used in the U.S. and around the world. The four most common techniques that are used are [7]

- Once-through cooling
- Wet cooling
- Dry cooling
- Hybrid cooling

2.2 Methods of Cooling

Different ways of cooling are used, depending upon the location of the plant, cooling load, weather conditions, and availability of water resources. Most thermal power plants use water to condense steam, i.e., they use wet cooling systems which use liquid water to condense steam [8]. A cooling technology that is best for a particular thermal power plant may not be efficient for another power plant, due to the factors just listed. The amount of water consumed by any power plant depends mainly on which type of cooling technology is being used. Also, each of the cooling technologies has its own advantages and disadvantages. Therefore, it is always important to find the optimal cooling technology for a particular location, weather conditions, and the available resources. Different methods of cooling are individually discussed in Sections 2.2.1-2.2.4.

2.2.1 Once-Through Cooling Systems

As the terminology indicates, once-though cooling systems withdraw water from a large-scale source, and use the water once for condensing the steam, then return most of the water to its source. As shown in Fig. 3, once-through cooling systems draw cool water from either water reservoirs (lakes) or rivers. Figure 3 shows that cooling water comes from the source (i.e., river) and is pumped through the condenser to condense the working fluid (low pressure steam and water mixture) exiting the turbine to become low temperature liquid water; and this liquid working fluid is then reused to generate steam in the boiler. After passing through the condenser, most of the cooling water is pumped back to the source, with some being used for other purposes in the power plant such as ash handling [7].

The temperature of the cooling water increases due to heat transfer from the power plant's working fluid, which is a mixture of steam and hot water, in the condenser. So, when this warmer cooling water is pumped back to the source, that warmer cooling water dissipates heat to the atmosphere and the earth through convection, radiation and evaporation. When the cooling water is withdrawn from a reservoir, part of this water is lost [due to evaporation] in the process of cooling the working fluid. This lost water has to be restored by rain or the water source itself [7].

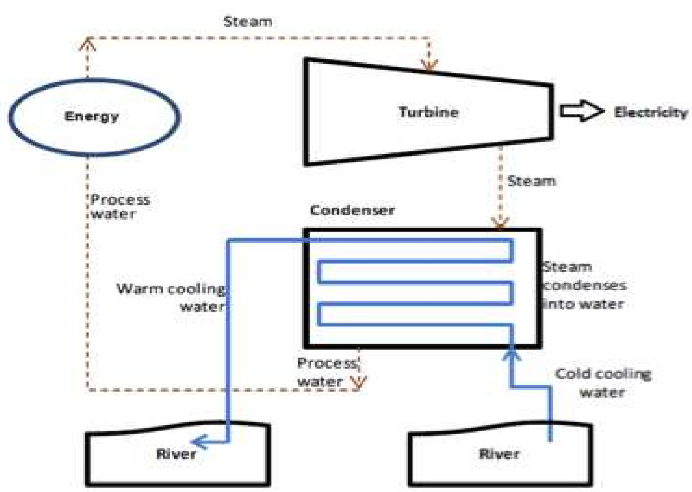

Figure 3. Schematic of a once-through cooling system (reproduced from Ref. 9).

At first glance, once-through cooling systems are the least expensive, easiest to construct and handle, and are the most effective system for condensing the steam [7]. Once-through cooling systems require abut 20,000-50,000 gal/MWh of water to condense the steam, but the amount of water that is lost (100-317 gal/MWh) is about one-fourth that of evaporative cooling systems. However, since large amounts of water are withdrawn from the source, heated, and then returned to the source, this process directly affects the ecological system [7]. Also, once-through cooling systems are only suitable for a thermal power plant if the thermal power plant is located close to a river or other significant water resources.

2.2.2 Wet Cooling Systems

Wet cooling systems are also called recirculating or evaporative cooling systems. Thermal power plants with wet cooling systems withdraw water from many different sources, such as surface water (rivers, lakes, and ponds), municipal water, and ground water. Cooling water withdrawn from these sources is then sent to the condenser to cool the mixture of steam and hot water, and the cooled working fluid is then reused in the power plant cycle [7].

After passing through the condenser, the cooling water is pumped into a cooling tower where it is cooled by evaporation into the ambient air. Large fans that force air over thin films of water aid this evaporation. The cooled water is then recirculated back to the condenser. As water evaporates from the cooling towers, there will be a need for make-up water, which is then withdrawn from external bodies of water. Also, due to evaporation inside cooling towers, dissolved salts and suspended solids are left behind which eventually reduce heat transfer from the cooling water to the air. Therefore, wet cooling towers have to be cleaned regularly [7]. Also, water consumption is 60-100 % higher in wet cooling as compared to that in once-through cooling [9].

Make-up water has to be continuously pumped to the cooling water system in order to meet the cooling loads. The capital costs of these recirculating cooling systems are ~ 39 USD/kW of electricity produced, as compared to once-through cooling (~19 USD/kW), dry cooling (~90 USD/kW) and hybrid cooling systems (~135 USD/kW) and are 3-15% more efficient (~35-42 %) than dry cooling systems; but they have some serious drawbacks. Requirements of high amounts of make-up water (480 -1100 gal/MWh), and a drop in the net energy of the plant due to energy consumption by large fans which are used to move the air, are some of the drawbacks of the wet cooling system. Since most thermal power plants do not have unlimited access to the natural resources such as rivers, lakes, ponds, etc., the majority of plants use wet cooling systems as compared to once-through cooling systems [7].

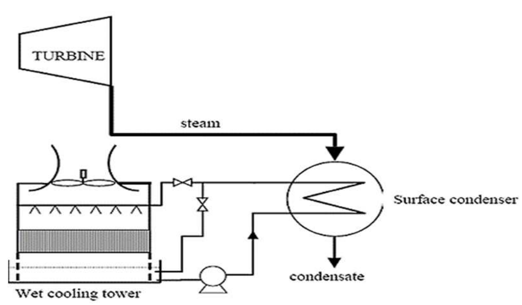

Figure 4. Schematic of a wet cooling evaporative system (reproduced from Ref. 10).

2.2.3 Dry Cooling Systems

Dry cooling systems, also called air-cooled condensers (ACC's), use air to condense the steam and water mixture. In a dry cooling system, air flowing past the tubes containing the low pressure steam and water mixture reduces the temperature of the low pressure steam and water mixture by means of direct heat transfer to the air. The air flow can be induced mechanically using large fans or by natural draft. Cooling water is not used since the heat from the mixture of low pressure steam and water mixture is directly transferred to the outside air through the tube walls. In hot climates, wet cooling systems are more efficient compared to dry cooling since the ambient air temperatures can be 40+ ^{o}C, which reduces the potential of a dry cooling system as compared with 20 ^{o}C (e.g., wet bulb temperature of water), which describes the potential of a wet cooling system.

Since the heat transfer to air is less efficient than evaporating water for a given cooling load [9], the number of large fans and tubes increases significantly as compared to that of a wet cooling tower. Although dry cooling systems consume much less water, the construction cost is approximately triple that of wet cooling systems [8]. However, during hot weather, there is a drop of 10-15% in the overall thermal efficiency of a power plant when using dry cooling systems due to the higher "cold reservoir" temperature, T_c of Eq. (2-1) [8]. Also, the net energy output of the plant decreases because the electricity consumed by the cooling equipment (fans) is greater as compared to electricity consumed by pumping equipment of other cooling techniques.

As of 2012, about 3% of the thermal power plants in the U.S. used dry cooling systems. This disparity with wet cooling is due to the high construction and operation costs, and the lower overall efficiency as compared to plants with other types cooling systems [10]. Dry cooling systems are used where water is scarce [9].

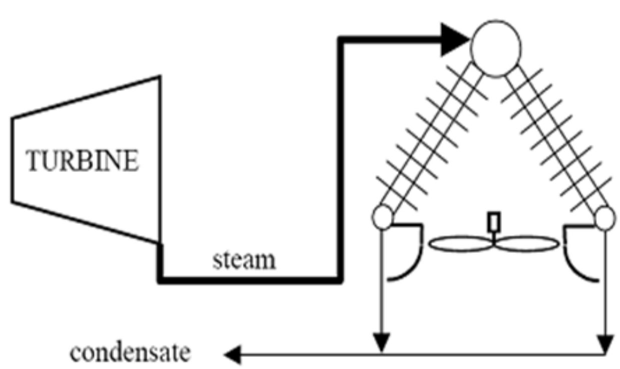

Figure 5. Schematic of dry cooling system (reproduced from Ref. 11).

2.2.4 Hybrid Cooling Systems

Hybrid cooling systems have both wet and dry cooling components that operate in combination to condense the mixture of low pressure steam and water going into the condenser. These types of cooling systems are designed to operate as wet cooling systems during hot periods, and as dry cooling systems supplemented with wet cooling systems during cooler seasons in order to maintain overall efficiency of the power plant, while reducing the consumption of water during the cooler periods of the year [10]. The drawback of hybrid cooling systems is that they are more expensive as compared to wet cooling systems alone. In addition, they require a significant amount of make up water during hotter periods of the year [200-500 gal/MWh]. Since the hybrid cooling system has to deal with both dry and wet cooling equipment, the maintenance costs are also high as compared to those of the other cooling systems [11].

Although hybrid cooling systems provide flexibility in using either dry, wet or both cooling systems, according to the season to reduce the usage of water consumption, the operating costs are well above those of wet cooling. Hybrid cooling systems require very high capital investments of approximately 135 USD/kW of electricity produced as compared to 39 USD/kW for wet cooling systems [10].

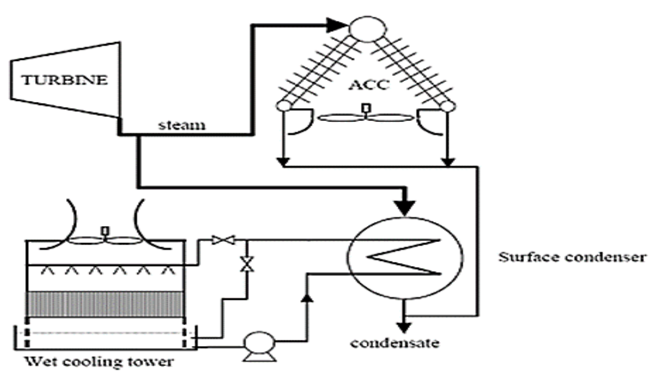

Figure 6. Schematic of a hybrid cooling system (reproduced from Ref. 11).

2.2.5 Cooling System Comparison

Each of the cooling technologies has advantages and disadvantages. As discussed in Sections 2.2.1 to 2.2.4, once-through cooling systems withdraw more water from the source but consume less water as compared to wet cooling systems. Wet cooling systems, although consuming more water, do not require an additional large water source as compared to once-through cooling systems [12]. Once-through and recirculating (wet) cooling systems also have different effects on the ecosystem, since once-through systems always return water to the source at a higher temperature than that at withdrawal, causing risks for aquatic life (fish, algae, etc.) or airborne life. So, the differences among various cooling systems can be evaluated in terms of cost, water consumed, environmental effects and overall efficiency. For a given power plant, cooling technology is chosen based on the location of the power plant, required efficiency, cost constraints and environmental effects.

Of the 1,655 operable cooling systems in the United States in 2012, more than 96% of them were once-through (43.444 %) or recirculating cooling systems (52.87 %) which used water (see Table 1); and the other 3.685 % were composed of both dry and hybrid cooling systems [9].

Table 1. Cooling system types by primary energy source (2012) (reproduced from Ref. 10).

Primary energy source	Once-through	Recirculating	Dry cooling	Wet & dry hybrid cooling	Total cooling systems
coal	398	368	4	1	771
natural gas	197	422	51	4	674
nuclear	50	44	0	0	94
other	74	41	1	0	116
total	**719**	**875**	**56**	**5**	**1,655**

2.3 Water Consumption in Thermal Power Plants

The agricultural and thermal power production sectors are the two largest users of water [7]. As discussed in Section 2.2, most of the water that is consumed in a power plant is consumed in the process of cooling; and the amount of water that is consumed depends on the type of cooling technique that is used by any particular power plant. Figure 7 shows the water demand of power plants for different types of cooling systems.

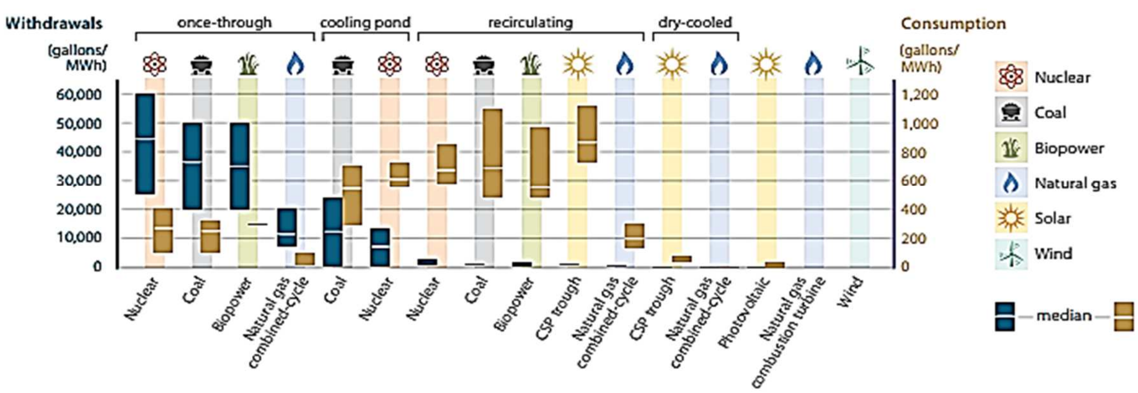

Figure 7. Water use by fuel and cooling technology (reproduced from Ref. 7).

The blue bars on the plots show water withdrawal (gal/MWh) and brown bars show water consumption (gal/MWh). Ranges reflect minimum and maximum water use values for selected technologies from NREL. Horizontal lines within rectangles indicate median values. For instance, a coal fired power plant with once-through cooling withdraws 20000 to 50000 gal/MWh, and consumes 400 to 1000 gal/MWh.

Based on the data collected from a 2010 study, focused on a sample of 21 power plants with once-through cooling systems in Texas, it was found that approximately 350 gallons of water was consumed per MWh of electricity produced [13]. Recirculating cooling systems consume about 50% more water than once-through cooling systems, while on the other hand, dry cooling uses and consumes less water, in the range of 1-4 gallons of water per MWh of electricity produced [10].

2.3.1 Statistics on Consumption of Water by Thermal Power Plants

As shown in Fig. 8, 2005 thermoelectric water withdrawals in the U.S. were 143,000 Mgal/day of fresh water and 58,000 Mgal/day of saline water. For the U.S., 41% of the total freshwater withdrawals were used for various purposes in thermoelectric power plants (see Fig. 8). In addition, more than 50% of the total saline water withdrawals were withdrawn for various purposes including cooling, ash handling, etc., by thermoelectric power plants [14].

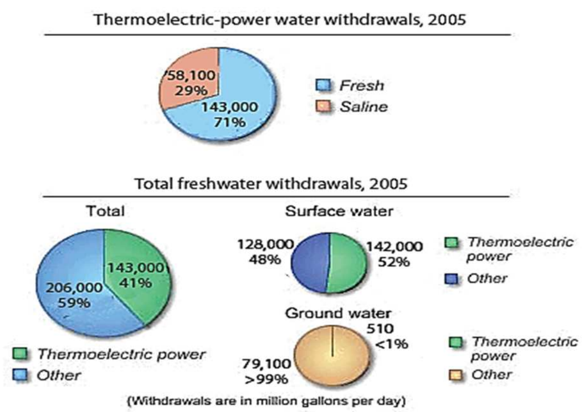

Figure 8. 2005 thermoelectric power water withdrawals in U.S. (reproduced from Ref. 14).

Figure 9 shows the water withdrawals for thermoelectric power production with increasing population from 1950 to 2005 [14].

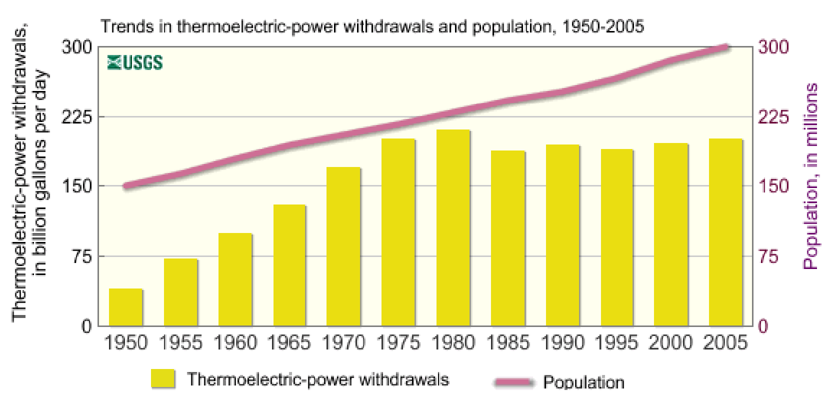

Figure 9. Thermoelectric water withdrawals and population trends of the U.S., 1950-2005 (reproduced from Ref. 14).

In the U.S., from 1950 to 1980, withdrawals by thermoelectric power plants increased from 40,000 Mgal/day to 210,000 Mgal/day. Figure 9 shows that, although the total population has continued to rise, withdrawals for thermoelectric power have stabilized since 1980 [14].

In the U.S., as a daily average in the year 2008, water-cooled thermoelectric power plants drew between 60 billion and 170 billion gallons of freshwater and consumed 2.8 to 5.9 billion gallons of that water [7]. The U.S.'s largest type of power producer, i.e., coal fired thermoelectric plants, was responsible for 70 % of those freshwater withdrawals, and 65% of that consumption [7]. These very large amounts of water were withdrawn from lakes, rivers or ponds; and, in places where there was a scarcity of these resources, ground water was used. In 2008, in the southwest, an average of 125 million to 190 million gallons of ground water was withdrawn every day to use in electric power production [7].

As discussed in Section 2.2, the cooling system for a power plant is chosen to match the water resources available near the plant. Contrary to the 2012 data of Table 1, in 2008, a study of cooling system types, reported that, for the U.S., 86 % of the power plants used once-through cooling systems since those plants had the advantage of being located near abundant water resources such as seas, lakes, and rivers [7]. As shown in Fig. 10, most of the inland power plants

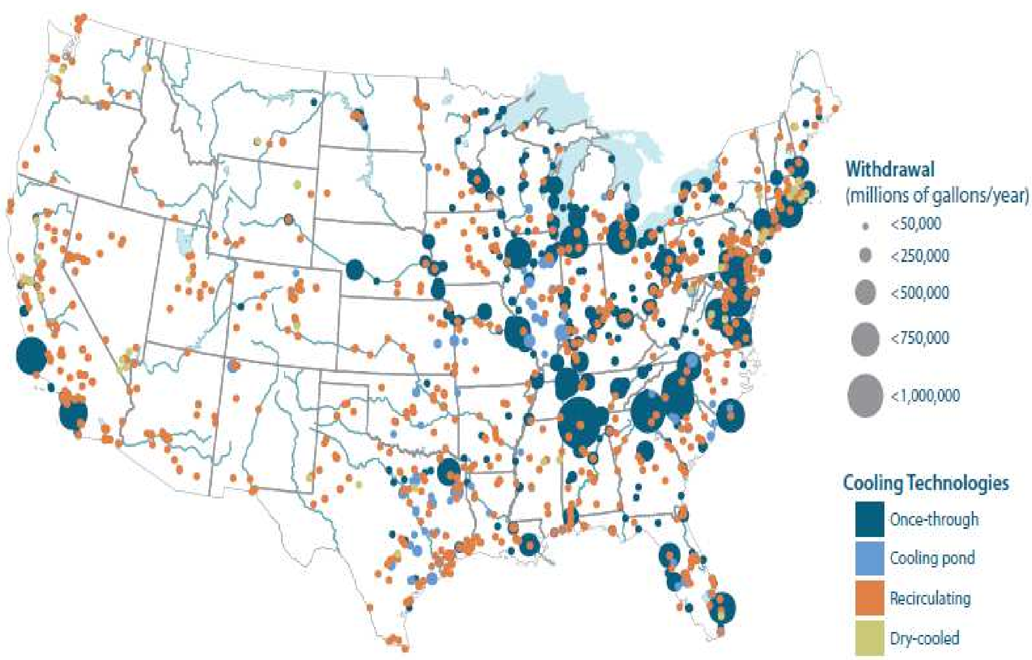

Figure 10. 2008 power plant water withdrawals by state (reproduced from Ref. 7).

used recirculating type cooling systems; and some inland plants that used once-through cooling systems were located in regions where there were ample sources of surface water [7]. As compared to the once-through cooling systems, recirculating cooling systems consumed about 500-700 gal more water per MWh of electricity produced [7].

A study conducted by “Energy and Water in a Warming World Initiative” reported the number of cases of water system stress caused by thermal power plants. For example, in the U.S. in 2008, 400 out of 2,016 watersheds were facing water supply stress due to power plants [7]. Figure 11 shows water supply stress across the U.S for 2008.

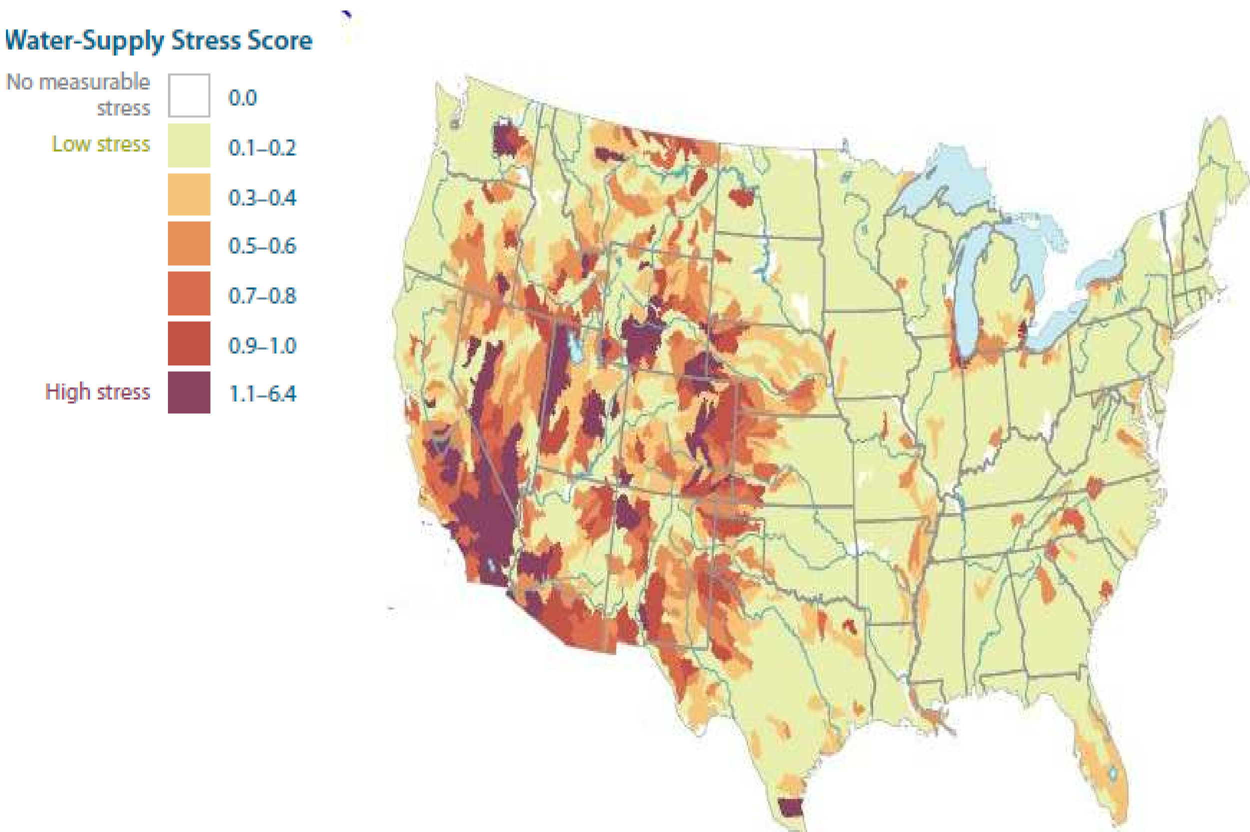

Figure 11. Water supply stress in the U.S. in 2008 (reproduced from Ref. 7).

Fresh water consumption by electric power generation is a big concern in many of the fast-growing economy states in the U.S. So adopting new water-conserving technologies for power production can help reduce the impact of future water shortages. Of the many alternative methods for cooling discharge water from a power plant condenser without consuming water, this thesis analyzes and focuses on one method (ground loop cooling).

2.4 Ground Loop Cooling Method

The ground loop cooling method was chosen, assuming that the earth is an infinite medium, which can be used as a heat sink, or as a thermal storage medium for heat. The earth can be used as sink by means of closed loop tubes in vertical or horizontal tubes in bore holes, which would be used as heat exchangers to either cool or heat the working fluid. Through all seasons, the earth's temperature remains relatively constant beyond a depth of 10-15 m, depending upon the location [15].

Although different regions of the U.S. encounter extreme temperatures from freezing in the winter to scorching heat in the summer, beyond a depth of 10-15 m, the temperature of the earth remains relatively constant and ranges from 10 ^{o}C to 16 ^{o}C, depending on the location and the type of the soil [15]. Figure 12 shows how temperature changes as a function of depth. The surface soil temperature and the temperature of the earth to a maximum depth of about 10 m are affected by incident solar radiation, rainfall, type of soil and surrounding air temperature. After 10 m, the temperature of the earth remains relatively constant and matches more or less the temperature of the ground water, and is referred to as mean earth temperature [15].

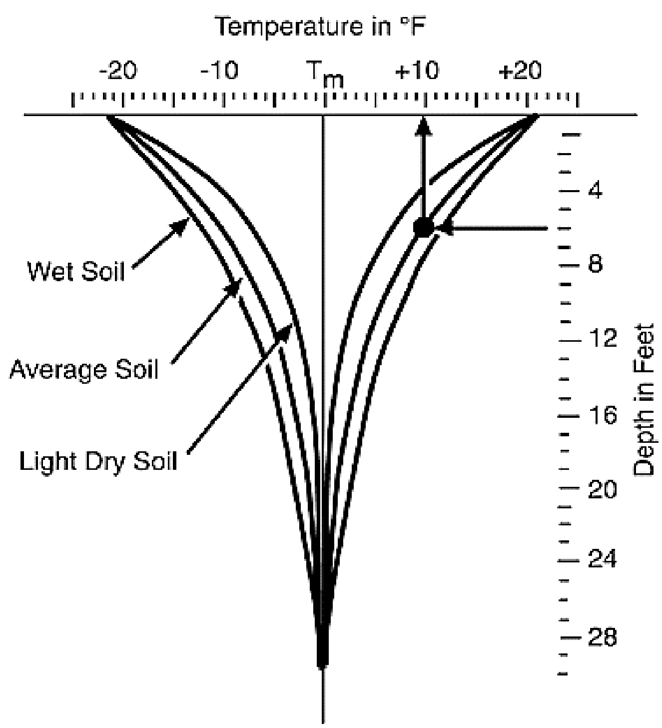

Figure 12. Temperature of the earth as a function of depth (reproduced from Ref. 15).

Figure 13 shows how the mean earth temperature varies across the United States. For example, in Kansas, the mean temperature below 10 m ranges from 54 ^oF to 60 ^oF [15].

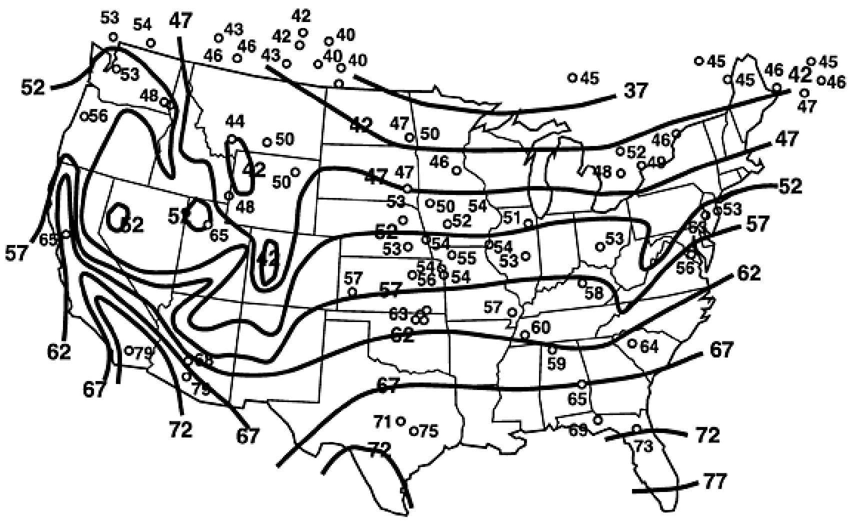

Figure 13. Mean earth temperature, T_m (^oF), contours across the United States (reproduced from Ref. 15).

Figure 14 shows how the temperature of the earth at different depths within the U.S changes versus time over a year. As can be seen, the ground temperature fluctuates less with increasing depth; and, after a depth close to 12 ft, the temperature remains relatively constant within 4 ^oF [15].

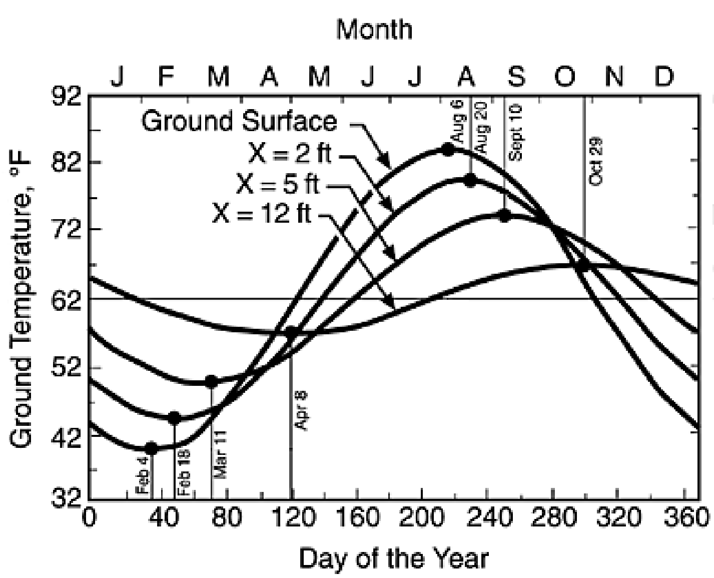

Figure 14. Ground temperature in the U.S. as a function of depth and time (reproduced from Ref. 15).

2.4.1 Ground Source Heat Pump (GSHP)

Many analytical and experimental studies have been performed on ground source heat pumps (GSHP) for cooling and heating of commercial and residential buildings [16]. Even with drawbacks, including high capital costs and lack of public awareness and trust in the GSHP's, there has been tremendous growth in the use of GSHP's for residential purposes due to the advantages from positive environmental and economic effects and high energy efficiency of GSHP's, [16]. Considering the previously mentioned advantages, such as constant and low earth temperature at large enough depths and the high efficiency of ground source heat pumps, there is an opportunity to use this method for cooling in a thermal power plant in order to reduce the water usage.

In designing a ground loop cooling system for a power plant, it is important to determine the bore hole depth needed to achieve the required bore hole exit water temperature and the distance that has to be provided between the bore holes. This all depends on the heat transfer to the earth from water flowing through the bore holes. This heat transfer to the earth in turn depends on other factors, such as the location of the bore holes, each bore hole's thermal interaction with the adjacent bore holes, temperature of the earth at different depths, and physical, thermal, and transport properties of the earth to which the heat is rejected. Therefore, it is important to determine the physical, thermal and transport properties of the earth.

2.4.2 Thermal Properties of the Earth

Thermal properties, like thermal conductivity and heat capacity, play fundamental roles in the design of ground loop cooling systems. The thermal conductivity of the earth varies with depth, soil type, rock composition, and the existence of different materials, which may form porous media in the earth at various depths. As shown in Table 2, the thermal conductivity of soil changes with composition and saturation. This plays a crucial role in the design of ground loop cooling systems.

Table 2. Thermal conductivities of different types of soil (Ref. 17)

Soil type	k (W/m-K)
Sand	0.77
Clay	1.11
Loam	0.91
Saturated sand	2.50
Saturated clay	1.67

It is also important to consider the depth to bedrock, since the thermal properties of bedrock vary depending on the type of material the bedrock is composed of; and, in most cases in the U.S., the depth to bedrock is far less than the bore hole depth chosen to conduct the simulations (L= 100 m and 150 m). Considering the previously mentioned factors of thermal property dependence on the composition of the earth and depth to bedrock, depth to bedrock at different locations was analyzed using an online tool "ArcGIS" [18]. Figure15 shows some of the ArcGIS images giving minimum depth to bedrock at randomly chosen locations in the U.S., such as Lawrence, KS, Oklahoma City, OK, and Portland, OR.

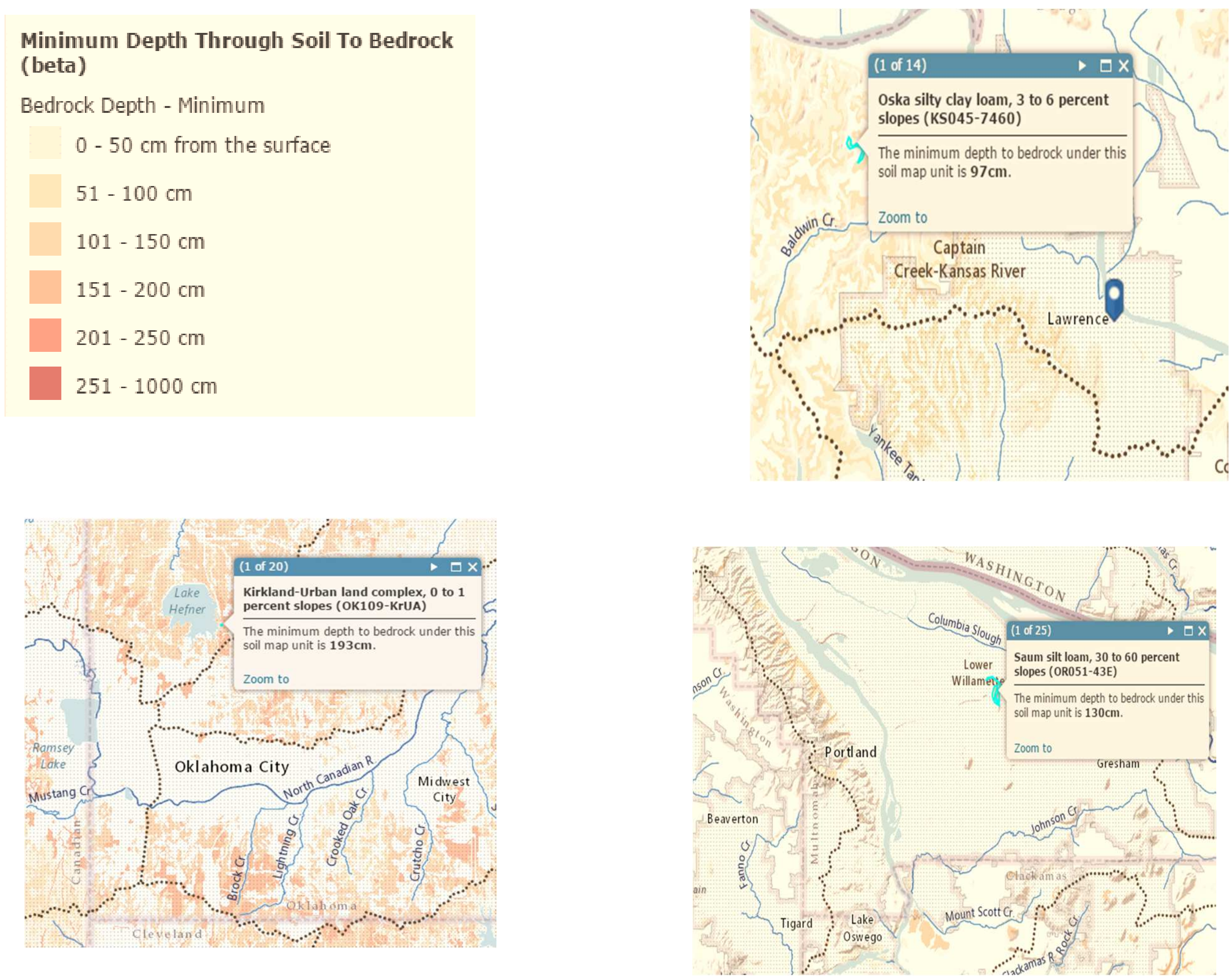

Figure 15. Minimum depth to bedrock at different locations across the U.S. (reproduced from Ref. 18).

The minimum depth to bedrock for most places across the U.S. is less than 10 m [18]. Bedrock is usually made up of different types of rock such as limestone, granite, igneous rock, metamorphic rock and different sediments. Thermal conductivities of these materials range from less than 2.0 W/m-K to greater than 5 W/m-K [17]. Considering this range in the value of the thermal conductivity of the earth for different locations, soil types, and depths, different cases were solved for values of k ranging from 0.5 W/m-K to 6 W/m-K; and the results are discussed in Chapter 4. In solving the heat transfer problem, it is necessary to determine the heat capacity and density of the material. Heat capacity and density of the earth were assumed to be of soil. The density of the earth was taken to be 2050 kg/m^3, and heat capacity was chosen to be 1840 J/kg-K [19].

Using these thermal properties and various boundary conditions, several methods were used to calculate bore hole depth and spacing that has to be provided between the bore holes. This detailed analysis is given in Chapters 3 and 4.

CHAPTER 3

METHODS

This chapter discusses the methods used to find the number of bore holes required and the spacing that has to be provided between the bore holes, both in one-dimensional and two-dimensional geometries.

As discussed in Chapter 2, once steam has passed through the turbines, it has to be condensed to water in order to be reused for producing more electricity. The condensing of the steam to water can be done by using different cooling techniques. Although wet cooling condenses the steam to water more efficiently than dry cooling (ACC's), considering the amount of water consumed in the process, there is a need to find alternatives to wet cooling techniques. One such techniques is ground loop cooling.

In the ground loop cooling technique, the warm cooling water coming out of the condenser is sent into the earth through a number of vertical tubes. The heat is then transferred from the warm cooling water to the earth, and this "cooled" cooling water is then reused to condense the low pressure steam in the power plant's condenser.

To substitute an alternative cooling technique for wet cooling, it is important to understand the amount of cooling required by a power plant for optimum efficiency. The amount of cooling required by any steam power plant depends on the thermal efficiency of the plant (see Eq. (2-1)), and not on the type of fuel used. Also, the higher the hot reservoir temperature (heat source), and the lower the cold reservoir temperature (external environment to which the heat is rejected), the higher the efficiency is (see Eq. (2-1)). Cooling load depends on the required temperature drop of the cooling water, mass flow rate of the cooling water, and the fluid which has to be cooled by any cooling system.

For installing a ground loop cooling system as a substitute for wet cooling, it is essential to determine the number of bore holes required and the spacing that has to be provided between the bore holes. In the ground loop cooling technique, warm water circulates through tubes transferring heat to the earth. Mathematical models were solved to predict the temperature distribution in the earth in order to arrive at the bore hole spacing that has to be provided between bore holes. A few methods for determining these values are discussed in Sections 3.1-3.2.

3.1 Temperature Distribution: One-Dimensional Transient Model

Initially, the spacing between the bore holes that has to be provided was calculated by solving a one-dimensional transient heat transfer model in cylindrical coordinates. The spacing that has to be provided can be determined by determining the radius at which the initial temperature of the earth remains unchanged. Therefore, the temperature distribution in the earth was solved in order to determine the radius at which the initial temperature of the earth was not affected due to the heat transfer from the hotter surface at the inner radius of the domain of interest.

A cylindrical model with an inner radius of r_i and an outer radius of r_o was considered, and boundary conditions were applied at the inner and the outer surfaces in order to solve the mathematical model. In order to assess the effect of inner diameter on the temperature distribution, the mathematical model was solved for two different inner diameters (0.1 m and 0.2 m). The outer diameter was chosen to be large enough that the earth at that location remained constant at the initial temperature of the earth. Earth temperature at depths below 10 m remains relatively constant at mean earth temperature (see Section 2.4), and in the U.S., mean earth temperature ranges from 10 ^oC to 15 ^oC [15]. Therefore, a close to average value of 12 ^oC (285 K) was taken for the initial temperature of the earth.

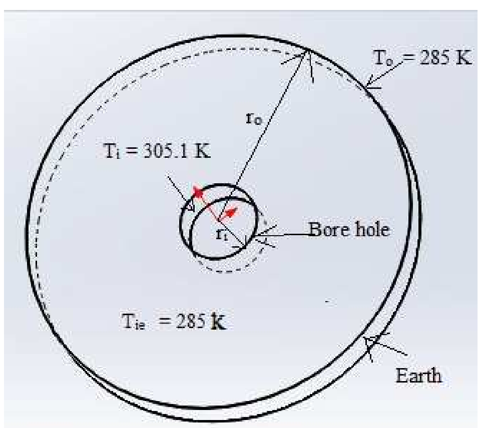

Figure 16. One-dimensional cylindrical model of earth and bore hole.

To solve the one-dimensional heat transfer model in cylindrical coordinates, the following assumptions were made:

- No temperature gradient in the direction of the water's flow (vertically in the bore hole).
- No internal heat generation in the earth.
- At a radius of 10 m, the earth's temperature is always a constant 285 K.
- Constant k, ρ, and C_p of the earth.

Constant temperature boundary conditions were assumed at both the inner and the outer radii of the cylindrical model (see Fig. 16). The temperature at the inner radius was taken to be 305.1 K, which is a typical temperature of the water at the exit of the condenser of a thermal power plant [6]. The transient model results were computed for different times with a maximum time of 4 months (10,368,000 s). The maximum time was chosen to be 4 months, since ground loop cooling would be efficient during the 4 summer months in the mid-latitudinal sections of the U.S. from June through September, during which time the ambient air temperature ranges from 18 ^{o}C to 40 ^{o}C. Since the thermal efficiency of a power plant is higher for lower values of T_c (see Eq. (2-1)), therefore, during the summer time, ground loop cooling would be more efficient than dry cooling. This is due to the temperature of the earth at depths below 10 m remaining relatively constant and ranging from 10 ^{o}C to 15 ^{o}C [15] as compared to high ambient temperatures of 18^{o} C to 40^{o} C. During the other 8 months of the year, the temperature of the air is lower, ranging from -10 ^{o}C to 15 ^{o}C. Thus, it is feasible to use dry cooling systems (ACC) during these periods and have minimal effect on the efficiency of the plant.

One-dimensional temperature distributions were computed for different time periods in order to determine the spacing that would have to be provided between the bore holes, if the ground loop cooling were used for only 1, 2 or 3 months. The minimum radius at which the temperature of the earth was relatively unchanged, within an error of 0.1 ^{o}C for any desired time period, was used in estimating the spacing needed between the bore holes.

In Sections 3.1.1-3.1.3, the temperature distribution in the radial direction at different times was calculated using the following methods; and the results were compared.

- Closed form solution
- Finite difference method (MS Excel)

3.1.1 Closed Form Solution

The closed form solution for transient one-dimensional heat conduction in the radial direction (without internal heat generation) was determined by solving the governing equation. The boundary value heat conduction equation in cylindrical coordinates is [20].

$$\frac{\partial^2 T_e}{\partial r^2} + \frac{1}{r}\frac{\partial T_e}{\partial r} = \frac{1}{\alpha}\frac{\partial T_e}{\partial \tau}$$

$$r_i \le r \le r_o \text{ , } \tau > 0 \text{ and } \alpha = \frac{k}{\rho C_p} \qquad (3\text{-}1)$$

The boundary conditions are

$$T_e(r = r_i, \tau > 0) = T_i \tag{3-2}$$

$$T_e(r = r_o, \tau > 0) = T_o \tag{3-3}$$

$$T_e(r_i \leq r \leq r_o, \tau = 0) = T_{ie} \tag{3-4}$$

Based on Eqs. (3-1)- (3-4), the temperature distribution is given by [20]

$$T_e(r, \tau) = \sum_{m=1}^{\infty} e^{-\alpha\beta_m^2\tau} K_o(\beta_m, r) \left[\int_{\tau'=0}^{\tau} e^{\alpha\beta_m^2\tau'} A(\beta_m, \tau')d\tau'\right] \text{ (K)} \tag{3-5}$$

where $A(\beta_m, \tau') = \alpha[r_i \frac{dK_o(\beta_m, r = r_i)}{dr} T_i - r_o \frac{dK_o(\beta_m, r = r_o)}{dr} T_o]$ (m-K/s) (3-6)

The kernel, $K_o(\beta_m, r)$, is the normalized eigenfunction, r_i is the inner radius, r_o is the outer radius, $T_e(r_i, \tau)$ and $T_e(r_o, \tau)$ are the temperatures of the walls at the inner and the outer radii, respectively. In addition [20],

$$K_o(\beta_m, r) = \frac{R_o(\beta_m, r)}{\sqrt{N}} \text{ (1/m)} \tag{3-7}$$

where $R_o(\beta_m, r)$ and N are

$$R_o(\beta_m, r) = \frac{J_o(\beta_m r)}{J_o(\beta_m r_o)} - \frac{Y_o(\beta_m r)}{Y_o(\beta_m r_o)} \text{ (no units)} \tag{3-8}$$

$$N = \frac{2}{\pi^2} \frac{1}{\beta_m^2 J_o^2(\beta_m r_o) Y_o^2(\beta_m r_o)} \left(1 - \frac{J_o^2(\beta_m r_o)}{J_o^2(\beta_m r_i)}\right) \text{ (m}^2\text{)} \tag{3-9}$$

β_m (eigenvalues) are the positive roots of [20]

$$\frac{J_0(r_i\beta_m)}{J_0(r_o\beta_m)} - \frac{Y_0(r_i\beta_m)}{Y_0(r_o\beta_m)} = 0 \tag{3-10}$$

Using r_i = 0.1 m, r_o = 10 m, T_i = 305.1 K, T_o = 285 K, T_{ie} = 285 K, k = 0.5, 2 or 4 W/m-K, ρ = 2050 kg/m^3, and C_p = 1840 J/kg-K, Eqs. (3-5)-(3-10) were simplified and solved to find $T_e(r,\tau)$. The simplified equations are shown in Appendix B. The first 8 values of β_m were calculated using Wolfram Alpha [21]; and then, using those 8 values for β_m, the next 90 values were calculated using Microsoft Excel. All of the β_m values calculated were not exact zeros of Eq. (3-10), but gave on the order of 10^{-14} to 10^{-10}. Only 98 values of β_m were computed, since the cumulative temperature at different radii and times calculated typically stabilized within an error of less than

±0.07 K after using 60 terms in the summation of the temperature equation, Eq. (B-3). The 98 β_m values and the calculation process for the β_m values using Excel are shown in Appendix A. The difference between two consecutive temperature values in the summation series when D_i =0.2 m, k = 4 W/m-K, and t = 10368000 s (120 days) is also shown in Appendix A (Fig. A-2). Figure 17 shows the cumulative earth temperature plotted versus m of β_m values for the Eq. (B-3) series at r = 2 m for k = 4 W/m-K, and D_i = 0.2 m.

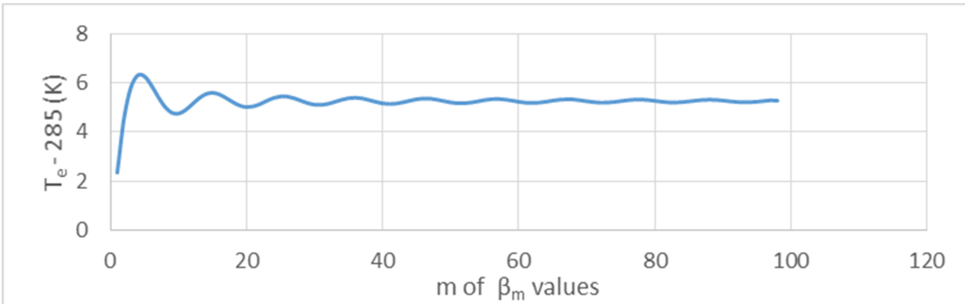

Figure 17. Cumulative temperature vs. m of β_m values at r = 2 m for k = 4 W/m-K, D_i = 0.2 m, and t =10368000 s.

Substituting the β_m values and the boundary conditions into Eq. (B-3), the temperatures at different radii and different times were calculated in order to determine the radius at which the initial temperature of the earth remained unchanged. This value of radius helped in determining the minimum spacing that must be provided between the bore holes. All of the results for the closed form solution are presented in Chapter 4. Major sections of the Excel sheet used to calculate the closed form solution when D_i = 0.2 m are shown in Appendix B. Table 3 shows the results for a sample case when k = 4 W/m-K, D_i = 0.2 m, and t = 10368000 s for different radii.

Table 3. Earth temperature for k = 4 W/m-K and D_i = 0.2 m at t = 10368000 s for different radii (98 β_m values).

r (m)	T_e (K)	r (m)	T_e (K)
1	293.75	6	285.88
2	290.28	7	285.53
3	288.40	8	285.29
4	287.21	9	285.13
5	286.42	10	285.00

Figure 18 shows the earth temperature plotted against radius when k = 4 W/m-K, D_i = 0.2 m, and t = 10368000 s (120 days). It can be seen that the initial earth temperature remained unchanged at approximately r = 9 m. Thus double this radius can be used as the minimum spacing needed between the bore holes for k = 4 W/m-K and D_i = 0.2 m at t = 10368000 s (120 days).

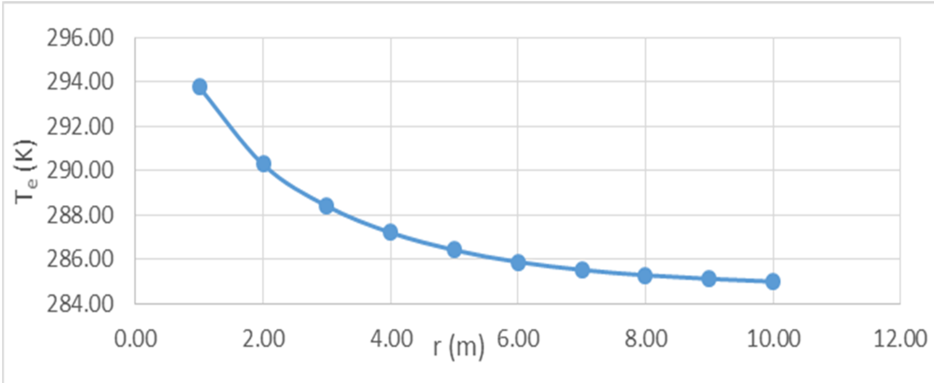

Figure 18. Earth temperature vs. radius at time t = 10368000 s for k = 4 W/m-K and D_i = 0.2 m.

The results from the closed form solution were then checked by solving the same problem using the Finite Difference method.

3.1.2 Finite Difference Method (EXCEL)

The one-dimensional transient conduction equation in cylindrical coordinates (Eqs. (3-1)-(3-4)) was also solved using the Finite Difference method with MS Excel. Temperature distribution results obtained using the Finite Difference method were compared with the results from the closed form solution of Section 3.1.1 and are shown in Chapter 4. When using the Finite Difference method, the outer and inner radii were kept constant and equal to 10 m and 0.1 m, respectively. The Finite Difference method was solved for different values of Δτ and Δr. This was done to check for the consistency of the solution with changing Δτ and Δr. Since the smaller the time and radius steps, the more accurate the results are, therefore, Δτ = 300 s and Δr = 0.05 m (where the results remained approximately unchanged) were used to solve the Finite Difference problem. Differences between temperatures for different values of Δτ and Δr are shown in Appendix F. Table 4 shows the input parameters used in solving the Finite Difference problem

Table 4. Input parameters for solving one-dimensional model using Finite Difference.

r_i (m)	0.1	k (W/m-K)	0.5, 2 or 4
r_o (m)	10	ρ (earth) (kg/m^3)	2050
T_{ie} (K)	285	C_p (J/kg-K)	1840
T_o (K)	285	T_i (K)	305.1

Stability Criterion

Stability criterion for the Finite Difference solution was [22]

$$\Delta\tau < \frac{\Delta r^2}{2\alpha} \tag{3-11}$$

So substituting $\Delta r = 0.05$ m and $\alpha = 1.06045 \times 10^{-6}$ m^2/s (k = 4 W/m-K) into Eq. (3-11) gave $\Delta\tau < 1178.75$ s. Also, $\Delta r^2/2\alpha$ increased for k = 2 and 0.5 W/m-K. Therefore, using $\Delta\tau = 300$ s satisfied the stability criterion for all of the cases and gave reliable results (see Appendix F) to validate the closed form solution [22]. The one-dimensional transient heat transfer problem in cylindrical coordinates was solved using the "Forward-Time Central-Space" Finite Difference method. The discretization may be written either in explicit or implicit form. The explicit form has been chosen here, and is [22]

$$T_{\tau+\Delta\tau,j} = T_{\tau,j} + \frac{\alpha\Delta\tau}{2r_j\,\Delta r^2}\left[\left(r_{j+1} + r_j\right)\left(T_{\tau,j+1} - T_{\tau,j}\right) - \left(r_{j-1} + r_j\right)\left(T_{\tau,j} - T_{\tau,j-1}\right)\right] \qquad (3\text{-}12)$$

where $\Delta r = r_j - r_{j-1}$. The results from the Finite Difference method are discussed in Section 4.2, where subscripts τ and j are time and radius points, respectively.

3.2 Two-Dimensional Temperature Distributions

Two-dimensional temperature distributions were found using ANSYS–CFX, a turbomachinery simulation software package, which uses CFD [23]. In solving the two-dimensional transient heat transfer problem, temperature distribution was calculated both radially and along the depth of the bore hole. First, to reduce the simulation time by reducing the number of elements, 3.6° wedge models of the water and earth domains were simulated instead of the complete 360° cylindrical model. Solving the 3.6° wedge model instead of the 360° cylindrical model helped in determining the approximate mass flow rates required for different depths of the bore hole in order to reach the desired bore hole exit water temperature.

To solve the two-dimensional problem for internal flow of water through a tube with conjugate heat transfer, the water and earth domains were first created using SolidWorks 2016 and then were imported to ANSYS-CFX. The different steps involved in creating, meshing and solving for temperature distributions in the earth domain and the bore hole exit water temperatures are discussed in Sections 3.2.1 and 3.2.3.

3.2.1 SolidWorks

The earth and water components have to be created as solid bodies in order to be meshed and simulated using ANSYS-CFX. These individual media are called "domains" in ANSYS-CFX terminology. SolidWorks 2016 was used to create a three-dimensional model of the combined domains of earth and water. First, instead of creating a 360 ^{o} complete model of the cylindrically shaped bore hole with its U-tube, a 3.6^{o} wedge was created, taking advantage of angular symmetry (since the heat transfer problem is two-dimensional and not dependent on angle). Creating the 3.6^{o} wedge (vertical bore hole and single tube, without U-tube) reduced the number of mesh nodes 100 times, which then reduced the computational time required by approximately 30 times. Since computer simulation time depends on the number of time steps, convergence of the results and number of nodes, simulation time reduced by 30 times as opposed to 100 times. The earth and water domains were created individually and then were connected using the assembly tool of SolidWorks. After determining the approximate mass flow rates required using the 3.6^{o} wedge, a complete 360^{o} three-dimensional model of the bore hole, U-tube, earth and water was created for complete analysis of the real-time installation of the ground loop cooling system. Steps that were used to create this model are discussed in Appendix E.

3.2.2 Overview of ANSYS-CFX

Sections 3.2.2 to 3.2.3.1 give an overview of the ANSYS set of programs. If the reader is already familiar with ANSYS, please skip to Section 3.2.3.2, which shows how the heat transfer problem was set up and solved. Figure 19 shows the ANSYS GUI and the five modules of CFX. ANSYS-CFX is one of two CFD codes that are part of the ANSYS set of programs. Another CFD code is ANSYS-FLUENT. The principal difference between the two codes is that the ANSYS-CFX solver uses the finite element method to discretize the domain, whereas ANSYS-FLUENT uses the finite volume method. In this study, ANSYS-CFX release 15.0 was used to run the simulations [23, 24].

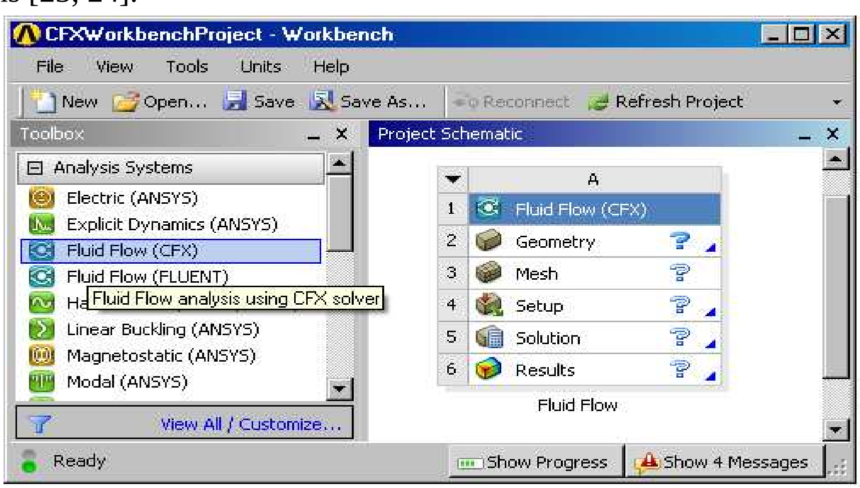

Figure 19. ANSYS GUI.

3.2.3 ANSYS-CFX Workflow

ANSYS-CFX is integrated into the ANSYS Workbench Environment, which offers users a graphical interface to access all of the functions within ANSYS with simple drag-and-drop operations. ANSYS-CFX itself consists of five modules: Geometry (Design Modeler), Meshing, Set up (CFX-Pre), Solution (CFX Solver), and Results (CFX-Post) [23], which are discussed in Sections 3.2.3.1 through 3.2.3.13

3.2.3.1 Design Modeler

Workbench 15.0 was first started. Then the Fluid Flow CFX-Analysis system was opened from the toolbar, or it also could be dragged to the main screen. By right clicking on the Design Modeler in the CFX-Analysis system, a drop-down menu appears, from which the parasolid (-x_t) file, which was created using SolidWorks, can be imported into the Design Modeler (Fig. 20). Then by double clicking on Design Modeler (Geometry), a new window appears; and, on the toolbar of the new window, double clicking on "generate" will generate the water and earth domains that were assembled using SolidWorks.

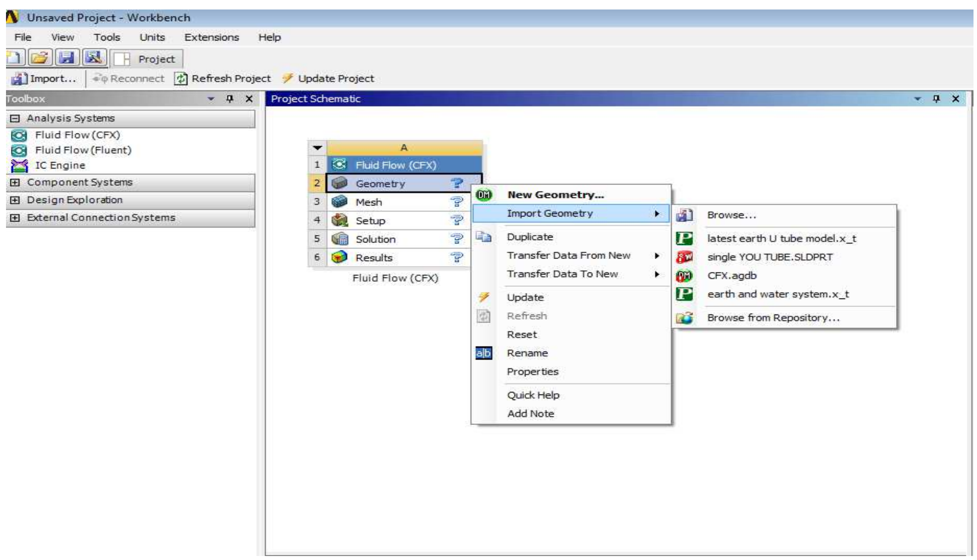

Figure 20. Importing the parasolid (-x_t) file into Design Modeler of ANSYS.

The two individual models of the earth and water domains appear as one body, which is comprised of two parts in Design Modeler. These two parts were selected and created as one single part. This was done by selecting both parts, and then right clicking gives the user an option to make them into one part. Making the water and earth domains into one single part in Design Modeler assured proper transfer of mesh, which in turn is related to the transfer of data from the water domain to the earth domain. Next, the Design Modeler was closed and the data from the Design Modeler was transferred to the meshing module of the CFX-Analysis systems.

3.2.3.2 Meshing

After the data was transferred from the Design Modeler to the Meshing Module, the Meshing was started by double clicking the Mesh tab of the CFX workspace. In Meshing, the earth and water domains were meshed to get fine grid refinement and enough elements in order to reduce errors in the final answer. The common mesh settings that were used in meshing the domains are listed in Table 5.

Table 5. Common mesh settings.

Defaults	
Physics Preference	CFD
Solver Preference	CFX
Relevance	100
Sizing	
Use Advanced Size Function	On: Proximity and Curvature
Relevance Center	Fine
Smoothing	Medium
Transition	Slow
Span Angle Center	Fine
Minimum Size of the Element	Default (0.156260 m)
Maximum Face Size	Default (15.6260 m)
Maximum Size of the Element	Default (31.2520 m)
Growth Rate	Default (1.10)
Minimum Edge Length	Default (7.854 m)

While leaving most of the settings at their defaults, solver preference and relevance were changed to CFX and 100, respectively. Changing the solver preference to CFX allowed the meshing application to set certain defaults that would help in creating mesh that was more favorable to CFX. Relevance, on the other hand, helped to control the fineness of the mesh. A high accuracy (+100) was chosen for the relevance since the finer the mesh, the more accurate the results were. Other settings, such as minimum size, maximum size, and growth rate could also be changed to mesh the model to required refinements. Growth rate represents the increase in the edge length of the element in the successive layers of elements. Minimum edge length is a default value, which cannot be changed and it provides a read-only indication of the smallest edge length in the model.

Figure 21 is a model of the earth and the water domains which were used for the analysis. Figure 21 shows the edges and sides of the 3.6° wedge model on which the different meshing operations were performed, which are shown in Table 6.

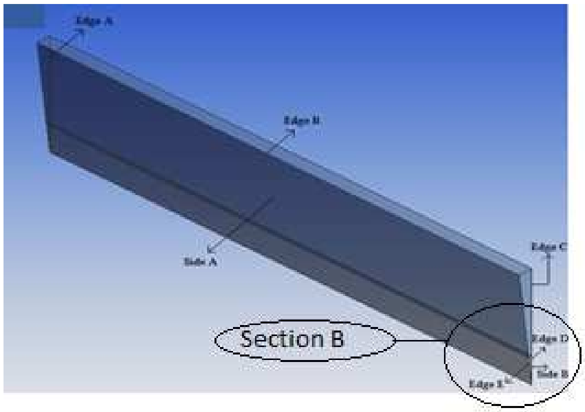

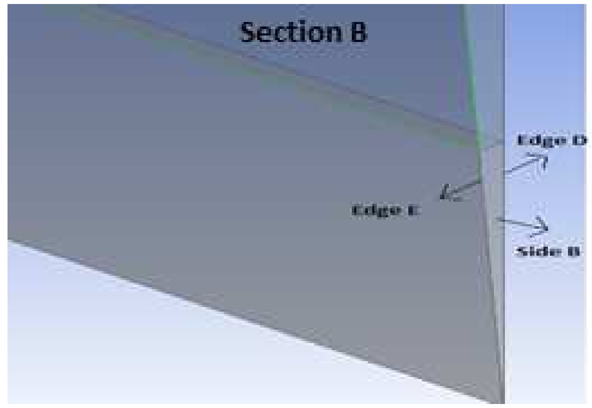

Figure 21. Model of the earth and water domains showing the edges and sides on which the meshing was performed with ANSYS-CFX.

Table 6. Methods followed in meshing the 3.6° wedge.

Domain	**Edge/Side**	**Method**	**Inputs**
Earth	Side A	Sweep Method	Manual Source/ /No Bias/ Sweep Number of Divisions 1
Earth	Side A	Mapped Face Meshing	Suppressed-No/ Constrain Boundary-No/Advanced Settings-Default
Earth	Edge A and C	Edge Sizing	Suppressed-No/Number of Divisons-100/ Bias Type ---- --- -- -/Bias Factor-250
Earth	Edge B	Edge Sizing	Suppressed-No/Number of Divisons-2500/ Bias Type ---- --- -- - /Bias Factor-10
Water	Side B	Sweep Method	Manual Source/Sweep Number of Divisions 2500/Bias Type ---- --- -- -/Bias Factor 10
Water	Edge D	Edge Sizing	Suppressed-No/Number of Divisons-40/ Bias Type --- --- ----/Bias Factor-10
Water	Edge E	Edge Sizing	Suppressed-No/Number of Divisons-40/ Bias Type - -- --- ----/Bias Factor-10
Water	Edge at the Interface	Edge Sizing	Suppressed-No/Number of Divisons-1/ No Bias

The following symbols listed in Table 6 "- -- --- ----, ---- --- -- -"are pictorial depictions of the bias types used in ANSYS-Meshing. For example, when an edge is selected with one of the two pictorial depictions for edge sizing, the side of the edge with more dashes will have more nodes, and the number of nodes decreases with decreasing number of dashes.

3.2.3.3 Meshing Quality

A good quality mesh is one that has the proper refinements around the areas of interest and enough elements to minimize error and maximize accuracy in the solution. The edges and shapes of the geometries should remain unaltered when meshing is performed. Since Bias factor was used in Sweep Meshing and Edge Sizing of the earth and water domains, to reduce the number of elements, the Bias factor played a key role in the quality of the mesh.

With element midside nodes dropped (nodes at the middle of the elements) and mesh morphing disabled (not allowing a change in Geometric Design to change the mesh in the solver for accuracy of the prediction), sample mesh statistics for a 3.6^o wedge with D_i = 0.2 m and L = 500 m are shown in Table 7. Mesh information for each individual run is given in Chapter 4.

Table 7. Mesh statistics.

Nodes	557723
Elements	332500

An All-Quad mesh (polygon with four sides) was preferred for computational purposes. (This is because All-Quad mesh has clean topology allowing for better results and animation of results.) So a sweep of the computational domain with Quad elements was attempted, but was disallowed by the meshing module due to the domain geometry of the domains. Therefore, the Quad/Tri option was selected for meshing the computational domain.

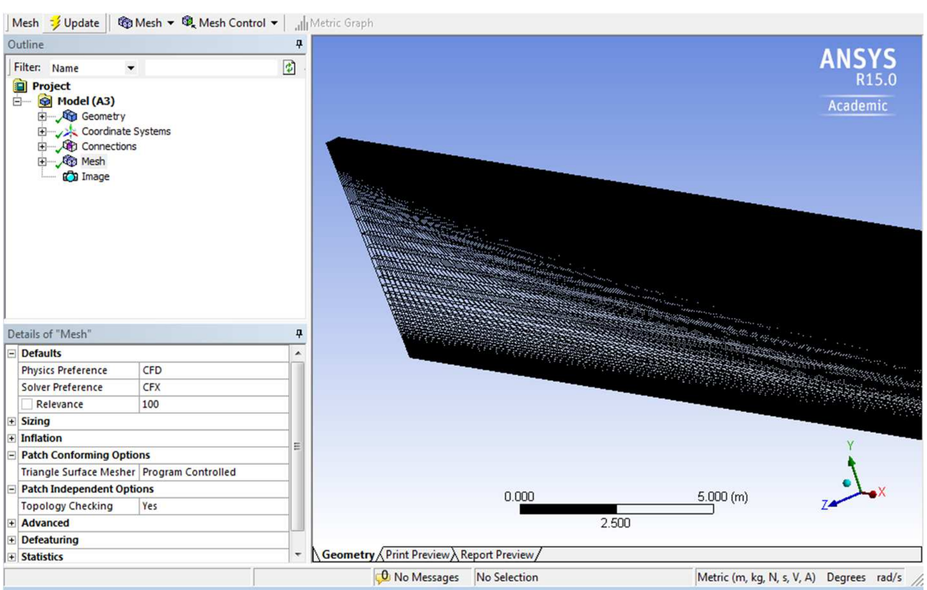

Figure 22. The mesh of the earth and water domains.

3.2.3.4 CFX-Pre (Set Up)

CFX-Pre was started by clicking on the set up module in the workbench workspace. The mesh data from the Meshing Module was transferred to the set up module automatically. The general method that was practiced in the set up module was to first select and assign the materials to both the earth and water domains. Then after giving the required initial and boundary conditions to both the domains and the solver and output controls for the solver, the set up module was closed and the problem was automatically transferred to the solution module of ANSYS-CFX.

Figure 23 shows what the CFX-Pre (set up) window looks like without giving any inputs.

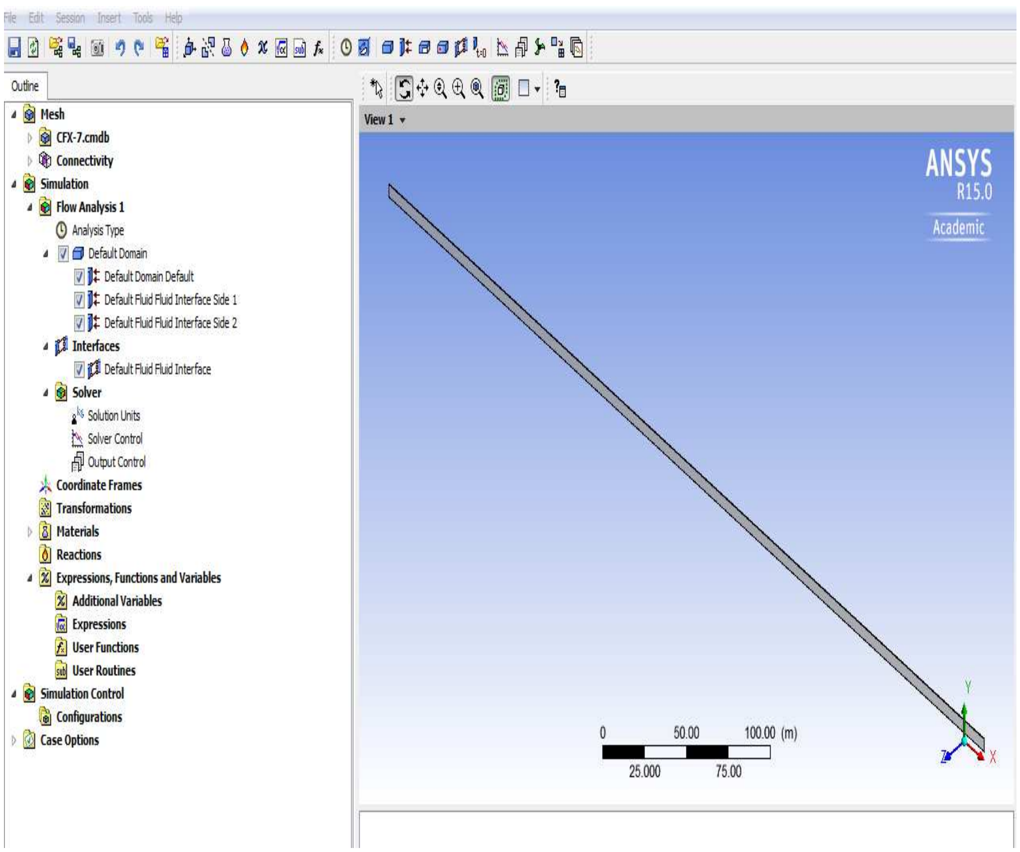

Figure 23. Default set up module.

Boundary conditions include inlet velocity components, opening conditions at the exit (defined in Section 3.2.3.8.2), wall temperatures at the outer wall, and symmetric conditions for both domains. All of the other edges and sides, which were not given as input parameters in the set up module, were considered as adiabatic walls by default by the set up module.

For solving different cases having different inlet velocities, opening temperatures, and material properties, the same mesh was used. Therefore, for every run conducted, the inlet parameters were changed accordingly in CFX-Pre; and various cases were solved.

3.2.3.5 Domains and Inlet Parameters Set Up

After the set up module was started, a window popped up, where all of the required boundary conditions and material properties could be assigned to the domains.

3.2.3.6 Domains and Material Set Up

The CFX-Pre considered both the water and earth domains as the same domain; and they were given same material and thermal properties. A new domain was created by selecting the domain icon on the tool bar and was named "Water". Then, on double clicking the "Water" domain, the details of the domain tab opened, where a material could be assigned to the domain; and fluids, heat transfer, and turbulence models could also be selected. The domain was also initialized in the same tab. Figure 24 shows how a water domain was set up.

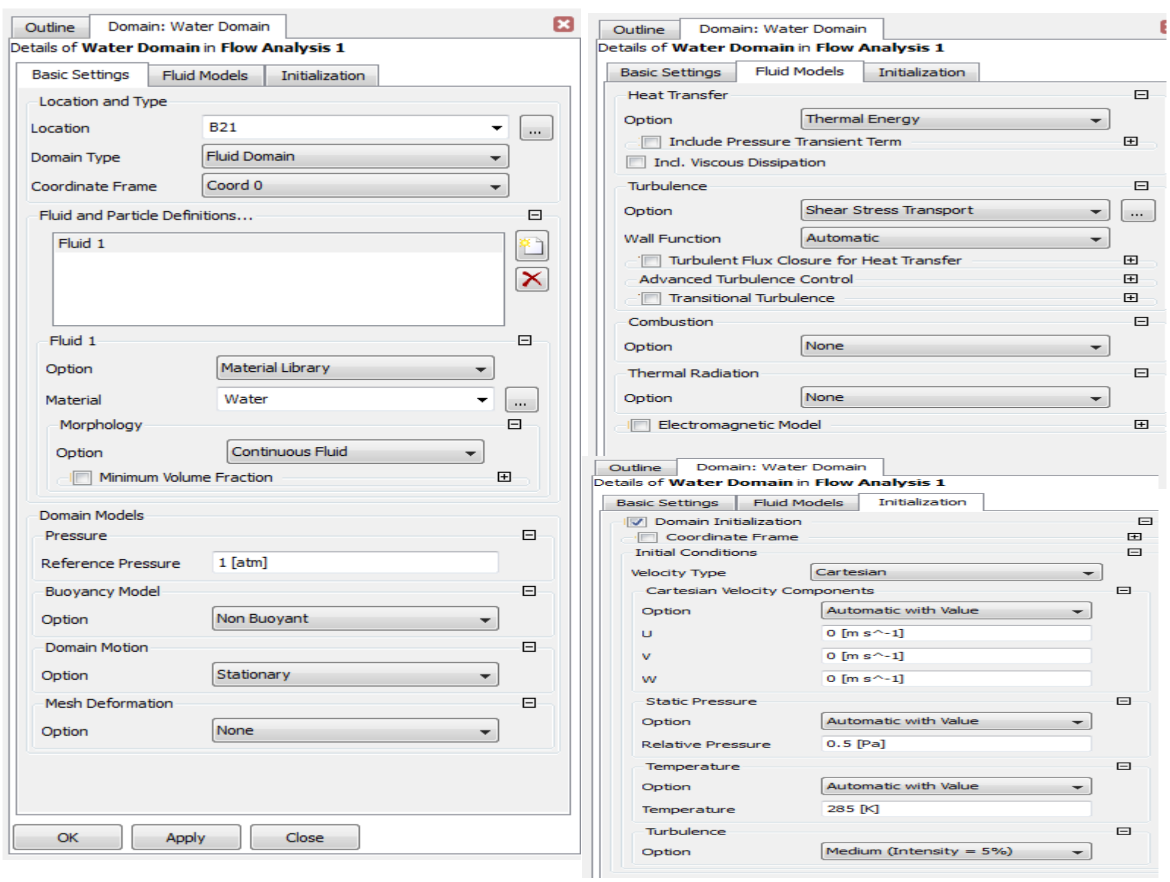

Figure 24. Details of the water domain.

Since the CFX-Pre materials library does not include the properties of soil, a new material was created by right clicking on the Materials tab and selecting “New Material”. In the Basic Settings tab of the Details of the New Material, i.e., “Earth”, the thermodynamic state was chosen to be solid; and, in the Material Properties tab, the values of coefficient of thermal conductivity, density, and heat capacity were assigned to the material. Figure 25 shows how the material “Earth” was added to the library of materials.

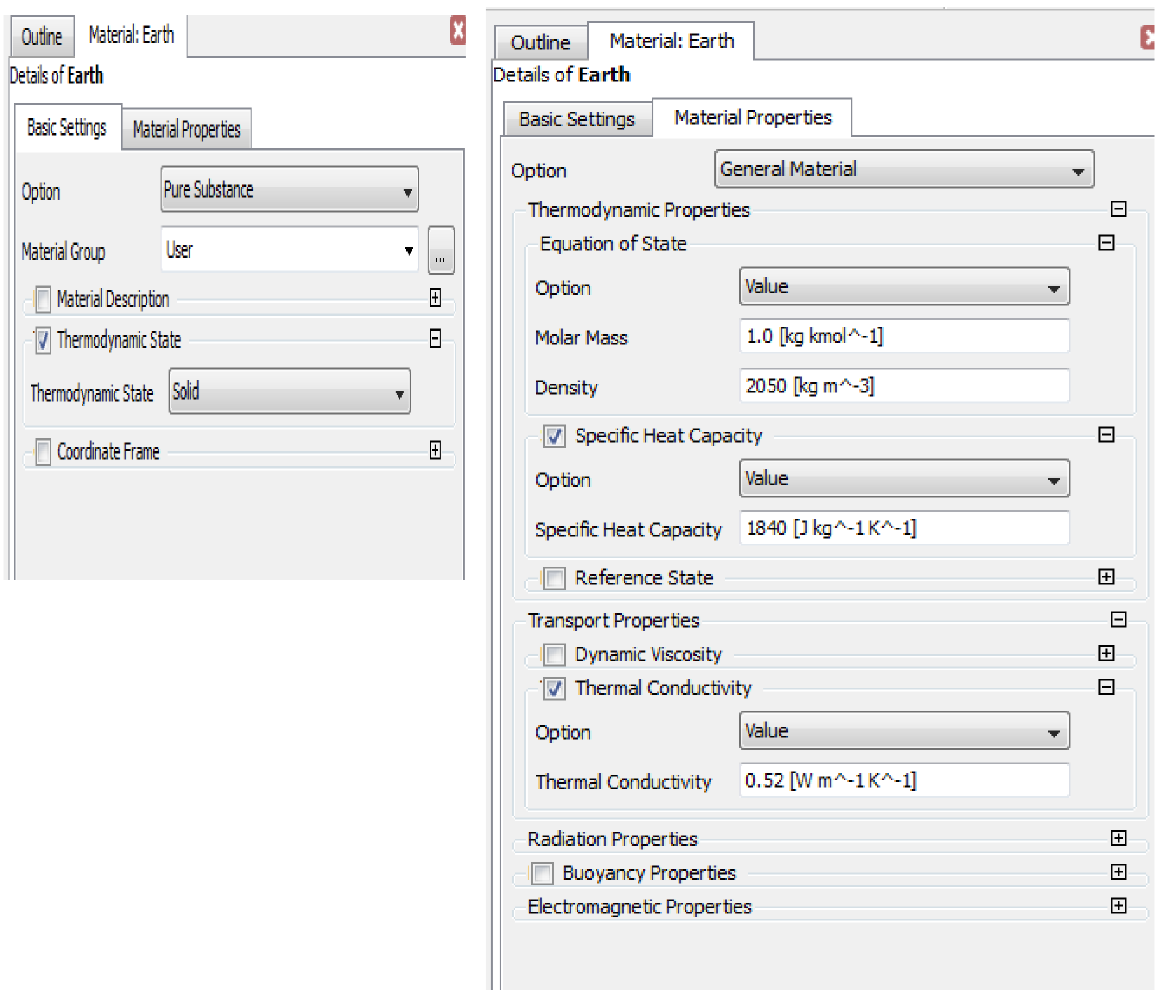

Figure 25. Adding earth to the material library.

Then, the default domain was renamed as “Earth”, and all of the “Earth” domain details, like location, material properties, domain type, and solid models, were given to the domain. In addition, the domain temperature was initialized to be the initial earth temperature. Figure 26 shows how an “Earth” domain was set up.

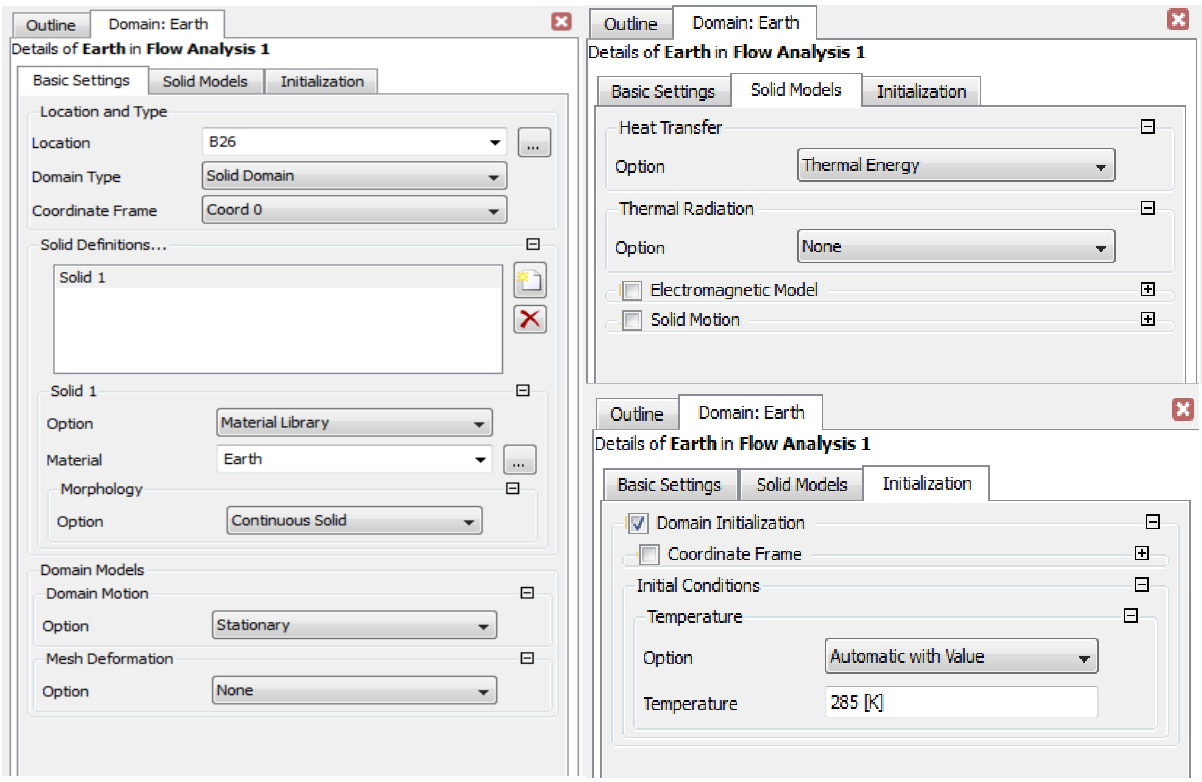

Figure 26. Earth model set up.

3.2.3.7 Analysis Type

The default Analysis Type was steady-state; but, on the contrary, our heat transfer problem was transient. Therefore, the steady-state option in the Analysis Type tab was changed to transient. Time duration was given as the total time chosen for the simulation, which was different for each of the various runs conducted. Time steps were given so that initial time steps were as small as 0.1 s with the maximum (final) time step becoming 3600 s or 4200 s, depending on the total time chosen for the simulation. This was done to decrease the computer simulation time by reducing the number of time steps and increase the accuracy of the results. These increments in time steps were achieved by creating an expression for ‘Δτ’, which was given as an input in the Time Step tab.

$$\Delta\tau = 0.1 + [1-\exp[-0.00005(\tau)]](4199.9)\ [s] \qquad (3\text{-}13)$$

The value 4199.9 (s) at the end of Eq. (3-13) was changed depending on the maximum time step that was chosen for any particular run, and depending on the convergence of the results. Initial time was given as 0 (s) for all of the runs. Figure 27 shows how an analysis type was set up.

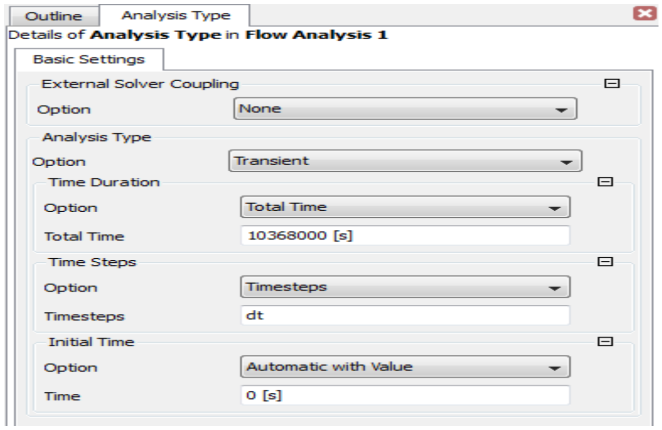

Figure 27. Analysis type set up.

3.2.3.8 Boundary Conditions Set Up (Parameters Set Up)

To solve the conjugate heat transfer problem with fluid flow, boundary conditions needed to be defined. Sections 3.2.3.8.1-3.2.3.10 show how different boundary conditions were defined in solving the transient heat transfer problem.

3.2.3.8.1 Inlet Set Up (Water Domain)

Inlet boundary conditions, such as velocity and static inlet temperature of the cooling water coming out of the condenser, were given as inputs for the water domain at the inlet. Also, the turbulence model was chosen to be of medium intensity, 5 %, for all of the runs except one run (10 %), where the effect of the turbulence intensity on the bore hole exit water temperature was assessed. Figure 28 shows how a typical “Inlet” boundary condition was set up for the water domain.

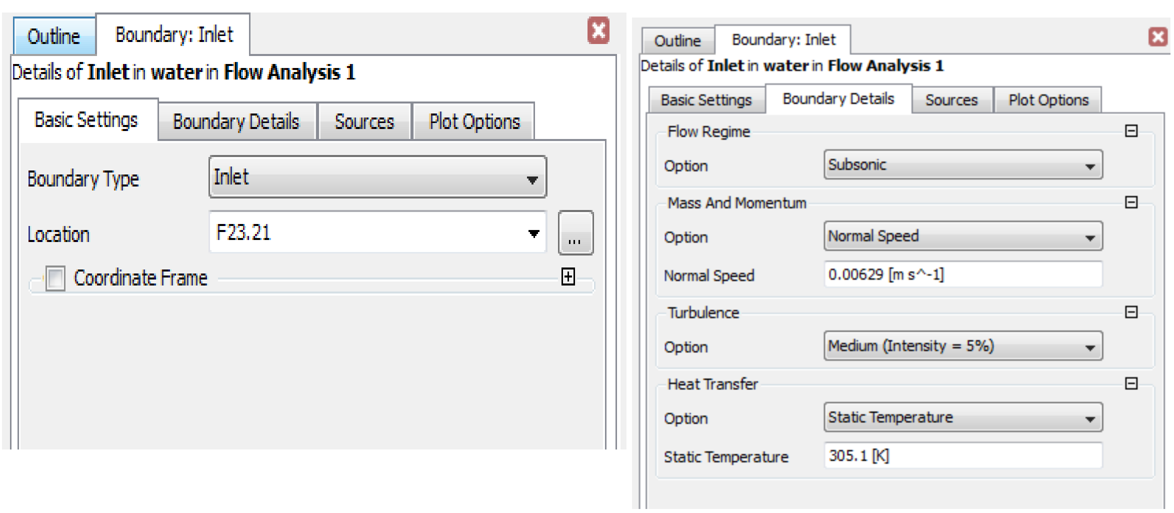

Figure 28. Inlet boundary condition set up.

The set up was done by right clicking on the water domain to insert a boundary condition, and this boundary condition was named “Inlet”. By double clicking the “Inlet” boundary condition under the water domain, the location and values (V_{in}, T_{in}) at the boundary were given.

3.2.3.8.2 Opening Set Up (Water Domain)

The Outlet Boundary Condition at the exit was given as an “Opening Boundary Type” instead of an “Outlet Boundary Type”. The Opening Boundary Condition is different from an “Inlet” or “Outlet” boundary condition since it allows flow in either direction as compared to allowing flow only in one direction (inlet or outlet). Using an “Outlet Boundary Type” is prefered, but doing so gave a floating point error while solving for the problem (“floating point error: having data with either too large or too small magnitude called 'overflow' or 'underflow,' respectively. Such data cannot be physically represented on computer for direct processing by arithmetic processing part of pocessor.”) Inputs, such as opening temperature, relative pressure at the “Outlet” and flow direction, were given as inputs at the boundary of the water domain at the exit of the tube. This boundary condition was named “Outlet”. Figure 29 shows how an Outlet Boundary was set up.

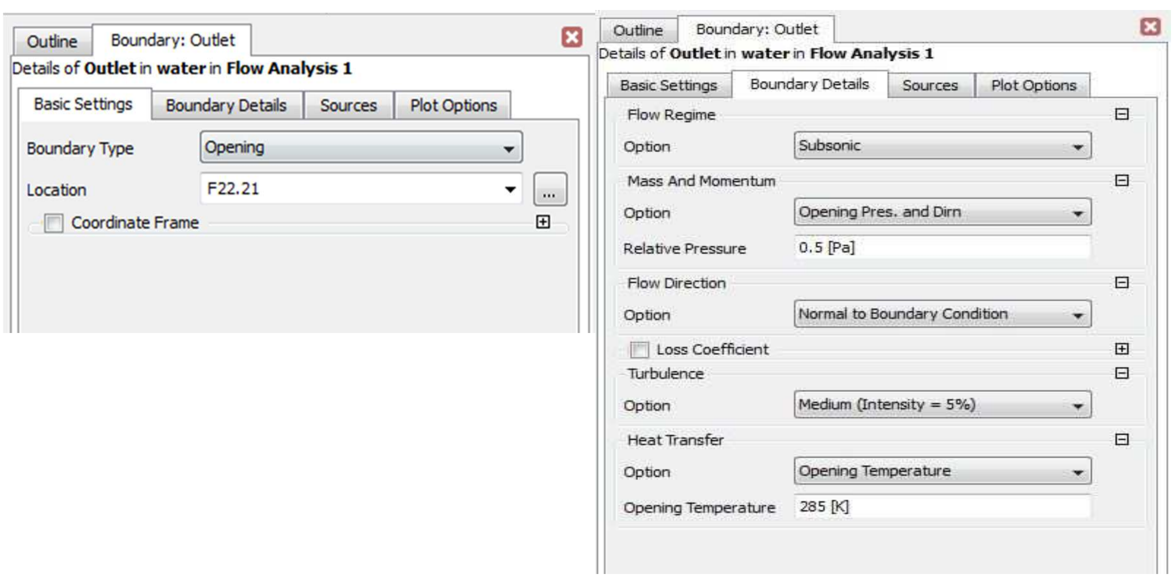

Figure 29. Outlet boundary condition set up.

The set up was done by right clicking on the water domain to insert a boundary condition, and this boundary condition was named “Outlet”. By double clicking the “Outlet” boundary condition under the water domain, the location and values at the boundary were given for the Outlet boundary.

3.2.3.8.3 Symmetry Set Up (Water and Earth Domains)

The Symmetry Boundary Condition was given for both the water and the earth domains. This symmetry condition was given to both of the domains (3.6° wedge), since they were designed as 3.6° wedges and have angular symmetry (the heat transfer problem is two-dimensional and not dependent on angle). This boundary condition required no other inputs except selecting the symmetric faces on both of the domains and choosing the Symmetry Boundary Condition.

3.2.3.9 Domain Interface

Interface boundary conditions were given for both the water and the earth domains at the interface between the domains. The CFX-Pre module automatically recognized the interface surfaces of both the domains and displayed it in the settings tab of the symmetry boundary. Also, CFX-Pre transferred the mesh from one domain to another. Figure 30 shows how the interface boundary conditions were set up.

A conservative interface flux boundary condition (this allows the solver to solve for the interface thermal resistance) was given to the water side of the interface. Although the tube walls at the interface were assumed to be smooth for most of the runs, wall roughs ness values were changed for two different runs in order to check the effect of roughness on the heat transfer from the cooling water to the earth domain.

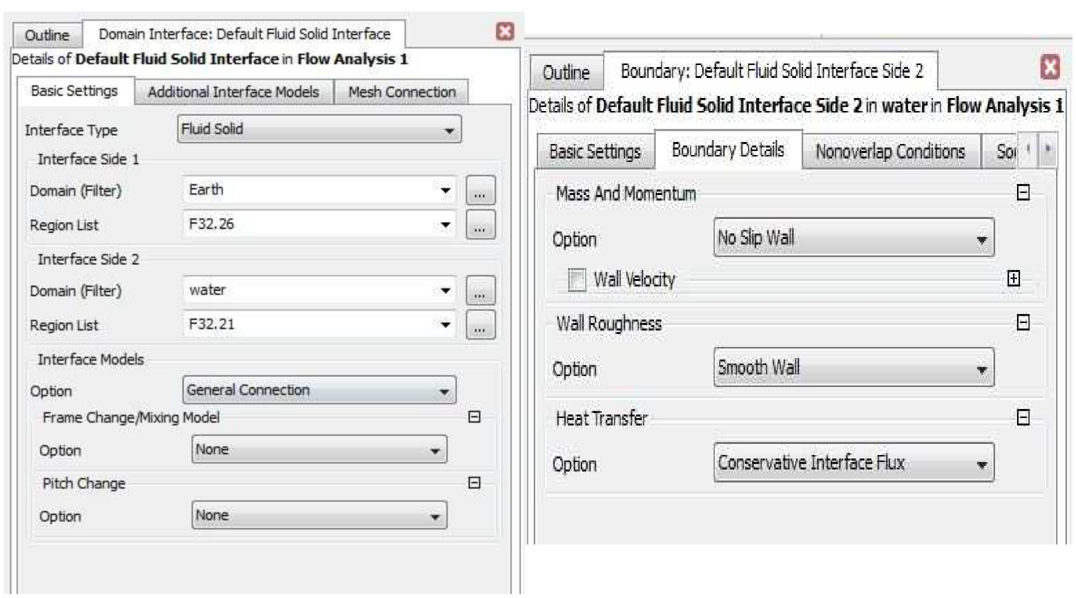

Figure 30. Interface boundary condition set up.

3.2.3.10 Wall Temperature (Earth Domain)

A constant temperature boundary condition was given to the earth domain at radius (r_o). The outer boundary of the earth domain at radius r_o was assumed to be at a constant temperature equal to the initial temperature of the earth (285 K). Figure 31 shows how the constant temperature boundary condition was set up.

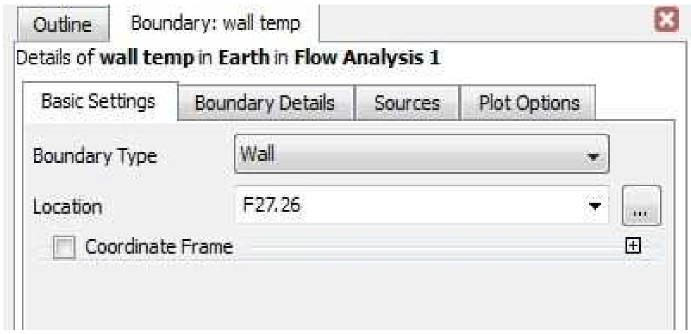

Figure 31. Details of constant temperature boundary condition at r_o (earth domain).

3.2.3.11 Solver Control Set Up

The CFX-Solver performed several coefficient iterations or loops, either to the specified maximum number or to the predefined residual target. Therefore, in the Solver Control Set Up, the maximum coefficient loops of convergence control was set to 10; and the residual target option was set to 1x 10^{-6}. Both the advection and turbulence schemes were set to high resolution; and a second order backward Euler scheme was chosen to solve the transient problem. Figure 32 shows how the Solver Control was set up.

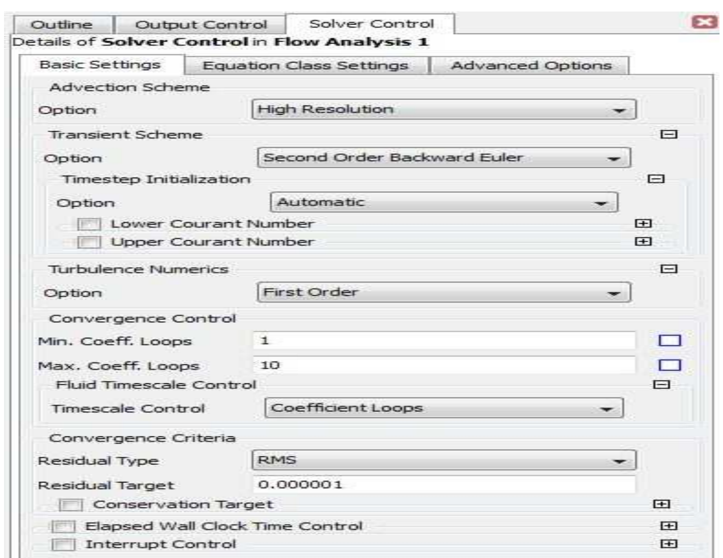

Figure 32. Solver control set up.

3.2.3.12 Output Control

Since the flow analysis was transient, output control for saving the transient results was set up using the Output Control option in CFX-Pre module. Results for the initial runs were saved at every time step; and, for the runs performed in the later stages, due to the amount of memory required to save the data, transient results were saved only at 120 time step intervals. Figure 33 shows how the output control was set up for saving the transient results.

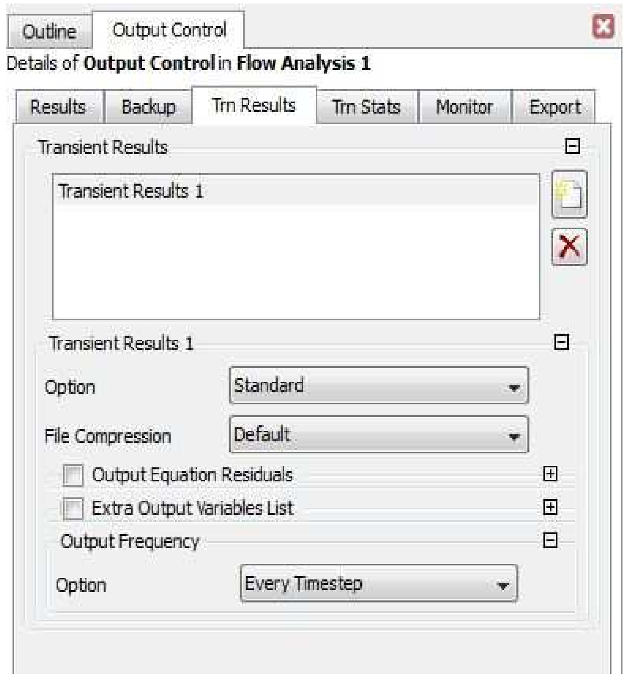

Figure 33. Details of the output control.

3.2.3.13 CFX-Post (Acquiring Solutions from CFX)

3.2.3.13.1 Starting the CFX-Solver Manager

The CFX-Solver Manager was started by double clicking on the solution tab in the CFX workspace. The Define Run dialog box was first displayed, which allowed the user to partition the problem and adjust the memory allocation for the Solver. The problem was first partitioned into parts, and all of the parts were then solved in parallel in order to reduce the simulation time. To fully utilize the quad core processer available, the problem was split into 8 parts, and all parts were solved simultaneously by using the HP MPI (Message Passing Interface) local parallel run mode. High memory was allocated to the Solver. Once the Define Run dialog box was set to the required settings, the run button in the bottom left corner was clicked to start the run.

3.2.3.13.2 Display Monitors

Display monitors showed the progress of a given run in terms of the residual values and a plot of the residuals. The display monitors also showed errors, if any, made while setting up the problem in the CFX-Pre module, in addition to licensing errors, and errors caused by the computer due to insufficient memory. For certain cases, the residuals did not converge to the target value of 1 x 10^{-6}. This could be seen on the display monitors and could be corrected by changing the mesh quality and time steps used. Convergence of 1x 10^{-4} for the residuals was also considered in some cases since the results achieved were reasonable. CFX-Post broke down the inputs given in CFX-Pre into readable code. Appendix H shows the code displayed on the display monitors for a general case. Figure 34 shows the display monitors for a sample run conducted on the 3.6^{o} wedge with k = 4 W/m-K.

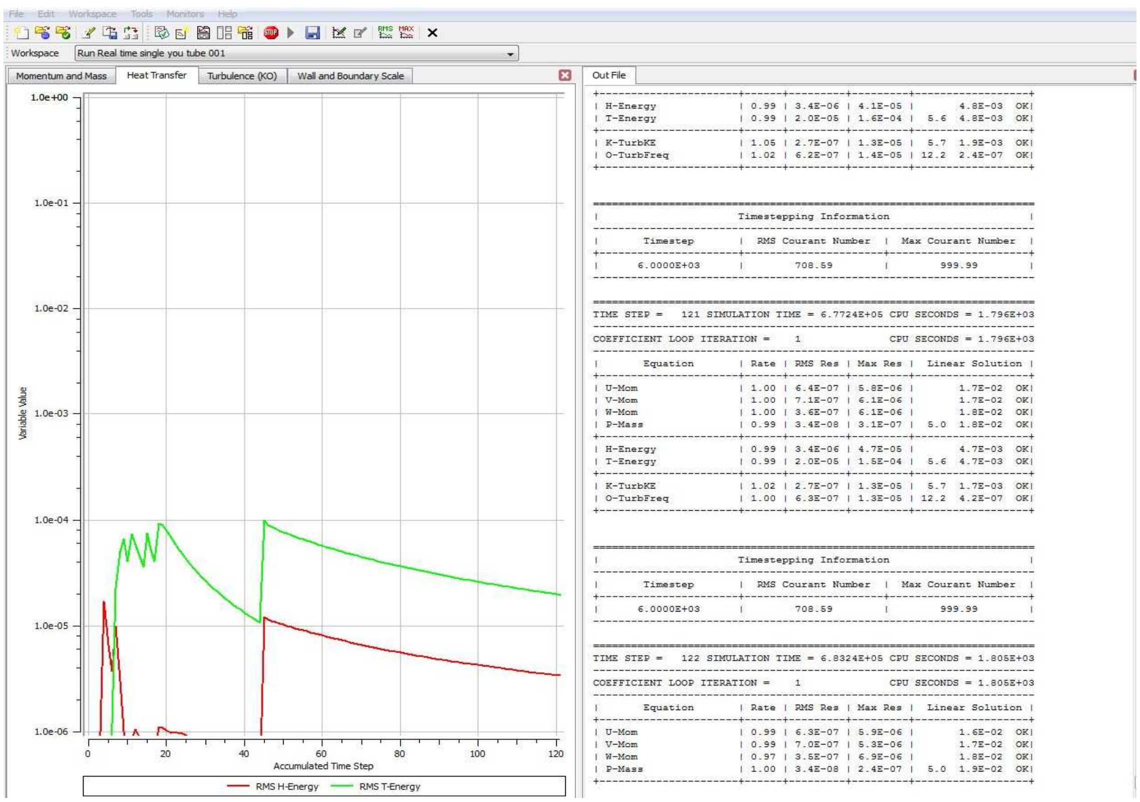

Figure 34. Display monitor results.

3.2.3.13.3 Solver Run Times

The computer used to run ANSYS-CFX was an Intel(R) core(TM) i7-2600 CPU processor running at 3.40 GHz with 8.00 GB of RAM. A 64-bit version of ANSYS 15.0 was used to run all of the cases. Parallel processing was used, i.e., the problem was split into various segments and all of those segments were solved simultaneously. Solving various segments in parallel, using several processers, took range of computer times to run various cases, depending on the total number of elements and time step expression used for solving the transient problem. To run a typical 3.6^{o} wedge model for 10368000 s (120 days) took approximately 11 hours, whereas, solving the cylindrical model with U-tube, L = 150 m and L = 100 m, took approximately 23 hours and 18 hours, respectively. The amount of space required to save the solution depended upon the number of time steps of the solution that were saved. Saving each of 2500 time steps required about 150 GB of space for the 3.6^{o} wedge model. On the other hand, saving at each time step for the cylindrical model with U-tube took about 350 GB. Considering the fact that each run required so much space to save the results at each time step, results were saved only at 120 time step intervals for the runs conducted later (runs conducted on the U-tube with L = 100 m) in order to reduce the space requirements. Saving the results at only 120 time steps took about approximately 16 GB.

After solving the problem for the total time given for a particular problem, results were extracted using CFX-Post (one of the five ANSYS-CFX modules) for each run. The results extracted for various runs are discussed in Section 4.4.

CHAPTER 4

RESULTS

This chapter gives a detailed discussion of the results obtained from the different solution methods. First, results for the one-dimensional temperature distribution using the closed form solution and the Finite Difference method are presented and discussed. Then, results obtained from ANSYS-CFX for the two-dimensional transient model are presented and discussed.

4.1 Results Obtained from the Closed Form Solution

As discussed in Section 3.1.1 and App. B, the closed form solution for the heat transfer problem (without fluid flow) in cylindrical coordinates was solved to obtain the results for one-dimensional temperature distribution. The results from that solution were then analyzed in order to find the radius at which the initial temperature of the earth (285 K) remained unchanged. This was done to estimate the spacing needed between bore holes, so that a bore hole did not thermally affect adjacent bore holes.

First, earth domain temperatures at different times and radii were calculated for different values of thermal conductivity (k), while keeping the inner diameter of the tube (D_i) constant and equal to 0.2 m, and keeping D_o = 20 m. The values of ρ = 2050 kg/m^3 and C_p = 1840 J/kg-K were kept constant for all cases. Table 8 show the one-dimensional temperatures above 285 K (ΔT_e) for different radii and times when using k = 0.5 W/m-K, where $\Delta T_e = T_e(r,t) - 285$ [K] .

Table 8. Temperature rise (ΔT_e) distribution at different times for k = 0.5 W/m-K and D_i = 0.2 m (closed form).

r (m)	ΔT_e (K) at t = 2592000 s (30 days)	ΔT_e (K) at t = 5184000 s (60 days)	ΔT_e (K) at t = 7776000 s (90 days)	ΔT_e (K) at t = 10368000 s (120 days)
0.5	6.42	7.85	8.58	9.06
1	2.28	3.77	4.64	5.24
2	0.13	0.62	1.13	1.57
3	-0.01	0.05	0.19	0.38
4	-0.02	-0.02	0.00	0.05
5	-0.03	-0.03	-0.02	-0.02
6	-0.03	-0.03	-0.03	-0.02
7	-0.02	-0.02	-0.02	-0.02
8	-0.01	-0.01	-0.01	-0.01
9	-0.01	-0.01	-0.01	-0.01
10	0.00	0.00	0.00	0.00

As can be seen from Fig. 35, for the given boundary and initial conditions (Eqs. (3-2)-(3-4)), initial earth temperature remained approximately unchanged, within an error of 0.05 K, for radius greater than 4 m for all times studied. Therefore, a distance of 8 m (2 x 4 m) can be used as the spacing that has to be provided between the bore holes when the thermal conductivity of the earth is assumed to be 0.5 W/m-K.

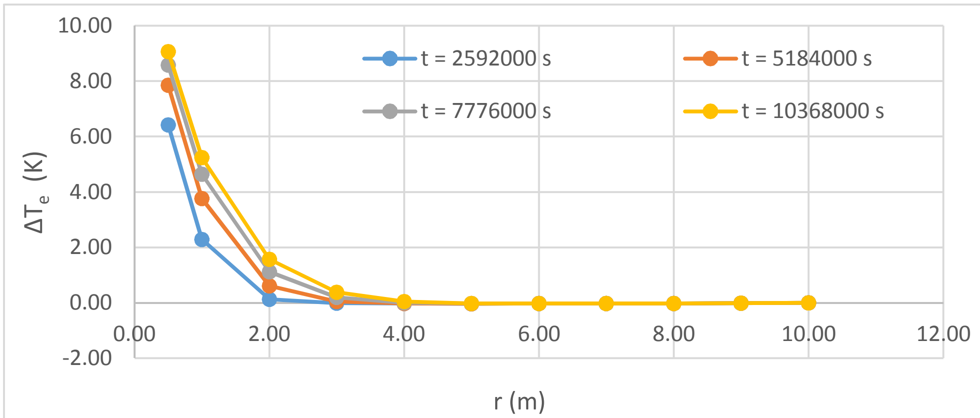

Figure 35. ΔT_e vs. radius at different times for k = 0.5 W/m-K and D_i = 0.2 m (closed form).

Next, Table 9 shows the one-dimensional temperatures above 285 K (ΔT_e) for different radii and times when using k = 2 W/m-K. Further information can be found in Fig. 36. Also, note that ΔT_e values at all radii when k = 0.5 W/m-K, t = 10368000 s (Table 8), are exactly the same as those for k = 2 W/m-K, t = 2592000 s (Table 9). This is because $T_e(r,\tau)$ depends on α and τ, as only the product of the two (see Eq. (B-3)). Therefore, when τ is halved and α is doubled, the value of $T_e(r,\tau)$ will be exactly the same.

Table 9. Temperature rise (ΔT_e) distribution at different times for k = 2 W/m-K and D_i = 0.2 m (closed form).

r (m)	ΔT_e (K) at t = 2592000 s (30 days)	ΔT_e (K) at t = 5184000 s (60 days)	ΔT_e (K) at t = 7776000 s (90 days)	ΔT_e (K) at t = 10368000 s (120 days)
0.5	9.06	10.07	10.58	10.92
1	5.24	6.58	7.28	7.74
2	1.57	2.8	3.55	4.07
3	0.38	1.15	1.75	2.22
4	0.05	0.42	0.82	1.18
5	-0.02	0.12	0.35	0.59
6	-0.02	0.02	0.13	0.27
7	-0.02	-0.01	0.04	0.11
8	-0.01	-0.01	0	0.04
9	-0.01	-0.01	0	0.01
10	0	0	0	0

As can be seen from Fig. 36, for the given boundary and initial conditions (Eqs. (3-2)-(3-4)), initial earth temperature remained approximately unchanged, within a maximum error of 0.04 K, for radius greater than 8 m for all times studied. Therefore, a distance of 16 m (2 x 8 m) can be used as the spacing that has to be provided between the bore holes when the thermal conductivity of the earth is assumed to be 2 W/m-K.

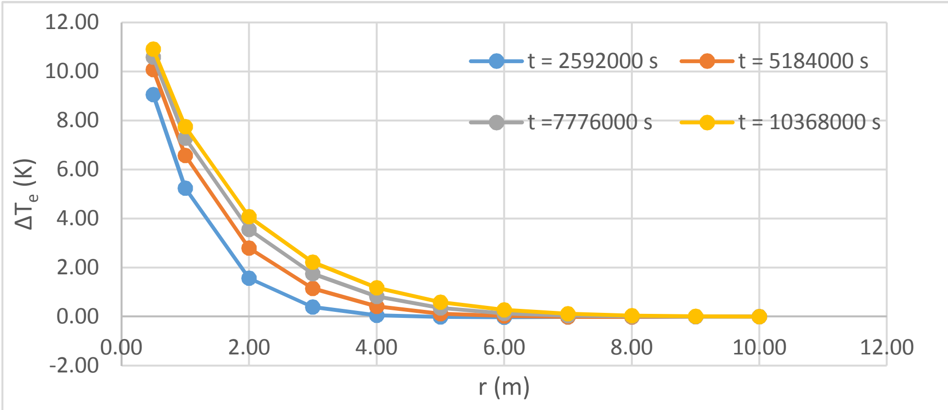

Figure 36. ΔT_e vs. radius at different times for k = 2 W/m-K and D_i = 0.2 m (closed form).

Finally, Table 10 shows the one-dimensional temperatures above 285 K (ΔT_e) for different radii and times when using k = 4 W/m-K. Further information can be found in Fig. 37. Also, note that ΔT_e values at all radii when k = 2 W/m-K, t = 5184000 s and t = 10368000 s (Table 9), are exactly the same as those of k = 4 W/m-K, t = 2592000 s and t = 5184000 s (Table 10), respectively. This is because $T_e(r,\tau)$ depends on α and τ, as only the product of the two (see Eq. (B-3)). Therefore, when τ is halved and α is doubled, the value of $T_e(r,\tau)$ will be exactly the same.

Table 10. Temperature rise (ΔT_e) distribution at different times for k = 4 W/m-K and D_i = 0.2 m (closed form).

r (m)	ΔT_e (K) at t = 2592000 s (30 days)	ΔT_e (K) at t = 5184000 s (60 days)	ΔT_e (K) at t = 7776000 s (90 days)	ΔT_e (K) at t = 10368000 s (120 days)
0.5	10.07	10.92	11.35	11.64
1	6.58	7.74	8.35	8.75
2	2.8	4.07	4.79	5.28
3	1.15	2.22	2.91	3.4
4	0.42	1.18	1.76	2.21
5	0.12	0.59	1.04	1.42
6	0.02	0.27	0.59	0.88
7	-0.01	0.11	0.32	0.53
8	-0.01	0.04	0.16	0.29
9	-0.01	0.01	0.06	0.13
10	0	0	0	0

As can be seen from Fig. 37, for the given boundary and initial conditions (Eqs. (3-2)-(3-4)), initial earth temperature remained approximately unchanged, within a maximum error of 0.13 K, for radius greater than 9 m for all times studied. Therefore, a distance of 18 m (2 x 9 m) can be used as the spacing that has to be provided between the bore holes when the thermal conductivity of the earth is assumed to be 4 W/m-K.

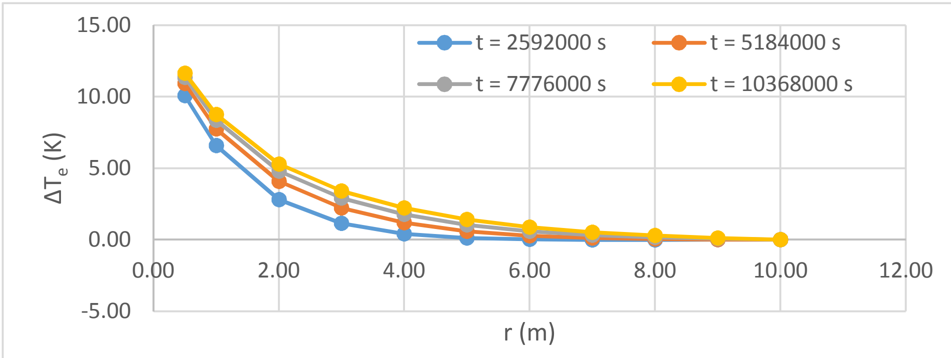

Figure 37. ΔT_e vs. radius at different times for k = 4 W/m-K and D_i = 0.2 m (closed form).

Before conducting runs using ANSYS-CFX, it was important to determine the effect of inner diameter on the temperature distribution. So a few more cases were solved by changing the inner diameter to 0.1 m. It was determined that for the decreased inner diameter to 0.1 m, the magnitudes of the differences between earth temperatures were approximately 0.10 K (max) to 0.01 K (min) (see Tables C-4 to C-6) compared to earth temperatures at similar conditions when D_i = 0.2 m (see Tables 8-10). The earth temperature results after changing the inner diameter of the earth to 0.1 m are discussed in Appendix C.

4.2 Results Using Finite Difference Method (MS Excel)

As stated in Section 3.1.2, the solution for the heat transfer problem in cylindrical coordinates was also found using the Finite Difference method in MS Excel. Then, these results are compared to the results from the closed form solution in Section 4.3. Equation (3-12) was used to solve the Finite Difference problem. Input parameters to solve the Finite Difference method such as r_i, r_o, ρ, C_p and k were taken from Table 4. The Finite Difference problem was solved using different values of Δr and $\Delta\tau$, while satisfying the stability criterion (Eq. (3-11)). This was done to check for consistency of the results. It was determined that, when the initially used Δr = 1 m and $\Delta\tau$ = 18000 s were reduced to Δr = 0.1 m and $\Delta\tau$ = 600 s, there was an approximate earth temperature difference of 1.691 K at r = 1.1 m and t = 10368000 s (120 days). Also, when Δr and $\Delta\tau$ were further reduced to Δr = 0.05 m and $\Delta\tau$ = 300 s, there was an approximate difference of

0.001 K for r = 1 m and t = 10368000 s (120 days) as compared to the earth temperatures calculated with $\Delta\tau$ = 600 s and Δr = 0.1 m. Since changing from $\Delta\tau$ = 600 s to 300 s did not the change the temperatures appreciably, $\Delta\tau$ = 300 s and Δr = 0.05 m were used to calculate all of the final temperature results (earth temperature rise above 285 K) using the Finite Difference method. The earth temperature results for $\Delta\tau$ = 600 s and 18000 s are compared in Appendix F.

Tables 11-13 and Figs. 38-40 show the one-dimensional temperature rise above 285 K (ΔT_e) at different radii and times determined using the Finite Difference method for various radii and times when using $\Delta\tau$ = 300 s, Δr = 0.05 m, D_i = 0.2 m, D_o = 20 m, ρ = 2050 kg/m^3, C_p = 1840 J/kg-K, and k = 0.5, 2, and 4 W/m-K.

Table 11. Temperature rise (ΔT_e) distribution at different times for k = 0.5 W/m-K and D_i = 0.2 m (Finite Difference method).

r (m)	ΔT_e (K) at t = 2592000 s (30 days)	ΔT_e (K) at t = 5184000 s (60 days)	ΔT_e (K) at t = 7776000 s (90 days)	ΔT_e (K) at t = 10368000 s (120 days)
0.5	6.89	8.32	9.05	9.53
1	2.18	3.67	4.54	5.14
2	0.12	0.61	1.12	1.56
3	0.00	0.06	0.21	0.40
4	0.00	0.00	0.03	0.08
5	0.00	0.00	0.00	0.01
6	0.00	0.00	0.00	0.00
7	0.00	0.00	0.00	0.00
8	0.00	0.00	0.00	0.00
9	0.00	0.00	0.00	0.00
10	0.00	0.00	0.00	0.00

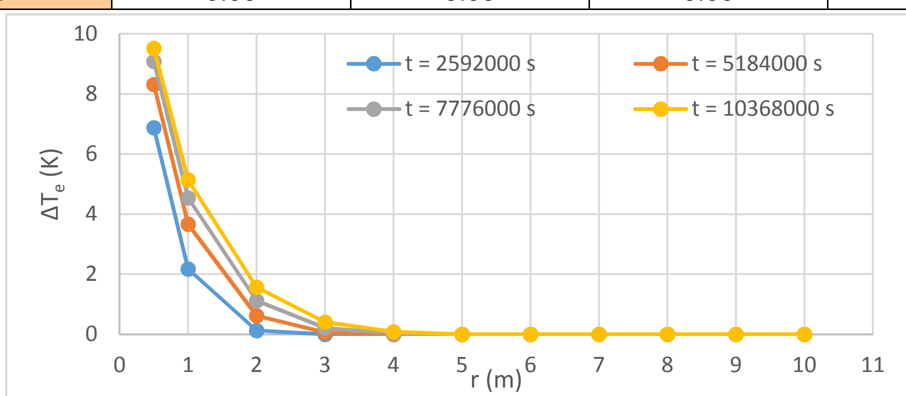

Figure 38. ΔT_e vs. radius at different times for k = 0.5 W/m-K and D_i = 0.2 m (Finite Difference method).

Table 12. Temperature rise (ΔT_e) distribution at different times for k = 2 W/m-K and D_i = 0.2 m (Finite Difference method).

r (m)	ΔT_e (K) at t = 2592000 s (30 days)	ΔT_e (K) at t = 5184000 s (60 days)	ΔT_e (K) at t = 7776000 s (90 days)	ΔT_e (K) at t = 10368000 s (120 days)
0.5	9.53	10.54	11.05	11.39
1	5.14	6.48	7.18	7.65
2	1.56	2.79	3.55	4.07
3	0.40	1.17	1.77	2.25
4	0.08	0.44	0.85	1.21
5	0.01	0.15	0.38	0.62
6	0.00	0.04	0.15	0.30
7	0.00	0.01	0.06	0.14
8	0.00	0.00	0.02	0.06
9	0.00	0.00	0.00	0.02
10	0.00	0.00	0.00	0.00

It can be noted from Tables 11 and 12 that ΔT_e values at all radii when k = 0.5 W/m-K, t = 10368000 s (Table 11), are exactly the same as those of k = 2 W/m-K (Table 12), t = 2592000 s. This is because $T_e(r,\tau)$ depends on α and τ, as only the product of the two (see Eq. (B-3)). Therefore, when τ is halved and α is doubled, the value of $T_e(r,\tau)$ will be exactly the same. Similarly from Tables 12 and 13, ΔT_e values at all radii when k = 2 W/m-K, t = 5184000 s and t = 10368000 s, are exactly the same as those of k = 4 W/m-K, t = 2592000 s and t = 5184000 s, respectively.

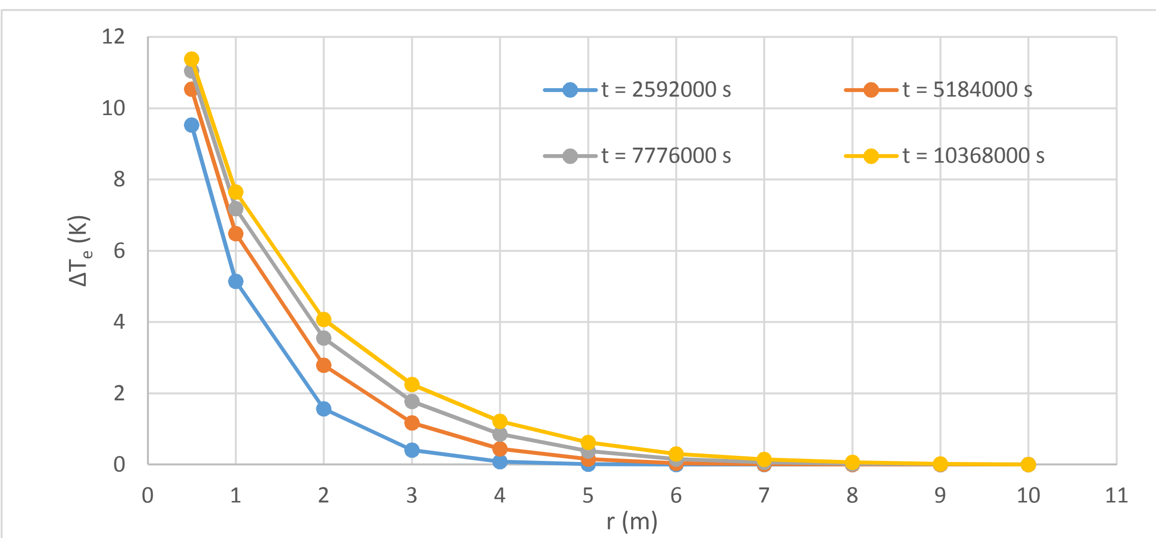

Figure 39. ΔT_e vs. radius at different times for k = 2 W/m-K and D_i = 0.2 m (Finite Difference method)

Table 13. Temperature rise (ΔT_e) distribution at different times for k = 4 W/m-K and D_i = 0.2 m (Finite Difference method).

r (m)	ΔT_e (K) at t = 2592000 s (30 days)	ΔT_e (K) at t = 5184000 s (60 days)	ΔT_e (K) at t = 7776000 s (90 days)	ΔT_e (K) at t = 10368000 s (120 days)
0.5	10.54	11.39	11.82	12.10
1	6.48	7.65	8.26	8.66
2	2.79	4.07	4.79	5.28
3	1.17	2.25	2.93	3.43
4	0.44	1.21	1.79	2.24
5	0.15	0.62	1.07	1.45
6	0.04	0.30	0.62	0.91
7	0.01	0.14	0.34	0.55
8	0.00	0.06	0.17	0.31
9	0.00	0.02	0.07	0.13
10	0.00	0.00	0.00	0.00

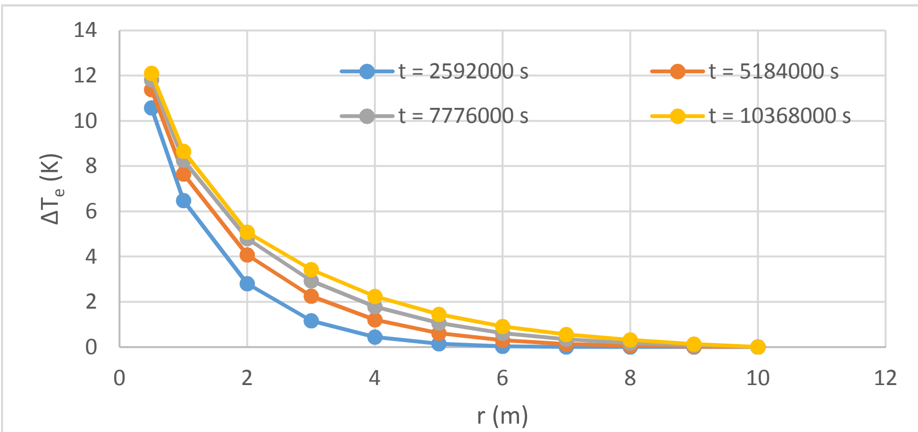

Figure 40. ΔT_e vs. radius at different times for k = 4 W/m-K and D_i = 0.2 m (Finite Difference method)

As can be seen from Figs. 38-40, initial earth temperature remained unchanged within an error of approximately 0.08 K (max) at 4 m for k = 0.5 W/m-K, 0.06 K (max) at 8 m for k = 2 W/m-K, and 0.13 K (max) at 9 m for k = 4 W/m-K. The large radii results (4 m, 8 m, and 9 m) obtained from Finite Difference results are reasonable when compared with those of the closed form solution. Differences between the two methods are computed and discussed in Section 4.3. These temperature distribution results are mainly useful for determining the minimum spacing that is needed between the bore holes.

4.3 Comparing Closed Form and Finite Difference Solutions

After solving the transient heat transfer problem in cylindrical coordinates using both the closed form (Tables 8-10) and Finite Difference (Tables 11-13) methods, the results were compared. Tables 14-16 show the differences between temperatures found using the two different methods for k = 0.5 W/m-K, 2 W/m-K, and 4 W/m-K, respectively. DT_e is the difference between the closed form solution and Finite Difference method temperatures

$$DT_e = T_{e\,(\text{Finite Difference method})} - T_{e\,(\text{closed form solution})} \tag{4-1}$$

Table 14. Difference between closed form solution and Finite Difference method temperatures at different times for k = 0.5 W/m-K and D_i = 0.2 m.

r (m)	DT_e (K) at t = 2592000 s (30 days)	DT_e (K) at t = 5184000 s (60 days)	DT_e (K) at t = 7776000 s (90 days)	DT_e (K) at t = 10368000 s (120 days)
0.5	0.47	0.47	0.47	0.47
1	-0.11	-0.10	-0.10	-0.10
2	-0.01	-0.01	-0.01	-0.01
3	0.01	0.01	0.01	0.02
4	0.02	0.02	0.02	0.02
5	0.03	0.03	0.03	0.03
6	0.03	0.03	0.03	0.03
7	0.02	0.02	0.02	0.02
8	0.01	0.01	0.01	0.01
9	0.01	0.01	0.01	0.01
10	0.00	0.00	0.00	0.00

Table 15. Difference between closed form solution and Finite Difference method temperatures at different times for k = 2 W/m-K and D_i = 0.2 m.

r (m)	DT_e (K) at t = 2592000 s (30 days)	DT_e (K) at t = 5184000 s (60 days)	DT_e (K) at t = 7776000 s (90 days)	DT_e (K) at t = 10368000 s (120 days)
0.5	0.47	0.47	0.47	0.47
1	-0.10	-0.10	-0.10	-0.10
2	-0.01	0.00	0.00	0.00
3	0.02	0.02	0.02	0.02
4	0.02	0.03	0.03	0.03
5	0.03	0.03	0.03	0.03
6	0.03	0.03	0.03	0.03
7	0.02	0.02	0.02	0.02
8	0.01	0.01	0.01	0.02
9	0.01	0.01	0.01	0.01
10	0.00	0.00	0.00	0.00

Table 16. Difference between closed form solution and Finite Difference method temperatures at different times for k = 4 W/m-K and D_i = 0.2 m.

r (m)	DT_e (K) at t = 2592000 s (30 days)	DT_e (K) at t = 5184000 s (60 days)	DT_e (K) at t = 7776000 s (90 days)	DT_e (K) at t = 10368000 s (120 days)
0.5	0.47	0.47	0.47	0.47
1	-0.10	-0.10	-0.10	-0.10
2	0.00	0.00	0.00	0.00
3	0.02	0.02	0.02	0.02
4	0.03	0.03	0.03	0.03
5	0.03	0.03	0.03	0.03
6	0.03	0.03	0.03	0.03
7	0.02	0.02	0.02	0.02
8	0.01	0.02	0.02	0.02
9	0.01	0.01	0.01	0.01
10	0.00	0.00	0.00	0.00

From Tables 14-16, it can be seen that the differences between the closed form solution and Finite Difference method temperatures are approximately 0.47 K at smaller radii, and the difference decreases with increasing radius. Also, it can be seen that the differences remain about the same for any given radius irrespective of time and thermal conductivity. The differences between temperatures at different radii varied from a minimum of zero to a maximum of 0.47 K. The results from the Finite Difference method were also compared with the results from ANSYS-CFX and are shown in Appendix D. For example, for k = 0.52 W/m-K and r = 0.3 m, the maximum difference observed was 0.57 K at t = 2592000 s (see App. D). The differences between the temperatures calculated by ANSYS CFX and Finite Difference methods are reasonable, but it is unknown as to whether these differences increase, decrease or remain the same as k increases.

4.4 CFD Results from ANSYS-CFX

A number of runs were conducted using ANSYS-CFX for various values of input parameters such as inlet velocity, thermal conductivity of the earth, roughness at the interface of the water and earth domains, inner tube diameter, bore hole depth, and operational time. Values for input parameters are clearly shown for each individual run.

First, as discussed in Section 3.2.1, a 3.6^o wedge was modeled instead of the full 360^o in order to reduce the simulation run time by approximately 30 times while reducing the number of nodes by a factor of 100. This 3.6^o wedge model for the earth and water domains was first created (one pipe going straight down, without any U-Tubes) and assembled using SolidWorks. Steps involved in creating the model are discussed in Appendix E. Then, the 3.6^o wedge model was imported into ANSYS-CFX for executing the simulations, as described in Section 3.2.3.1.

Simulations were also conducted on the complete 360^o cylindrical model for a U-tube having a range of the input variable values. This was done in order to determine the number of bore holes required to reach target exit temperature for different simulation times. Conducting simulations on the 3.6^o wedge, before simulating the actual 360^o cylindrical model with U-tube, helped in determining the approximate mass flow rate of the water required to achieve a 10 ^{o}C water temperature drop from the inlet to the exit. 10 ^{o}C was the cooling water temperature change assumed to be needed for the condenser of a power plant [8].

4.4.1 Initial Conditions

As discussed in Section 2.4, across the U.S., earth temperature beyond a depth of 10 m remains relatively constant, ranging from 10 ^{o}C to 16 ^{o}C [15] depending on the location and the soil type. Considering this fact, the initial temperature of the earth was chosen to be in the middle of that range, at 12 ^{o}C (285 K), for all runs.

4.4.2 Boundary Conditions

4.4.2.1 Inlet Temperature of Water

In the ground loop cooling method, the warm cooling water exiting the condenser will be sent to the ground loop system to be cooled. Since the temperature of the cooling water exiting a typical power plant's condenser is approximately 32.1 ^{o}C, an inlet ground loop temperature of T_{in} = 305.1 K was used for all runs [6]. Since many of the cooling systems of a thermal power plant operate with a cooling water temperature change of approximately 10 ^{o}C [6], the target bore hole exit water temperature was chosen to be 295 K. Various runs were performed by changing other boundary conditions (e.g., inlet water velocity) until the temperature at the bore hole exit was less than or equal to the target of 295 K when t = 10368000 s (4 months).

4.4.2.2 Wall Temperature

A temperature of 285 K (T_o), equal to the initial temperature of the earth, was given to the outer boundary of the cylinder at radius r_o. Since all of the results from the one-dimensional transient problem indicated that the initial temperature of the earth at radii greater than 9 m was not affected, a larger value of r_o, equal to 10 m, was chosen for the undisturbed outer radius of the

CFX model. Using the previously discussed boundary and initial conditions (Eqs. (3-2)-(3-4)), different runs were conducted; and the results obtained are discussed in Sections 4.4.3- 4.4.10.

4.4.2.3 Thermal Conductivity

As discussed in Section 2.4.2, thermal conductivity of the earth ranges from 0.5 W/m-K to over 5 W/m-K. Considering this variability in thermal conductivity of the earth, several runs were conducted using different values of k; and the results were analyzed and compared

4.4.3 ANSYS-CFX Runs on 3.6º Wedge with $D_i = 0.2$ m

Figure 41 shows the 3.6º wedge model used to conduct the simulations using ANSYS-CFX. Warm cooling water exiting the condenser is sent into the bore hole inlet (left side of Fig. 41). While transferring heat to the earth domain, this warm cooling water reduces in temperature and exits the bore hole at a lower temperature than at the inlet. Runs were conducted at different mass flow rates ($\dot{m}$) and inner radii (r_i) of the tube until water at the bore hole exit was 10º C cooler than at the inlet at all of the times with a maximum time of 10368000 s (4 months). The final mass flow rate was used as an approximate value for the follow-on runs conducted with the 360º cylindrical model having the U-tube (Sections 4.4.7 and 4.4.8).

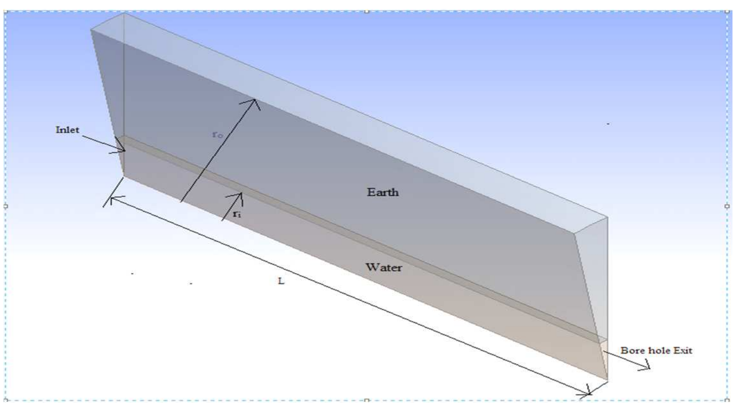

Figure 41. Scale model of 3.6º wedge of the water and earth domains used to conduct the simulations.

Table 17 shows thermal properties given to the earth domain and the dimensions used in designing the 3.6º wedge for the runs conducted with an inner diameter of the tube equal to 0.2 m.

Table 17. Common input values for the runs conducted on the 3.6º wedge with D_i = 0.2 m.

r_i (m)	r_o (m)	L (m)
0.1	10	500
k (W/m-K)	C_p (J/kg-K)	ρ (kg/m^3)
0.52	1840	2050

For the Table 17 values of radii (r_i) and depth (L), a mesh file was created. Table 18 shows typical mesh statistics for the results presented in Sections 4.4.3.1- 4.4.3.8.

Table 18. Mesh statistics for 3.6^o wedge with D_i = 0.2 m and L = 500 m.

Domain	Nodes	Elements
Earth	255102	125000
Water	280112	205000

Runs were conducted for different values of inlet velocity while keeping the input values from Table 17 and Table 19 (boundary conditions) unchanged. The results, such as the earth's temperature distribution and bore hole exit water temperatures, were calculated for different cases of inlet velocity and are discussed in Sections 4.4.3.1- 4.4.3.8.

Table 19. Common boundary conditions given to both domains (3.6^o wedge).

Boundaries			
Boundary - Default Fluid Solid Interface Side 1		Boundary - Default Fluid Solid Interface Side 2	
Type	INTERFACE	Type	INTERFACE
Location	F32.26	Location	F32.21
Heat Transfer	Conservative Interface Flux	Heat Transfer	Conservative Interface Flux
Boundary – Earth Symmetry		Mass and Momentum	No Slip Wall
Type	SYMMETRY	Wall Roughness (e)	Smooth Wall
Location	F28.26, F29.26	Boundary – Outlet	
Boundary - Earth Default		Type	OPENING
Type	WALL	Location	F22.21
Location	F30.26, F31.26	Flow Direction	Normal to Boundary Condition
Heat Transfer	Adiabatic	Flow Regime	Subsonic
Boundary - Wall Temperature		Heat Transfer	Opening Temperature
Type	WALL	Opening Temperature (T_{op})	2.850×10^2 [K]
Location	F27.26	Mass And Momentum	Opening Pressure and Direction
Settings		Turbulence	Medium Intensity and Eddy Viscosity Ratio
Heat Transfer	Fixed Temperature	Boundary - Water Symmetry	
Fixed Temperature	2.850×10^2 [K]	Type	SYMMETRY
		Location	F24.21, F25.21

4.4.3.1 Run 1 with V_{in} = 0.030510 m/s and t = 2592000 s (3.6° Wedge, r_i = 0.1 m)

With the common input values of Tables 17 and 19 and the input values given for the water domain at the inlet (see Table 20), a run was conducted for a total time of t = 2592000 s (1 month). For the initial runs, t = 2592000 s (1 month) was used as opposed to t = 10368000 s (4 months) (which took approximately 11 hours of computer simulation time), so as to reduce the computational time in determining the mass flow rates that can be used to achieve the target bore hole exit water temperature. The time steps were determined using the expression

$$\Delta\tau = 0.1 + [1-\exp(-0.00005000\,(\tau))]\,(3599.9)\ [\mathrm{s}] \qquad (4\text{-}2)$$

Results, including earth temperature distributions and bore hole exit water temperatures at different times, were produced using CFX-Post and are discussed in the following pages.

Table 20. Input values given at the inlet boundary of the water domain for Run 1.

Boundary – Inlet	
Type	INLET
Location	F23.21
Heat Transfer	Static Temperature
T_{in}	305.1 K
Mass And Momentum	Normal Speed
V_{in}	3.0510×10^{-2} m/s
Turbulence (I)	Medium Intensity and Eddy Viscosity Ratio (5%)
Wall Roughness (e)	0 m
Opening Temperature (T_{op})	285 K

The results were saved for all time steps. Area averaged water temperature (Eq. (4-3)) was plotted against depth along the bore hole at 10 different locations and is shown in Fig. 42. Area averaged water temperature at the outlet is the sum of the product of temperature and area of each water element at the outlet divided by the total area of the outlet.

$$T_{exit} = \text{“areaAve (Temperature)@Outlet”} \qquad (4\text{-}3)$$

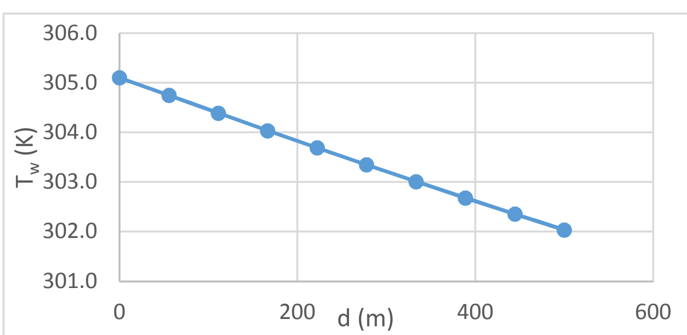

Figure 42. Water temperature vs. depth along the bore hole for t = 2592000 s and V_{in} = 0.030510 m/s (3.6° wedge, r_i = 0.1 m, L = 500 m).

The water temperature at t = 2592000 s for different locations along the bore hole decreased linearly due to the heat transfer to the earth (see Fig. 42). Since the water temperature at 500 m did not reduce by 10°C from the inlet at 0 m, to meet the target of 295 K, in the following runs, the inlet velocity was decreased for each run until the target temperature for water at the bore hole exit was achieved.

Table 21 shows the radial temperature rise distributions (ΔT_e) in the earth domain at different depths, where $\Delta T_e = T_e - 285$ [K].

Table 21. Earth temperature rise (ΔT_e) at different depths along the bore hole for V_{in} = 0.030510 m/s and t = 2592000 s (3.6° wedge, r_i = 0.1 m, L= 500 m).

	ΔT_e [K]					
r [m]	d = 0.1 m	d = 100 m	d = 200 m	d = 300 m	d = 400 m	d = 500 m
0.1	19.95	19.25	18.62	18.01	17.42	16.85
1.2	1.36	1.3	1.24	1.18	1.12	1.07
2.3	0.05	0.05	0.04	0.04	0.04	0.04
3.4	0	0	0	0	0	0
4.5	0	0	0	0	0	0
5.6	0	0	0	0	0	0
6.7	0	0	0	0	0	0
7.8	0	0	0	0	0	0

The initial temperature of the earth domain remained unchanged at a radius greater than approximately 2.3 m for all depths and at time equal to 2592000 s (see Figs. 43 and 44). Also, Fig. 44 shows that the earth temperature changes are smooth (consistent) both radially and along the depth of the bore hole indicating that the earth temperature distribution results shown in Fig. 43

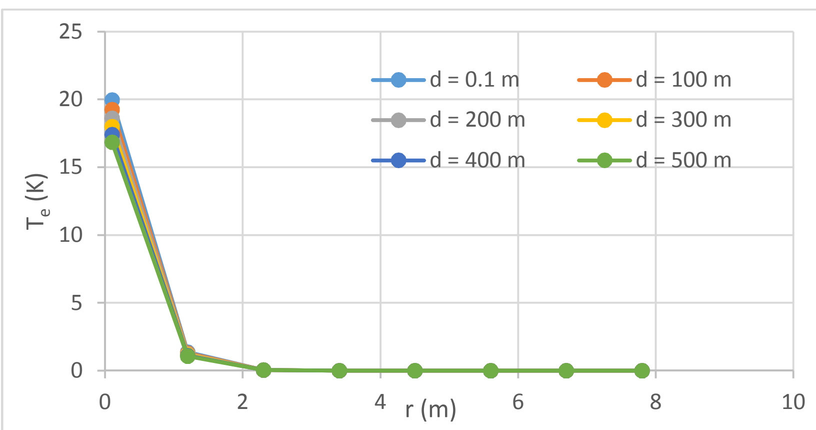

Figure 43. Earth temperature vs. radius at different depths along the bore hole for t = 2592000 s and V_{in} = 0.030510 m/s (3.6° wedge, r_i = 0.1 m, L = 500 m)

are representative of the results all along the bore hole. Although the bore hole exit water temperature did not hit the target of 295 K, a distance of 4.6 m (2 x 2.3 m) can be used as the minimum spacing that has to be provided between the bore holes if the inputs from Table 20 are used.

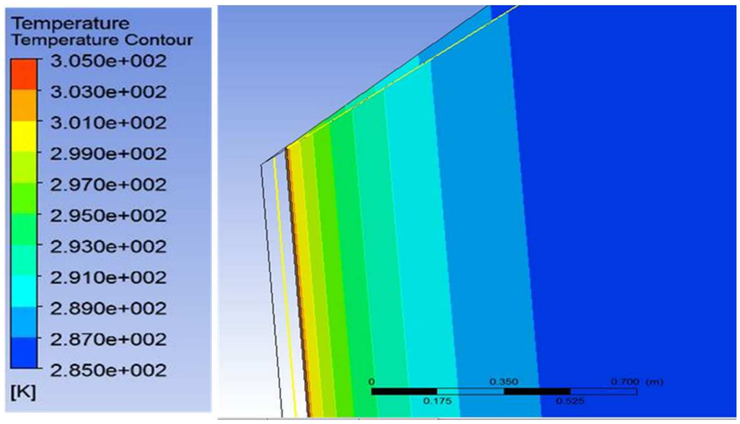

Figure 44. Temperature contours in the uppermost section of the vertical radially symmetric side of the earth domain for t = 2592000 s and V_{in} = 0.030510 m/s (3.6° wedge, r_i = 0.1 m, L = 500 m).

Area averaged bore hole exit water temperature was plotted against time to see the transient behavior of the heat rejected by warm cooling water to the earth domain (see Fig. 45).

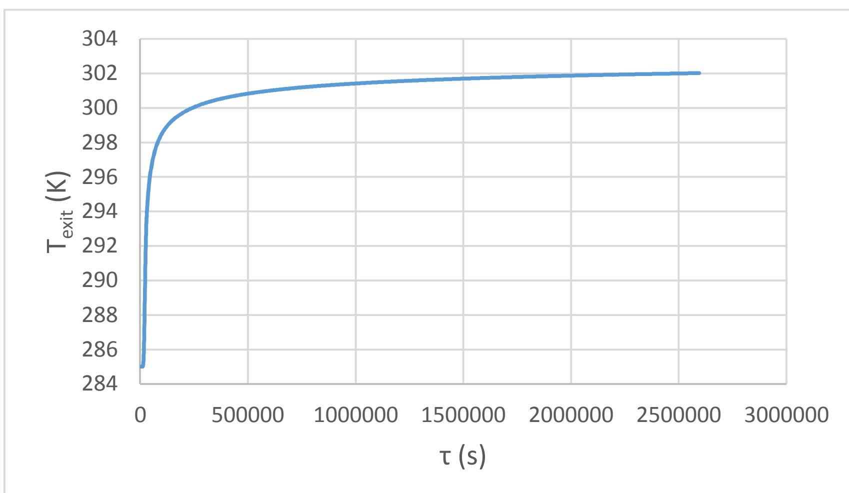

Figure 45. Bore hole exit water temperature vs. time for V_{in} = 0.030510 m/s (3.6° wedge, r_i = 0.1 m, L = 500 m).

As can be seen from Fig. 45, the water at the bore hole exit starts to be flatter at a relatively constant temperature after 500000 s (5.7 days). Taking into account the target exit temperature of 295 K required to maintain the cycle efficiency of the power plant at all times, further runs were conducted at reduced mass flow (inlet water velocity), and are discussed in the following sections. Results for all of the runs conducted are summarized in Section 4.4.6.

4.4.3.2 Run 2 with V_{in} = 0.01525 m/s and t = 2592000 s (3.6° Wedge, r_i = 0.1 m)

Run 2 was conducted with V_{in} = 0.01525 m/s while keeping all of the other inputs the same as those of Run 1. Table 22 shows the input values of inlet velocity, inlet temperature and other parameters given for the water domain of Run 2. The results were extracted using CFX-post and are discussed in the following pages.

Table 22. Input values given at the inlet boundary of the water domain for Run 2.

Boundary – Inlet	
Type	INLET
Location	F23.21
Flow Regime	Subsonic
Heat Transfer	Static Temperature
T_{in}	305.1 K
Mass And Momentum	Normal Speed
V_{in}	1.525×10^{-2} m/s
Turbulence (I)	Medium Intensity and Eddy Viscosity Ratio (5%)
Roughness (e)	0 m
Opening Temperature (T_{op})	285 K

With the input values for the water domain at the inlet (see Table 22), and the common settings (see Tables 17 and 19), a run was conducted for total time of t = 2592000 s (1 month). The time steps were determined using Eq. (4-2).

Radial temperature rise distributions ($\Delta T_e = T_e - 285$ [K]) in the earth domain for different depths at t = 2592000 s were extracted by CFX-post, and the results are shown in Table 23.

Table 23. Earth temperature rise (ΔT_e) at different depths along the bore hole for t = 2592000 s and V_{in} = 0.01525 m/s (3.6° wedge, r_i = 0.1 m, L = 500 m).

	ΔT_e [K]					
r [m]	d =0.1 m	d = 100 m	d = 200 m	d = 300 m	d = 400 m	d = 500 m
0.1	19.92	18.45	17.27	16.16	15.11	14.12
1.2	1.35	1.22	1.11	1.01	0.92	0.84
2.3	0.05	0.04	0.04	0.03	0.03	0.03
3.4	0	0	0	0	0	0
4.5	0	0	0	0	0	0
5.6	0	0	0	0	0	0
6.7	0	0	0	0	0	0
7.8	0	0	0	0	0	0
8.9	0	0	0	0	0	0

As can be seen from Figs. 46 and 47, and Table 23, for all depths along the bore hole, the initial temperature of the earth remained relatively unchanged at radii greater than approximately 2.3 m. Although the bore hole exit water temperature did not hit the target of 295 K, if the inlet velocity of 0.01525 m/s (Run 2) is used, a distance of 4.6 m (2 x 2.3 m) can be used as the minimum spacing that has to be provided between the boreholes. Also, Fig. 47 shows that the earth temperature changes are smooth (consistent) both radially and along the depth of the bore hole indicating that the earth temperature distribution results shown in Fig. 46 are representative of the results all along the bore hole.

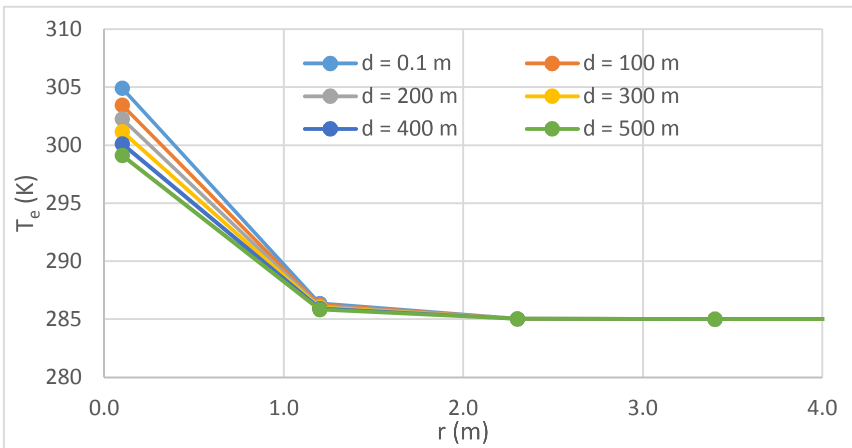

Figure 46. Earth temperature vs. radius at different depths along the bore hole for $t = 2592000$ s and $V_{in} = 0.01525$ m/s (3.6° wedge, $r_i = 0.1$ m, $L = 500$ m).

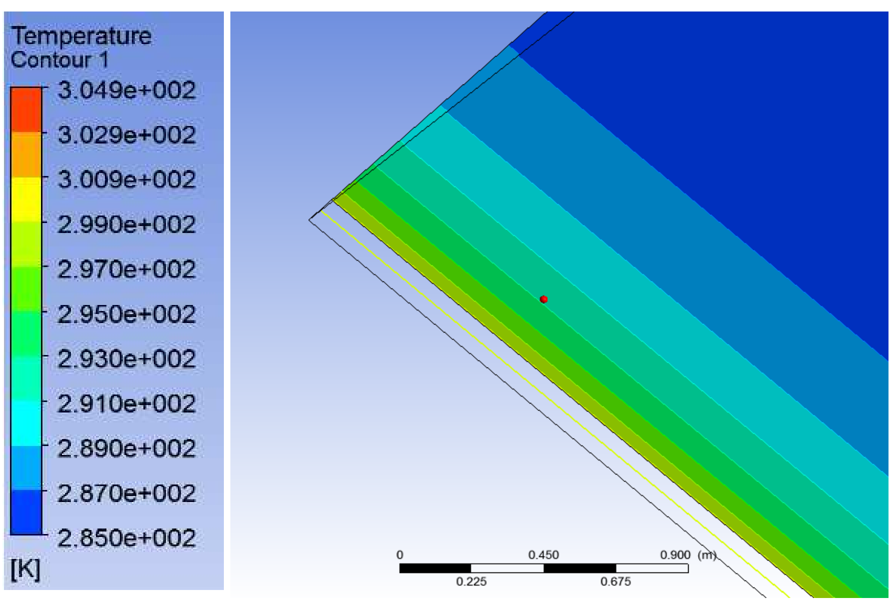

Figure 47. Temperature contours in the uppermost section of the vertical radially symmetric side of the earth domain for $V_{in} = 0.01525$ m/s and $t = 2592000$ s (3.6° wedge, $r_i = 0.1$ m, $L = 500$ m).

Figure 48 was plotted to see if, at any depth, the area averaged bore hole exit water temperature at t = 10368000 s (4 months) reached the bore hole exit water temperature of 295 K.

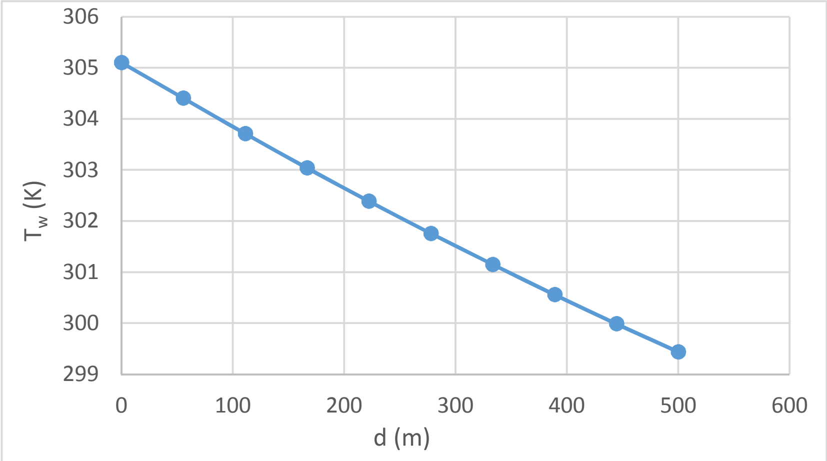

Figure 48. Water temperature vs. depth along the bore hole for t = 2592000 s and V_{in} = 0.01525 m/s (3.6° wedge, r_i = 0.1 m, L = 500 m).

As can be seen from Fig. 48, for Run 2, at V_{in} = 0.01525 m/s, the temperature of water at a depth of 500 m was lower than for Run 1, decreasing by 2.5 °C.

Figure 49 shows the area averaged bore hole exit water temperature at different times for a maximum time of 2592000 s. Although the bore hole exit water temperature at the maximum time decreased by 2.5° C from Run 1, the target temperature of 295 K was not achieved at this flow rate for any times greater than approximately 100000 s. A new run was conducted by further decreasing the mass flow rate in order to achieve the target bore hole exit water temperature, and the results are discussed in Sections 4.4.3.3.

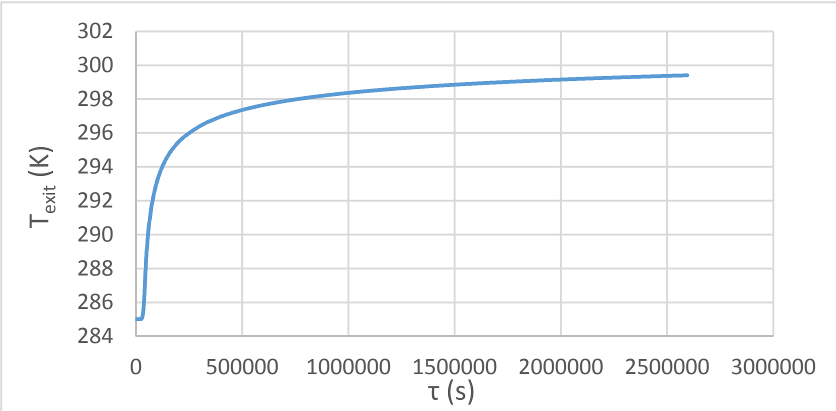

Figure 49. Bore hole exit water temperature vs. time for V_{in} = 0.01525 m/s (3.6° wedge, r_i = 0.1 m, L = 500 m).

4.4.3.3 Run 3 with V_{in} = 0.00621 m/s and t = 2592000 s (3.6º Wedge, r_i = 0.1 m)

Run 3 was conducted with V_{in} = 0.00621 m/s while keeping all of the other inputs the same as those of Run 1. Table 24 shows the input values of inlet velocity, inlet temperature and other parameters given for the water domain of Run 3. Different results were them extracted using CFX-post and are discussed in the following pages.

Table 24. Input values given at the inlet boundary of the water domain for Run 3.

Boundary – Inlet	
Type	INLET
Location	F23.21
Heat Transfer	Static Temperature
T_{in}	305.1 K
Mass And Momentum	Normal Speed
V_{in}	6.210×10^{-3} m/s
Turbulence (I)	Medium Intensity and Eddy Viscosity Ratio (5%)
Wall roughness (e)	0 (m)
Opening Temperature (T_{op})	285 K

This run was conducted for a total time of t = 2592000 s (1 month). The time steps were determined using Eq. (4-2).

Results were then extracted using CFX-Post and are presented in Table 25 and Figs. 50-53. To determine the minimum spacing needed between the bore holes, radial temperature rise distributions at different depths along the bore hole were produced by CFX-Post. Table 25 shows the radial temperature rise distributions ($\Delta T_e = T_e - 285$ [K]) at different depths along the bore hole for t = 2592000 s.

Table 25. Earth temperature rise (ΔT_e) at different depths along the bore hole for t = 2592000 s and V_{in} = 0.00621 m/s (3.6º wedge, r_i = 0.1 m, L = 500 m).

	ΔT_e [K]					
r [m]	d = 0.1 m	d = 100 m	d = 200 m	d = 300 m	d = 400 m	d = 500 m
0.1	19.78	16	14	12	10	8
1.2	1.33	1	1	1	1	0
2.3	0.05	0	0	0	0	0
3.4	0	0	0	0	0	0
4.5	0	0	0	0	0	0
5.6	0	0	0	0	0	0
6.7	0	0	0	0	0	0
7.8	0	0	0	0	0	0
8.9	0	0	0	0	0	0

It can be seen from Table 25 that most of the ΔT_e values are rounded numbers without decimal digits. This is due to an error made in exporting the results from CFX-post. Therefore, Table 25 values have possible errors of ± 1.0 K; and the values could not be corrected due to the inaccessibility of ANSYS-CFX software while revising this thesis.

As can be seen from Figs. 50 and 51, and Table 25, at any depth along the bore hole, the initial earth temperature remained essentially unchanged at a radius greater than approximately 2.3 m. So, for an inlet velocity of 0.00621 m/s (Run 3), a distance of 4.6 m (2 x 2.3 m) can be used as the minimum spacing needed between the bore holes. Also, Fig. 51 shows that the earth temperature changes are smooth (consistent) both radially and along the depth of the bore hole indicating that the earth temperature distribution results shown in Fig. 50 are representative of the results all along the bore hole

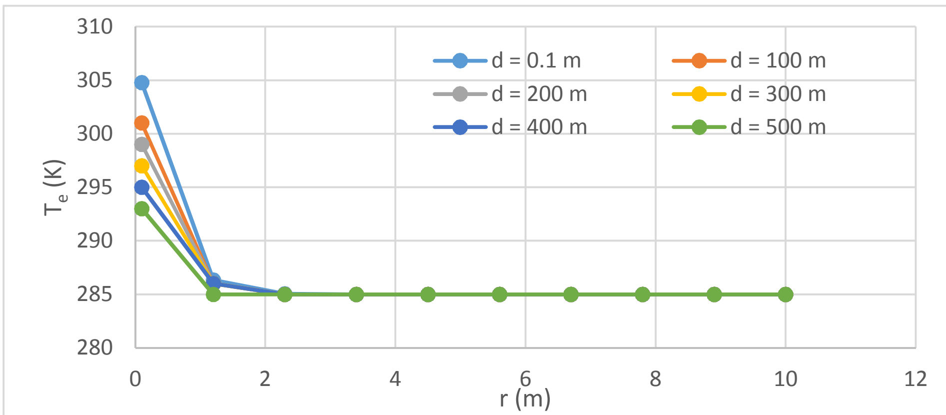

Figure 50. Earth temperature vs. radius at different depths along the bore hole for t = 2592000 s and V_{in} = 0.00621 m/s (3.6^o wedge, r_i = 0.1 m, L = 500 m).

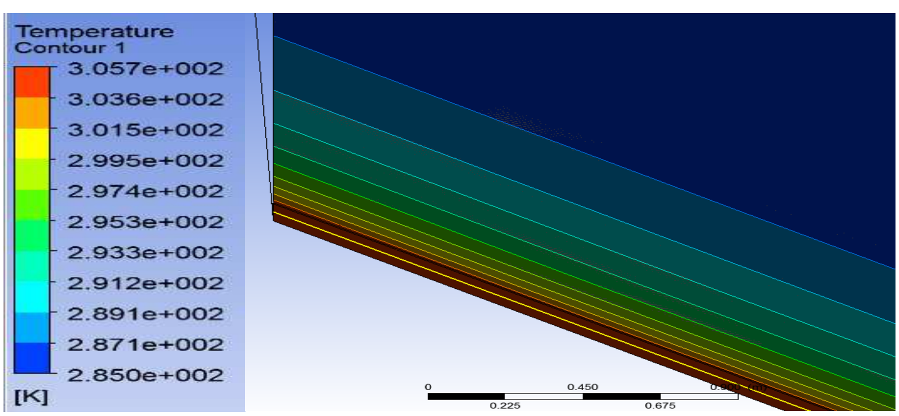

Figure 51. Temperature contours in the uppermost section of the vertical radially symmetric sides of the earth and water domains at t = 2592000 s and V_{in} = 0.00621 m/s (3.6^o wedge, r_i = 0.1 m, L = 500 m).

Figure 52 shows the area averaged water temperature at different depths along the bore hole for time equal to 2592000 s. It can be seen that, at depths between 389 m and 444 m, area averaged water temperature dropped below the required target temperature of 295 K.

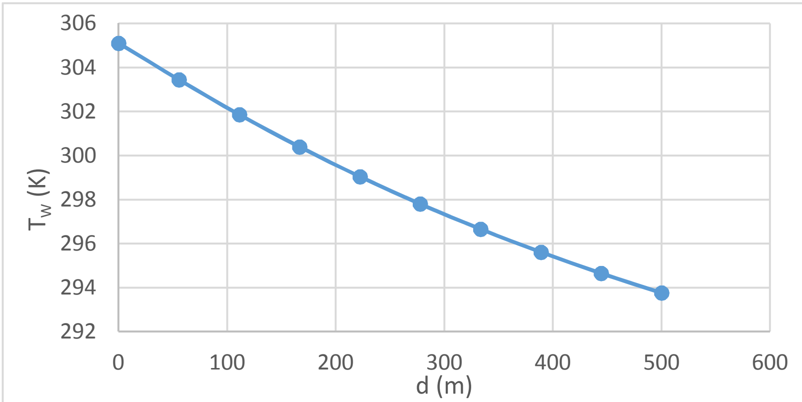

Figure 52. Water temperature vs. depth along the bore hole for t = 2592000 s and V_{in} = 0.00621 m/s (3.6^o wedge, r_i = 0.1 m, L = 500 m).

Figure 53 shows the area averaged bore hole exit water temperature plotted against time for a maximum time of 2592000 s.

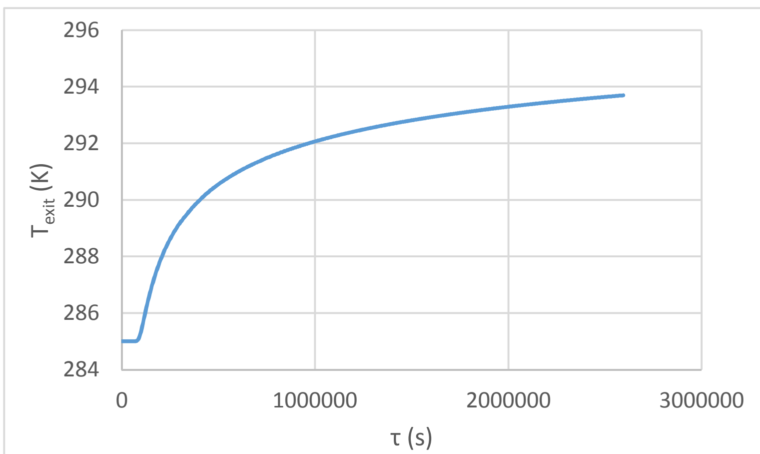

Figure 53. Bore hole exit water temperature vs. time for V_{in} = 0.00621 m/s (3.6^o wedge, r_i = 0.1 m, L= 500 m).

As can be seen from Fig. 53, bore hole exit water temperature remained below the target temperature of 295 K at all of the intermediate times, for a maximum time of 2592000 s. The bore hole exit water temperature will be less than 295 K during the initial times as shown in Fig. 53. These low temperatures during the initial times will have a positive effect on the cycle thermal efficiency of the power plant. Further discussion of the effects of these low temperatures [during initial times] on the thermal efficiency of the power plant is provided in Section 4.4.11.

Since the approximate value of water inlet velocity needed to reach the target bore hole exit temperature of 295 K was determined to be 0.00621 m/s, a few more runs were conducted at the same inlet velocity by changing the turbulence intensity options, roughness, and opening temperature to see how they affected the exit temperature of the water. Results for these changes are discussed in Sections 4.4.3.4 - 4.4.3.6.

4.4.3.4 Run 4 with V_{in} = 0.00621 m/s and t = 2592000 s (Changing I)

This section shows the results obtained when changing the turbulence intensity (I) of the flow. Table 26 shows the input values of inlet velocity, inlet temperature and other parameters given for the water domain of Run 4.

Table 26. Input values given at the inlet boundary of the water domain for Run 4.

Boundary – Inlet	
Type	INLET
Location	F23.21
Heat Transfer	Static Temperature
T_{in}	305.1 K
Mass And Momentum	Normal Speed
V_{in}	6.210×10^{-3} m/s
Turbulence (I)	High Intensity and Eddy Viscosity Ratio (10 %)
Wall Roughness (e)	0 m
Opening Temperature (T_{op})	285 K

Table 26 shows that the turbulence option was changed to high intensity (10 %) as compared to the previous runs, where the turbulence model was of medium intensity (5 %).

The bore hole exit water temperature was computed and compared to the bore hole exit water temperature from Run 3 at a maximum time of 2592000 s (1 month). This was done to see if changing the turbulence option affected the heat transfer from the water to the earth domain. The bore hole exit water temperature was computed by using Eq. (4-3) under the calculator tab on CFX-Post. Area averaged water temperature at the outlet (bore hole exit water temperature) is the sum of the product of temperature and area of each water element at the outlet divided by the total area of the outlet. Table 27 shows the bore hole exit water temperature for the runs using the two different turbulence options.

Table 27. Bore hole exit water temperature for two different turbulence options.

Turbulence (I)	Medium Intensity (5 %)	High intensity (10 %)
T_{exit} (K)	293.695	293.695

The area averaged bore hole exit water temperatures for both turbulence options remained the same (see Table 27). So, for all of the following runs, while changing the other inputs, the turbulence intensity option was kept constant and equal to medium intensity (5 %).

4.4.3.5 Run 5 with V_{in} = 0.00621 m/s and t = 2592000 s (Changing T_{op})

For Run 5, while keeping all of the other inputs the same as those of Run 3, the value of opening temperature at the exit was changed to 295 K as compared to the 285 K used for all previous runs. Opening boundary condition is different from the inlet and the outlet boundary conditions since it allows flow in both the directions as compared to flow only in one direction (inlet or outlet) [23]. When the flow direction is into the domain, the pressure value is taken to be total pressure based on the normal component of the velocity. When flow is leaving the domain, the pressure value is taken to be relative static pressure. In this case, since the flow was leaving the domain, the relative pressure was taken to be 0.5 Pa normal to the outlet boundary. Since our problem was transient, assuming that the flow direction at the bore hole exit while solving the problem would change and flow occurred into the water domain, the opening temperature [temperature of the inflow (if any)] was given two different values of 285 K and 295 K in order to analyze the effect of T_{op} on the bore hole exit water temperature.

The bore hole exit water temperature was computed using Eq. (4-3), and compared with the bore hole exit water temperature from Run 3 at a time equal to 2592000 s. This was done to see if changing the opening temperature at the outlet affected the heat transfer from the warm cooling water to the earth domain. As can be seen from Table 28, bore hole exit water temperature did not change due to the change in the opening temperature at the outlet. Considering the results from this run, it was clear that there was no inflow into the domain at the bore hole exit. If there were flow into the water domain, the bore hole exit water temperature should be different for the two different opening temperatures. Therefore, the opening temperature was kept constant and equal to 285 K for all of the following runs.

Table 28. Bore hole exit water temperature for two different opening temperatures at the outlet.

T_{op} (K)	285	295
T_{exit} (K)	293.695	293.695

4.4.3.6 Runs 6 and 7 with V_{in} = 0.00621 m/s and t = 2592000 s (Changing e)

Runs 6 and 7 were conducted by changing the wall surface roughness at the water and earth domain interface, as compared to using a smooth surface as in Run 3. The bore hole exit water temperature was computed and compared to the exit temperature from Run 3. Table 29 shows that the exit temperature of the water changed very little with change in roughness at the interface. Since the change in temperature was so small, the effect of roughness on heat transfer across the interface was not considered, and all following runs were conducted considering a smooth surface (e = 0 m) at the interface.

Table 29. Bore hole exit water temperature for different surface roughnesses at the interface.

e (m)	0	0.005	0.05
T_{exit} (K)	293.695	293.695	293.652

4.4.3.7 Run 8 with V_{in} = 0.00621 m/s and t = 10368000 s (3.6º Wedge, r_i = 0.1 m)

After checking for the effect of turbulence, roughness and opening temperature at the outlet on the bore hole exit water temperature, Run 8 was conducted by changing the total time to 10368000 s (4 months), keeping all other inputs same as those for Run 3. Since this thesis was aimed at using ground loop cooling for the 4 summer months of the year [in mid-latitudes of the U.S.], the total time of the run was changed to 10368000 s (4 months). Table 30 shows the input values given for the water domain at the inlet for Run 8.

Table 30. Input values given at the inlet boundary of the water domain for Run 8.

Boundary – Inlet	
Type	INLET
Heat Transfer	Static Temperature
T_{in}	305.1 K
Mass And Momentum	Normal Speed
V_{in}	6.210×10^{-3} m/s
Turbulence (I)	Medium Intensity and Eddy Viscosity Ratio (5 %)
Wall Roughness (e)	0 m
Opening Temperature (T_{op})	285 K

With the input values given to the water domain at the inlet and the common input values of Tables 17 and 19, a run was conducted for a total time of t = 10368000 s (4 months), and the results are discussed in the following pages. The time steps were determined using Eq. (4-4). The maximum time step of Eq. (4-4) was changed from 3599.9 s (used in Eq. (4-2)) to 4199.9 s in order to reduce the computational time.

$$\Delta\tau = 0.1 + [1\text{-}\exp(-0.0000500\,(\tau))]\,(4199.9)\ [s] \tag{4-4}$$

To determine the minimum spacing needed between the bore holes, temperature distributions of the earth domain ($\Delta T_e = T_e - 285$ [K]) at different depths along the bore hole were computed and are shown in Table 31.

Table 31. Earth temperature rise (ΔT_e) at different depths along the bore hole for t = 10368000 s and V_{in} = 0.00621 m/s (3.6^o wedge, r_i = 0.1 m, L = 500 m).

	ΔT_e [K]					
r [m]	d = 0.1 m	d = 100 m	d = 200 m	d = 300 m	d = 400 m	d = 500 m
0.1	19.85	17.09	15.02	13.18	11.56	10.13
1.2	4.02	3.43	2.96	2.54	2.19	1.88
2.3	1.08	0.9	0.76	0.65	0.54	0.46
3.4	0.23	0.19	0.16	0.13	0.11	0.09
4.5	0.04	0.03	0.02	0.02	0.02	0.01
5.6	0	0	0	0	0	0
6.7	0	0	0	0	0	0
7.8	0	0	0	0	0	0

Table 31 and Fig. 54 show that the initial earth temperature at any location along the depth of the bore hole and time equal to 10368000 s (4 months) does not change appreciably beyond a radius greater than approximately 4.5 m. Therefore, a distance of 9 m (2 x 4.5 m) can be used as the minimum spacing that is needed between the bore holes when using inputs from Table 30.

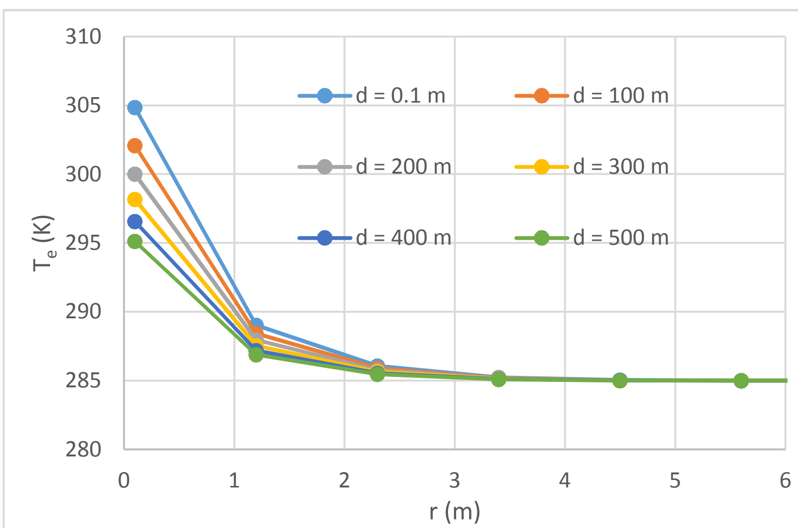

Figure 54. Earth temperature vs. radius at different depths along the bore hole for t = 10368000 s and V_{in} = 0.00621 m/s (3.6^o wedge, r_i = 0.1 m, L = 500 m)

Figure 55 shows the area averaged bore hole exit water temperature plotted against time. As can be seen from Fig. 55, bore hole exit water temperature remained below the target temperature of 295 K for about 7000000 s. After 7000000 s, the temperature did not rise much. At the end of 10368000 s (4 months), the temperature of the water at the exit was 295.52 K. Note that the earth temperature from Table 51 and Fig. 54 at d = 500 m and t = 10368000 s was 295.13 K, which is reasonable since the water is transferring heat to the earth.

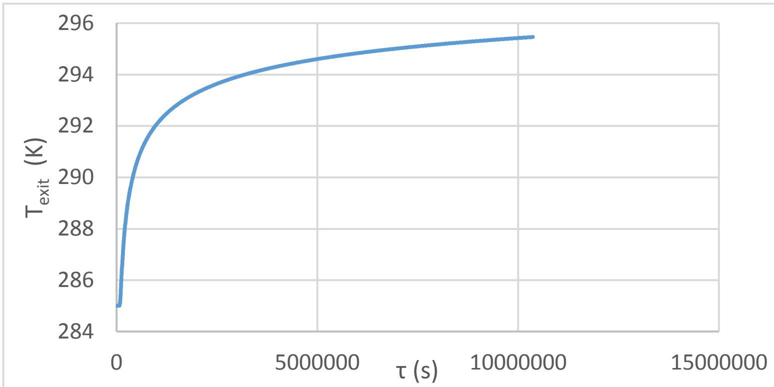

Figure 55. Bore hole exit water temperature vs. time for V_{in} = 0.00621 m/s (3.6° wedge, r_i = 0.1 m, L = 500 m).

Figure 56 shows the area averaged water temperature at different depths of the bore hole. Since the temperature of the water at depth 500 m was 295.52 K, which is fairly close to the required target temperature of 295 K (see Fig. 56), a few more runs were conducted by changing

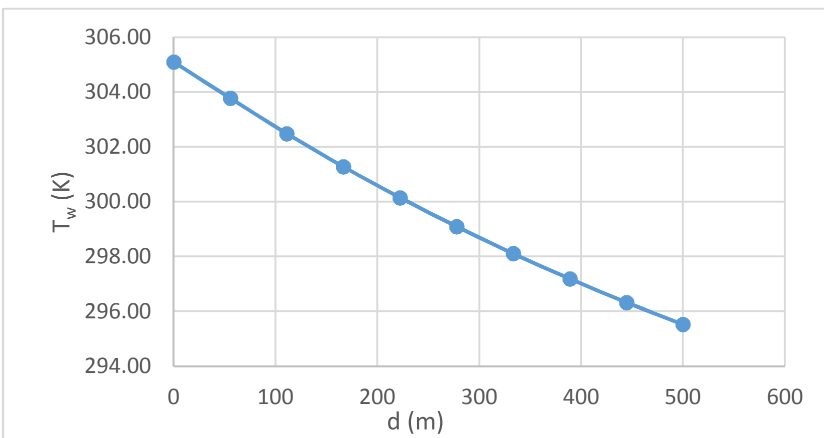

Figure 56. Water temperature vs. depth along the bore hole for t = 10368000 s and V_{in} = 0.00621 m/s (3.6° wedge, r_i = 0.1 m, L = 500 m).

the inlet velocity of water. This was done in order to produce an equation for bore hole exit water temperature (T_{exit}) as a function of inlet velocity of water (V_{in}). Although the results for all of the runs are not discussed in detail in this thesis, the bore hole exit water temperatures at time 10368000 s (4 months) for different inlet velocities are discussed in Section 4.4.3.8.

4.4.3.8 Exit Temperature Estimates for Different Inlet Velocities (D_i = 0.2 m)

Three more runs were conducted for different inlet velocities, keeping all of the other input parameters unchanged from Run 8. Using the values from Table 32, an equation for bore hole exit water temperature as a function of inlet velocity was determined.

$$T_{exit}\,[K] = (329.36\,\frac{s^{0.014}K}{m^{0.014}})\,(V_{in}^{0.014}) \tag{4-5}$$

Table 32. Bore hole exit water temperature for different inlet velocities for t = 10368000 s and D_i = 0.2 m.

V_{in} (m/s)	T_{exit} (K)
0.0078625	296.992
0.00698889	296.246
0.006621053	295.851
0.00621	295.520

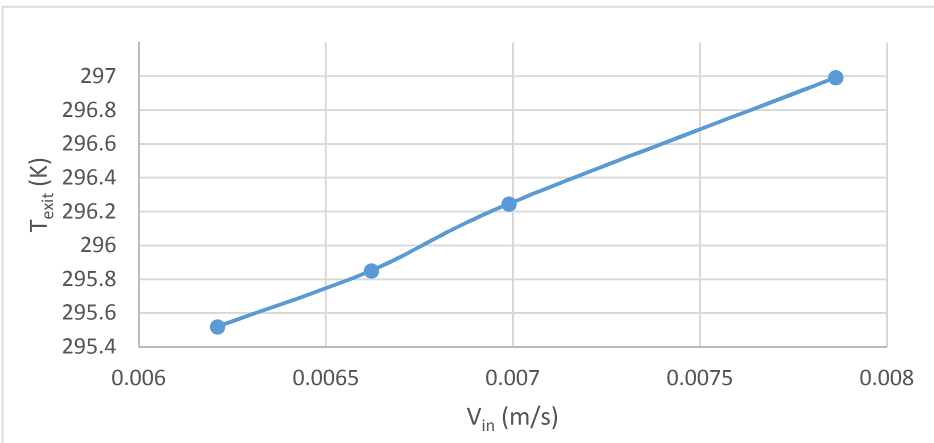

Figure 57. Bore hole exit water temperature vs. inlet velocity at t = 10368000 s for D_i = 0.2 m.

Equation (4-5) can be used to determine the bore hole exit water temperature for inlet velocities in the range of 0.00621 m/s to 0.078625 m/s and for the 3.6° wedge with D_i = 0.2 m. Since the 3.6° wedge models cannot be practically installed, because there is no riser (return pipe) for the warm cooling water to come up, Eq. (4-5) was not used to determine the water inlet velocity required to reach 295 K at the bore hole exit.

4.4.4 ANSYS-CFX Runs on 3.6° Wedge with D_i = 0.25 m

Runs were conducted by changing D_i from 0.2 m (Section 4.4.3) to 0.25m and 0.3 m (Section 4.4.5) to determine the effect of inner diameter on the temperature distribution in the earth and the bore hole exit water temperature. Table 33 shows thermal properties used for the earth domain and the dimensions used in designing the 3.6^o wedge for runs conducted when D_i = 0.25 m.

Table 33. Common input values for the runs conducted on the 3.6^o wedge with D_i = 0.25 m.

r_i (m)	r_o (m)	L (m)
0.125	6	500
k (W/m-K)	C_p (J/kg-K)	ρ (kg/m^3)
0.52	1840	2050

For the Table 33 values of radius and depth for the domains, a mesh file was created and different simulations were performed. Table 34 shows the common mesh statistics for the runs conducted on the 3.6^o wedge with D_i = 0.25 m.

Table 34. Mesh statistics for 3.6^o wedge with D_i = 0.25 m and L= 500 m.

Domain	Nodes	Elements
Earth	255102	125000
Water	307623	207500

Inputs from Table 33 and common input values of Table 19 were used to perform four runs at different inlet velocities. All of the runs were conducted for a total time of t = 10368000 s (4 months). The time steps were computed using Eq. (4-4). Detailed results for V_{in} = 0.00621 m/s are discussed in Section 4.4.4.1; and bore hole exit water temperatures for the four different water inlet velocities are discussed in Section 4.4.4.2.

4.4.4.1 Run 2-1 with V_{in} = 0.00621 m/s and t = 10368000 s (3.6^o Wedge, r_i = 0.125 m)

This section discusses the results when the inner diameter was changed from 0.2 m to 0.25 m, while keeping all other inputs the same as those of Run 3. Table 35 shows the input values given for the water domain at the inlet of Run 2-1.

Table 35. Input values given at the inlet boundary of the water domain for Run 2-1.

Boundary – Inlet	
Type	INLET
Location	F23.21
Heat Transfer	Static Temperature
T_{in}	305.1 K
Mass And Momentum	Normal Speed
V_{in}	6.210 x 10^{-3} m/s
Turbulence (I)	Medium Intensity and Eddy Viscosity Ratio (5 %)
Wall Roughness (e)	0 m
Opening Temperature T_{op}	285 K

With inputs to the water domain at the inlet (see Table 35) and common input values from Tables 19 and 33, a run was conducted for a total time of t = 10368000 s (4 months). Different results were then extracted using CFX-Post and are presented as follows.

Figure 58 shows the area averaged water temperature (see Eq. (4-3)) at different locations along the depth of the bore hole.

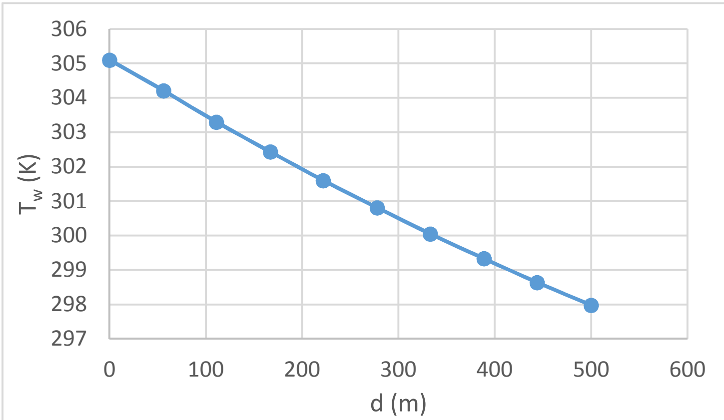

Figure 58. Water temperature vs. depth along the bore hole for t = 10368000 s and V_{in} = 0.00621 m/s (3.6° wedge, r_i = 0.125 m, L = 500 m).

As can be seen from Fig. 58, area averaged water temperature, for time equal to 10368000 s (4 months) at different locations along the bore hole, decreases with increasing depth and exits the bore hole at 297.98 K. Since the water temperature at d = 500 m (bore hole exit) and t = 10368000 s did not hit the target of 295 K, a few more runs were conducted using different inlet velocities, while keeping all of the other inputs the same as those of Run 2-1; and the results are discussed in Section 4.4.4.2. Figure 59 shows how the bore hole exit water temperature changes with time.

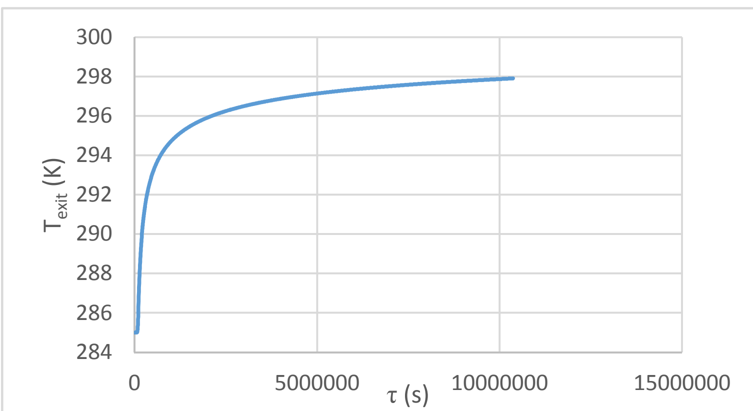

Figure 59. Bore hole exit water temperature vs. time for V_{in} = 0.00621 m/s (3.6° wedge, r_i = 0.125 m, L = 500 m).

Figure 59 shows that the water temperature at the bore hole exit becomes greater than 295 K for time greater than 13 days (1123200 s). Considering this fact, a few more runs at different flow rates were conducted in order to determine the exact inlet velocity at which the bore hole exit water temperature remained below or equal to 295 K for all times; and the results are shown in Section 4.4.4.2.

To determine the minimum spacing needed between the bore holes, radial temperature distributions (ΔT_e, where $\Delta T_e = T_e - 285$ [K]) at different locations along the bore hole depth were produced and are shown in Table 36.

Table 36. Earth temperature rise (ΔT_e) at different depths along the bore hole for t = 10368000 s and V_{in} = 0.00621 m/s (3.6^o wedge, r_i = 0.125 m, L = 500 m).

ΔT_e [K]						
r [m]	d = 0. 1 m	d = 100 m	d = 200 m	d = 300 m	d = 400 m	d = 500 m
0.1	19.88	17.87	16.37	14.98	13.71	12.54
0.8	7.17	6.43	5.84	5.3	4.8	4.35
1.4	3.39	3.02	2.72	2.45	2.2	1.98
2.1	1.57	1.39	1.24	1.1	0.98	0.88
2.7	0.67	0.59	0.52	0.46	0.4	0.36
3.4	0.26	0.23	0.2	0.17	0.15	0.13
4	0.09	0.08	0.07	0.06	0.05	0.05
4.7	0.03	0.03	0.02	0.02	0.02	0.01
5.3	0.01	0.01	0.01	0	0	0

As can be seen from Table 36 and Figs. 60 and 61, initial temperature of the earth remained unchanged at radii greater than approximately 4.7 m at a time equal to 10368000 s (4 months) and at any depth along the bore hole.

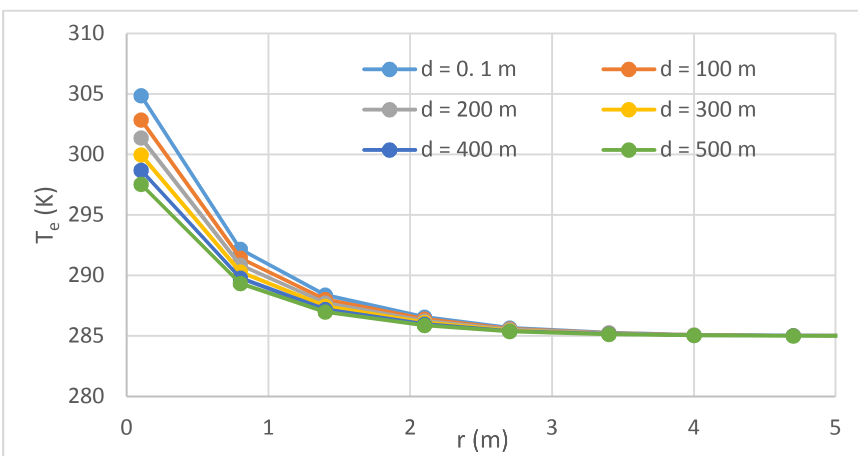

Figure 60. Earth temperature vs. radius at different depths along the bore hole for V_{in} = 0.00621 m/s and t = 10368000 s (3.6^o wedge, r_i = 0.125 m, L = 500 m).

Figure 61 shows the temperature contours for both the water and the earth domains near the inlet section for the maximum time of the simulation. Also, Fig. 61 shows that the earth temperature changes are smooth (consistent) both radially and along the depth of the bore hole indicating that the earth temperature distribution results shown in Fig. 60 are representative of the results all along the bore hole.

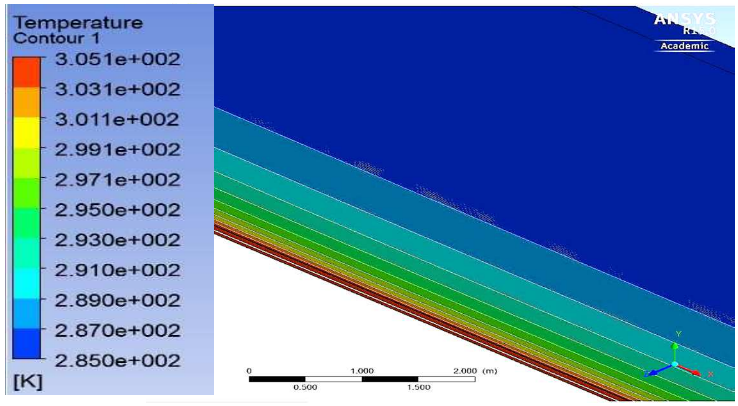

Figure 61. Temperature contours in the uppermost section of the vertical radially symmetric sides of the earth and water domains for t =10368000 s and V_{in} = 0.00621 m/s (3.6^o wedge, r_i = 0.125 m, L = 500 m).

Since the area averaged temperature at the bore hole exit was not equal to or below the required target temperature of 295 K, a few more runs were conducted with different inlet velocities, keeping the other parameters the same as they were in Run 2-1. Although the results for all of the runs are not discussed in detail, bore hole exit water temperatures were calculated for different inlet velocities and are discussed in Section 4.4.4.2.

4.4.4.2 Exit Temperature of Water for Different Inlet Velocities at 10368000 s (D_i = 0.25 m)

Table 37 shows the bore hole exit water temperature at total time equal to 10368000 s (4 months) for different inlet velocities when D_i = 0.25 m and k = 0.52 W/m-K.

Table 37. Bore hole exit water temperature at different inlet velocities for t = 10368000 s and D_i = 0.25 m.

V_{in} (m/s)	T_{exit} (K)
0.0041933	295.359
0.00449286	295.822
0.00571818	297.347
0.00621	297.980

Using the values from Table 37 and Fig. 62, an equation for the bore hole exit water temperature as a function of inlet velocity was produced.

$$T_{exit}\ [K] = \left(333.5\frac{s^{0.0222}K}{m^{0.0222}}\right)\left(V_{in}^{0.0222}\right) \quad (4\text{-}6)$$

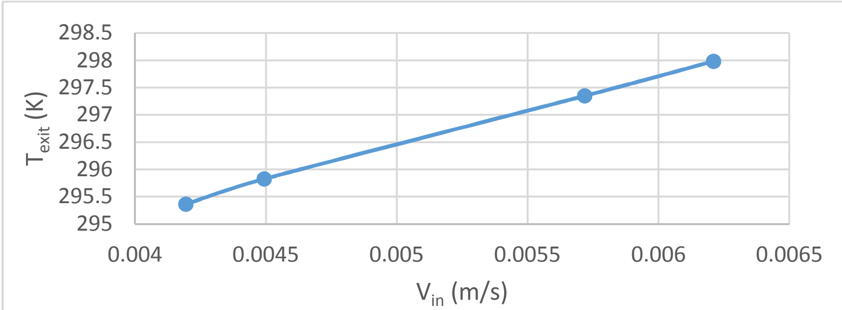

Figure 62. Bore hole exit water temperature vs. inlet velocity at t = 10368000 s for D_i = 0.25 m.

Equation (4-6) can be used to determine the bore hole exit water temperature at any inlet velocity in the range of 0.0041933 m/s to 0.00621 m/s, for the 3.6° wedge with D_i = 0.25 m and k = 0.52 W/m-K. Since the 3.6° wedge models cannot be practically installed, because there is no riser (return pipe) for the warm cooling water to come up, Eq. (4-6) was not used to determine the water inlet velocity required to reach 295 K at the bore hole exit.

4.4.5 ANSYS-CFX Runs on 3.6° Wedge with D_i = 0.3 m

Table 38 shows thermal properties given to the earth domain and the dimensions used in designing the 3.6° wedge for runs conducted with D_i = 0.3 m.

Table 38. Common input values for the runs conducted on the 3.6° wedge with D_i = 0.3 m.

r_i (m)	r_o (m)	L (m)
0.15	6	500
k (W/m-K)	C_p (J/kg-K)	ρ (kg/m³)
0.52	1840	2050

For the Table 38 values of radius and depth for the domains, a mesh file was created and different simulations were performed. Results including temperature distributions and bore hole exit water temperatures obtained from this simulations are discussed in Sections 4.4.5.1 and 4.4.5.2. Table 39 shows the common mesh statistics for runs conducted with the 3.6° wedge having D_i = 0.3 m.

Table 39. Mesh statistics for 3.6° wedge with D_i = 0.3 m and L = 500 m.

Domain	Nodes	Elements
Earth	255102	125000
Water	302621	205000

Inputs from Table 38 and common input values of Table 19 were used to perform four runs at different inlet velocities. All of the runs were conducted for a total time of 10368000 s. The time steps were determined using Eq. (4-4).

4.4.5.1 Run 3-1 with V_{in} = 0.0041933 m/s and t = 10368000 s (3.6° Wedge, r_i = 0.15 m)

Run 3-1 was conducted on a 3.6° wedge with D_i = 0.3 m. Table 40 shows the input values of inlet velocity, inlet temperature and other parameters given for that water domain of Run 3-1.

Table 40. Input values given at the inlet boundary of the water domain for Run 3-1.

Boundary – Inlet	
Type	INLET
Location	F23.21
Heat Transfer	Static Temperature
T_{in}	305.1 K
Mass And Momentum	Normal Speed
V_{in}	4.1933 x 10^{-3} m/s
Turbulence (I)	Medium Intensity and Eddy Viscosity Ratio (5 %)
Wall Roughness (e)	0 m
Opening Temperature (T_{op})	285 K

With the input values given to the water domain at the inlet (see Table 40) and common settings (see Table 19), a run was conducted for a total time of t = 10368000 s (4 months). Results, including bore hole exit water temperatures and earth temperature distributions, are discussed in the following pages.

To determine the minimum spacing needed between the bore holes, radial temperature rise distributions in the earth domain, $\Delta T_e = T_e - 285$ [K]), at different locations along the depth of the bore hole at a time equal to 10368000 s, were computed and are shown in Table 41.

Table 41. Earth temperature rise (ΔT_e) at different depths along the bore hole for t = 10368000 s and V_{in} = 0.0041933 m/s (3.6° wedge, r_i = 0.15 m, L = 500 m).

ΔT_e (K)						
r (m)	d = 0.1 m	d = 100 m	d = 200 m	d = 300 m	d = 400 m	d = 500 m
0.2	19.86	17.58	15.95	14.47	13.12	11.88
0.8	7.49	6.62	5.94	5.33	4.78	4.29
1.4	3.57	3.13	2.79	2.48	2.2	1.95
2.1	1.66	1.45	1.27	1.12	0.98	0.86
2.8	0.72	0.61	0.54	0.47	0.4	0.35
3.4	0.28	0.24	0.21	0.18	0.15	0.13
4.1	0.1	0.09	0.07	0.06	0.05	0.05
4.7	0.03	0.03	0.02	0.02	0.02	0.01

The initial earth temperature did not change appreciably after a radius of approximately 4.7 m at maximum time and any depth along the bore hole (see Fig. 63 and Table 41). Therefore, a distance of 9.4 m (2 x 4.7 m) can be used as the minimum spacing that has to be provided between the bore holes for the given input values of D_i = 0.3 m and k = 0.52 W/m-K (for inputs of Tables 19, 38, and 40)

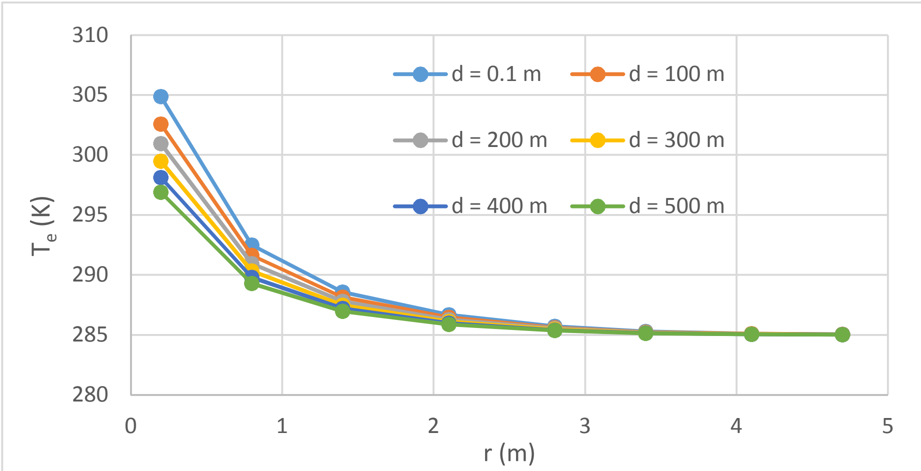

Figure 63. Earth temperature vs. radius at different depths along the bore hole for V_{in} = 0.0041933 m/s and t = 10368000 s (3.6^o wedge, r_i = 0.15 m, L = 500 m).

Figure 64 shows the area averaged water temperature at different depths along the bore hole for t = 10368000 s.

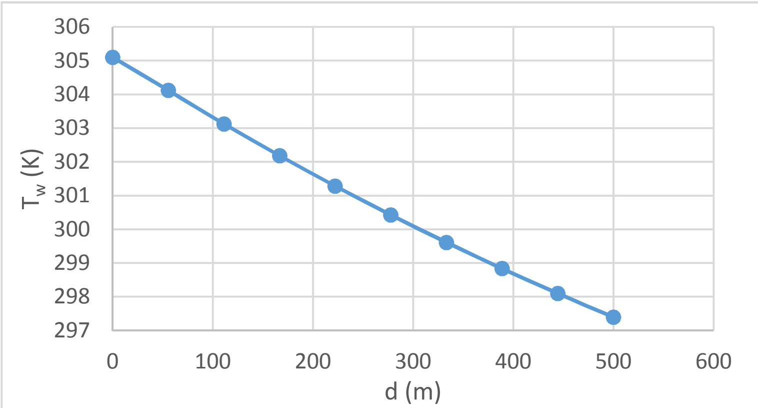

Figure 64. Water temperature vs. depth along the bore hole for V_{in} = 0.0041933 m/s and t = 10368000 s (3.6^o wedge, r_i = 0.15 m, L = 500 m).

For the given inlet velocity of 0.0041933 m/s and total time equal to 10368000 s, the water temperature at a depth of 500 m does not reach the required target temperature of 295 K (see Fig. 64).

Figure 65 shows the area averaged bore hole exit water temperature plotted against time.

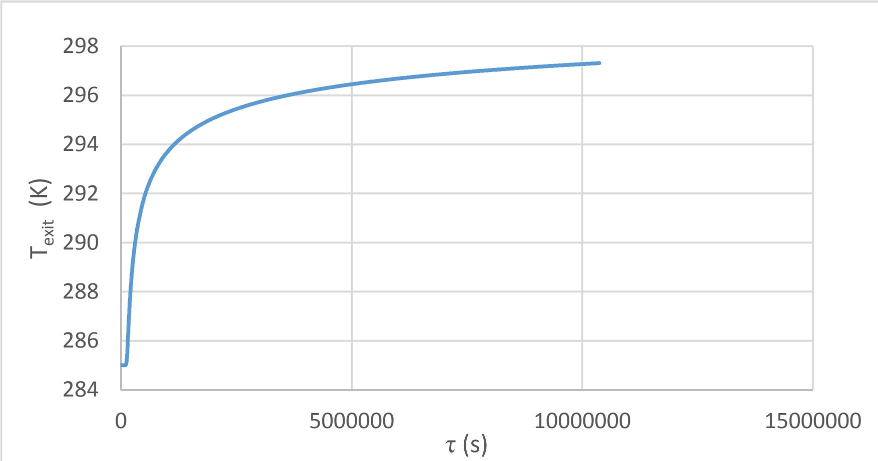

Figure 65. Bore hole exit water temperature vs. time for V_{in} = 0.0041933 m/s (3.6^o wedge, r_i = 0.15 m, L = 500 m).

For t = 10368000s, water temperature at the bore hole exit was higher than the target temperature of 295 K (see Fig. 65). Considering this fact, a few more runs were conducted by changing the inlet water velocity. Although not all of the results are discussed in detail, the bore hole exit water temperatures for different inlet velocities are discussed in Section 4.4.5.2.

4.4.5.2 Exit Temperature of Water for Different Inlet Velocities at 10368000 s (D_i = 0.3 m)

This section deals with the bore hole exit water temperatures for different velocities when D_i = 0.3 m. Table 42 shows the bore hole exit water temperatures at a time equal to 10368000 s (4 months) for different inlet velocities when the inner diameter is 0.3 m.

Table 42. Bore hole exit water temperature at different inlet velocities for t = 10368000 s and D_i = 0.3 m.

V_{in} (m/s)	T_{exit} (K)
0.003310526	295.816
0.00349444	296.172
0.00393125	296.919
0.00419333	297.401

Using the values from Table 42 and Fig. 66, an equation for the bore hole exit water temperature as a function of inlet velocity was developed.

$$T_{exit}\ [K] = (336.11\ \frac{s^{0.0224}\ K}{m^{0.0224}})\ (V_{in}^{0.0224}) \qquad (4\text{-}7)$$

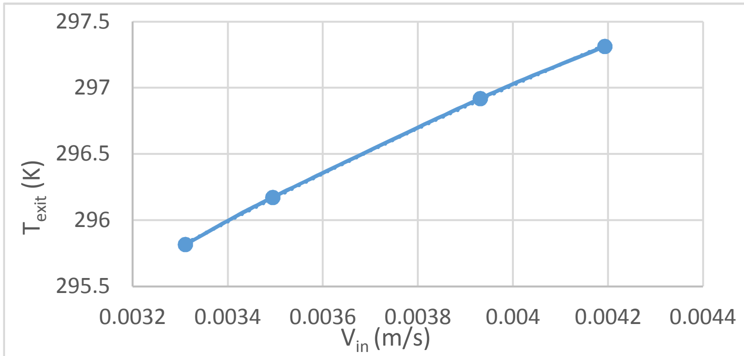

Figure 66. Bore hole exit water temperature vs. inlet velocity at t = 10368000 s for D_i = 0.3 m.

Equation (4-7) can be used to determine the exit temperature of water at any inlet velocity, in the range of 0.0033105 m/s to 0.0041933 m/s, for the 3.6° wedge with D_i = 0.3 m and k = 0.52 W/m-K. Since the 3.6° wedge models cannot be practically installed, because there is no riser (return pipe) for the warm cooling water to come up, Eq. (4-7) was not used to determine the water inlet velocity required to reach 295 K at the bore hole exit.

4.4.6 Summary of All Results with the 3.6° Wedge

This section provides a summary of the results, including the bore hole exit water temperatures and minimum spacing needed between the bore holes, for all of the runs conducted on the 3.6° wedge for different inner tubing diameters.

The following show how to compute the number of bore holes. Assuming the total mass flow rate of the cooling water coming out of the condenser to be "$\dot{M}$", the total number of bore holes required to maintain the cycle thermal efficiency of the plant can be calculated by dividing that total mass flow rate by the flow rate of water through each bore hole, $\dot{m}$, needed to reach the bore hole exit water temperature of 295 K.

$$B_{Num} = \frac{\dot{M}}{\dot{m}} \tag{4-8}$$

Mass flow rate through each bore hole, can be calculated using

$$\dot{m} = \rho_w A_c V_{in} \tag{4-9}$$

where the density of water (ρ_w = 997 kg/m^3) was found at 305.1 K (inlet temperature of water), A_c is the cross-sectional area of the tube, and V_{in} is the water inlet velocity (which is different for different cases).

A typical fossil-fueled 1000 MW power plant operating at full capacity with η = 40% would reject about 1500 MW, which requires 35727.73 kg/s of circulating cooling water, based on a 10 °C difference in temperatures from the inlet to the outlet of a cooling system (with $C_{p(water)}$ = 4198.42 J/kg-K) [6]. Table 43 shows summary results for the runs conducted on the 3.6° wedge with D_i = 0.2 m and t = 2592000 s. $\dot{m}$ and B_{Num} were calculated using Eqs. (4-9) and (4-8), respectively.

Table 43. Summary of results for D_i = 0.2 m and t = 2592000 s.

D_o (m)		20	
k (W/m-K)		0.52	
C_p (J/kg-K)		1840	
ρ (kg/m³)		2050	
T_{in} (K)		305.1	
V_{in} (m/s)	$\dot{m}$ (kg/s)	T_{exit} (K)	B_{Num}
0.030510	0.955624	302.021	37387
0.01525	0.477656	299.405	74798
0.00621	0.194508	293.695	183683

The minimum spacing that has to be provided between the bore holes is equal to two times the radius at which the initial earth temperature remained unchanged.

$$B_{Spacing} = r_{unchanged} \; x \; 2 \tag{4-10}$$

For all of the cases shown in Table 43, the maximum radius at which the initial temperature of the earth remained unchanged was determined to be 4.5 m. Therefore, 9 m is the minimum spacing needed between bore holes.

Using Table 32, Table 44 was produced to show summary results for the runs conducted on the 3.6° wedge with D_i = 0.2 m and t = 10368000 s. For those runs, the maximum radius at which the initial temperature of the earth remained unchanged did not exceed 4 m.

Table 44. Summary of results for D_i = 0.2 m and t = 10368000 s.

D_o (m)			20
k (W/m-K)			0.52
C_p (J/kg-K)			1840
ρ (kg/m³)			2050
T_{in} (K)			305.1
V_{in} (m/s)	$\dot{m}$ (kg/s)	T_{exit} (K)	B_{Num}
0.0078625	0.246282	296.992	145068
0.00698889	0.218907	296.246	163210
0.006621053	0.207381	295.851	172281
0.00621	0.194508	295.520	183683

Since the minimum spacing that has to be provide is no greater than 8 m for a total time of 10368000 s, outer radius for the runs conducted on the 3.6° wedge with D_i = 0.25 m and 0.3 m was changed to a conservative value of 6 m (greater than r = 4 m i.e., radius at which the earth temperatures remains unchanged when D_i = 0.2 m) instead the of 10 m used for D_i = 0.2 m. This helped to reduce the computer simulation time, due to the smaller number of elements.

Using Table 37, Table 45 was produced to show summary results for the runs conducted on the 3.6° wedge with D_i = 0.25 m and t = 10368000 s. The minimum spacing between the bore holes for all of those cases did not vary much compared to the spacing of 8 m for results from Table 44. For all of the cases from Table 45, the minimum radius at which the initial temperature of the earth remained unchanged was determined to be 4.7 m. Therefore, the minimum spacing between bore holes should be 9.4 m.

Table 45. Summary of results for D_i = 0.25 m and t = 10368000 s

D_o (m)		12	
k (W/m-K)		0.52	
C_p (J/kg-K)		1840	
ρ (kg/m^3)		2050	
T_{in} (K)		305.1	
V_{in} (m/s)	$\dot{m}$ (kg/s)	T_{exit} (K)	B_{Num}
0.00621	0.303918	297.980	117557
0.00571818	0.279848	297.347	127668
0.00449286	0.219881	295.822	162487
0.0041933	0.205222	295.359	174093

Using Table 42, Table 46 was produced to show summary results for the runs conducted on the 3.6° wedge with D_i = 0.3 m and t = 10368000 s.

Table 46. Summary of results for D_i = 0.3 m and t = 10368000 s.

D_o (m)		12	
k (W/m-K)		0.52	
C_p (J/kg-K)		1840	
ρ (kg/m^3)		2050	
T_{in} (K)		305.1	
V_{in} (m/s)	$\dot{m}$ (kg/s)	T_{exit} (K)	B_{Num}
0.00419333	0.29552	297.401	120898
0.00393125	0.27705	296.919	128958
0.00349444	0.246266	296.172	145078
0.003310526	0.233305	295.816	153137

For all of the cases shown in Table 46, the maximum radius at which the initial temperature of the earth remained unchanged was determined to be 4.7 m. Therefore, the minimum bore hole spacing that must be provided is 9.4 m (2 x 4.7 m). Number of bore hole required are not discussed, because, the 3.6^o wedge models were solved primarily to determine the spacing that is needed. Also, the 3.6^o wedge models cannot be practically installed (because there is no return pipe). Therefore, discussing the number the number of bore holes required for different cases solved on the 3.6^o wedge does not address the issue of number of bore holes required to maintain the thermal efficiency of a power plant. This concludes the results from the runs conducted on the 3.6^o wedge.

4.4.7 ANSYS-CFX Runs of Cylindrical Model with U-Tube When L = 150 m and D_i = 0.2 m

After conducting multiple runs on the 3.6 ^{o} wedge model, a conclusion was drawn on the range of inlet velocities (to use V_{in} in the range of 0.00621 m/s), in order to limit the number of trials needed for meeting the target bore hole exit water temperature. These inlet velocities were used for runs conducted on the cylindrical model of the earth with a U-shaped tube as shown in Fig. 67.

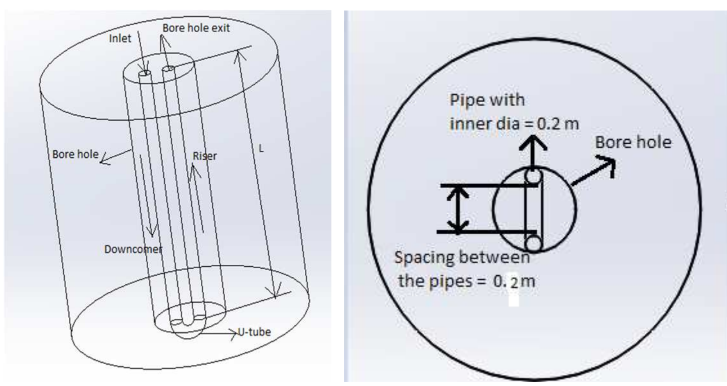

Figure 67. Three-dimensional model of the water and earth domains used for runs conducted with the cylindrical model with U-tube.

For all runs that were conducted using the cylindrical model of the earth (ρ = 2050 kg/m^3, C_p = 1840 J/kg-K were kept constant for all the runs) with a U-shaped tube, the inner diameter of the tube was set to 0.2 m. This was done since increasing the inner diameter above 0.2 m was not showing much effect on the exit water temperature, and decreasing the inner diameter would increase the number of bore holes required (Section 4.4.6). The spacing between the tubes was set to 0.2 m, which makes the total diameter of the bore hole equal to 0.6 m (2 tubes of 0.2 m diameter and spacing of 0.2 m) (see Fig. 67). The outer diameter was set to 12 m. While keeping the inner radius (r_i = 0.1 m), outer radius (r_o = 6 m) and spacing between the tubes constant, various runs were conducted by changing the depth of the bore holes and thermal conductivity of the earth. These runs were conducted using different inlet velocities until the target bore hole exit water temperature was reached or enough bore hole exit water temperature values were obtained to interpolate for the target bore hole exit water temperature (295 K). Not all results for every run are discussed in detail in this thesis. However, the results for one value of inlet velocity are presented for each value of thermal conductivity and length of the bore hole in Sections 4.4.7.1-4.4.7.4.

First, various runs were conducted keeping the length of the bore hole constant and equal to 150 m, while changing the inlet velocity of the water and thermal conductivity of the earth (ρ and C_p were kept constant and equal to the values in Table 17). All of the runs were conducted for a total of time of t = 10368000 s (4 months). The time steps were determined using Eq. (4-4).

Table 47 shows the common boundary conditions used in the runs conducted on the cylindrical model of the earth with a U-shaped tube [for Sections 4.4.7 and 4.4.8 results].

Table 47. Common input boundary conditions given for both domains (U-tube).

Boundary- Default Fluid Solid Interface Side 1		Boundary-Outlet	
Type	INTERFACE	Type	OPENING
Loaction	F12.14, F13.14	Location	F19.15
Heat Transfer	Conservative Interface Flux	Flow Direction	Normal to Boundary Condition
Boundary- Earth Default		Flow Regime	Subsonic
Type	WALL	Heat Transfer	Opening Temperature
Location	F16.14, F17.14	Opening Temperature	285 [K]
Heat Transfer	Adiabatic	Mass and Momentum	Opening Pressure and Direction
Boundary- Wall Temp		Turbulence	Medium Intensity and Eddy Viscosity Ratio
Type	WALL	Boundary-Insulated	
Location	F18.14	Type	WALL
Heat Transfer	Fixed Temperature	Location	F21.15
Fixed Temperature	285 [K]	Heat Transfer	Adiabatic
Boundary- Default Fluid Solid Interface Side 2		Mass and Momentum	No Slip Wall
Type	INTERFACE	Wall Roughness	Smooth Wall
Location	F12.15, F13.15		
Heat Transfer	Conservative Interface Flux		
Mass and Momentum	No Slip Wall		
Wall Roughness	Smooth Wall		

Table 48 shows the mesh statistics for the cylindrical model for a 150 m depth bore hole.

Table 48. Common mesh statistics for L =150 m.

Domain	Nodes	Elements
Earth	4533300	4410784
Water	242424	198880
All Domains	4775724	4609664

4.4.7.1 Run 4-1 with V_{in} = 0.00621 m/s, t = 10368000 s, L= 150 m, and k = 0.52 W/m-K

Run 4-1 was conducted on the cylindrical model of the earth with U-tube at V_{in} = 0.00621 m/s, L = 150 m, D_i = 0.2 m, D_o = 12 m, and k = 0.52 W/m-K for a total time of 10368000 s (4 months). Results, including bore hole exit water temperatures and earth temperature distributions, are discussed in the following pages. Table 49 shows the input values of inlet velocity, inlet temperature and other parameters used for the water domain for Run 4-1.

Table 49. Input values given at the inlet boundary of the water domain for Run 4-1.

Boundary – Inlet	
Type	INLET
Location	F20.15
Heat Transfer	Static Temperature
T_{in}	3.051 x 10^2 K
Mass And Momentum	Normal Speed
V_{in}	6.210 x 10^{-3} m/s
Turbulence (I)	Medium Intensity and Eddy Viscosity Ratio (5 %)
Wall Roughness (e)	0 m
Opening Temperature (T_{op})	285 K

With the common input values of Table 47 and the input values selected for the water domain at the inlet (see Table 49), a run was conducted. Figure 68 shows the water temperature at different locations along the depth of the bore hole at a time equal to 10368000 s, for the inputs from Tables 47 and 49. Bore hole exit water temperature was 300.62 K, which was high compared to the target bore hole exit water temperature of 295 K. Figure 69 shows the area averaged bore hole exit water temperature (Eq. (4-3)) plotted versus time. Considering this result, more runs were conducted at different inlet velocities, keeping the earth thermal conductivity unchanged, and are shown in Table 50. Also, earth temperature at the top section of the bore hole (Fig. 70), when t =

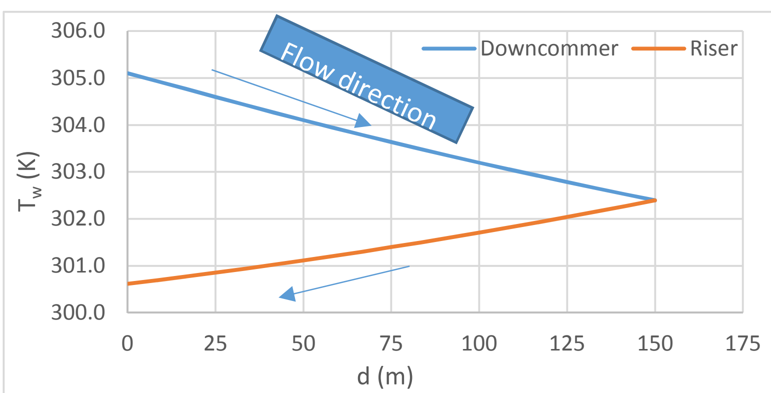

Figure 68. Water temperature vs. depth along the bore hole for V_{in} = 0.00621 m/s and t =10368000 s (U-tube, L = 150 m).

10368000 s, is higher than the water temperature in the riser at the same location (Fig. 70). This is due to the heat transfer from the warmer cooling water in the downcomer. Therefore, water in the riser starts to increase in temperature at the top section of the riser, which is not desirable, because this means that earth is transferring heat to the water (reversed direction). Therefore, the bore hole length has to be chosen so that the water temperature is always greater than the earth temperature.

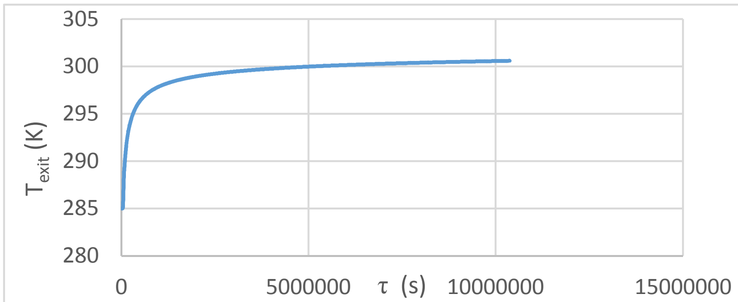

Figure 69. Bore hole exit water temperature vs. time for k = 0.52 W/m-K and V_{in} = 0.00621 m/s (U-tube, L = 150 m).

The water temperature at the bore hole exit becomes greater than 295 K for times greater than approximately 310,000 s (Fig. 69). Although the earth temperatures (Fig. 70) at the top section of the bore hole are greater than the exit water temperature, the water temperature drops along the depth of the bore hole (Fig. 68). Since the water temperature continues to drop, even at the exit, it must be assumed that the earth temperatures in other planes (e.g., perpendicular to the vertical plane shown in Fig. 71) are lower than the exit water temperature; but this is not known since those temperature profiles were not extracted from the CFX results [which are no longer available].

Earth temperatures at different radii and different locations along the depth of the bore hole were extracted by CFX-Post. Figure 70 shows the temperature of the earth plotted versus radius at different depths. The inequality in earth temperatures at d = 150 m and r = 0.3 m (Fig. 70) between the downcomer and the riser sides is discussed in Section 4.4.7.3.

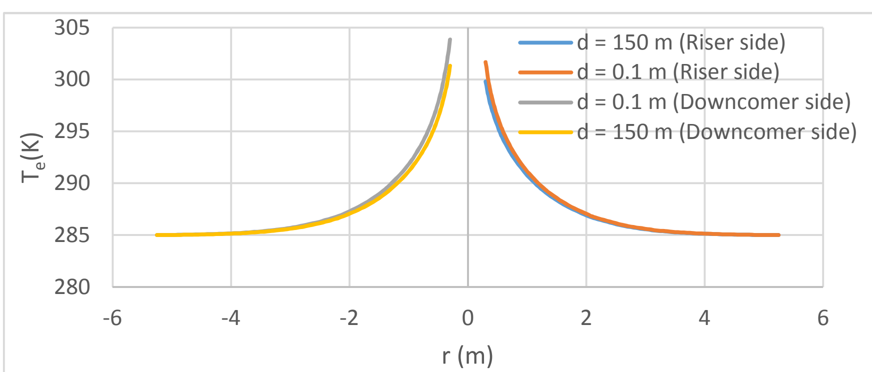

Figure 70. Earth temperature vs. radius at different depths along the bore hole for V_{in} = 0.00621 m/s, t = 10368000 s, and k = 0.52 W/m-K (U-tube, L = 150 m).

Figure 71 shows temperature contours (temperature distributions in the earth and water domains) for the uppermost section of the vertical plane through both the earth and water domains. Also, Fig. 71 shows that the earth temperature changes are smooth (consistent) both radially and along the depth of the bore hole indicating that the earth temperature distribution results shown in Fig. 70 are representative of the results all along the bore hole.

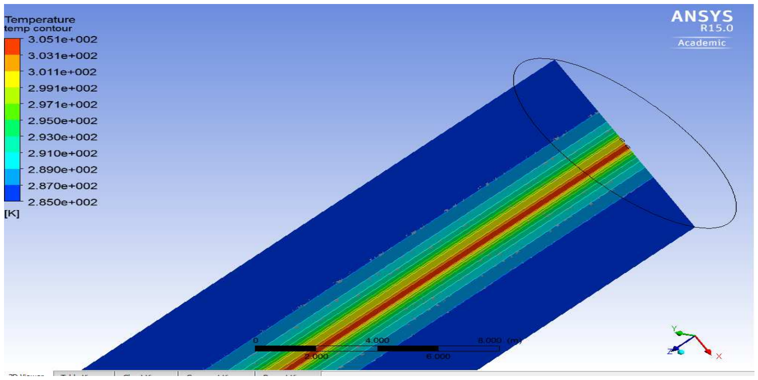

Figure 71. Temperature contours in the uppermost section of the vertical plane through both domains for t =10368000 s, V_{in} = 0.00621 m/s, and k = 0.52 W/m-K (U-tube, L = 150 m).

The initial earth temperature was not affected at radii greater than 4 m for both the downcomer and riser tubes (see Figs. 70 and 71). The minimum bore hole spacing needed for Run 4-1 remained similar to the results from the 3.6^{o} wedge with 0.2 m diameter, which was 8 m.

To determine the exact inlet water velocity required to reach 295 K at the bore hole exit, a few more runs were conducted by changing the inlet water velocity while keeping all other inputs constant and the same as those of Run 4-1. Table 50 shows the bore hole exit water temperatures for these inlet velocities with k = 0.52 W/m-K and L = 150 m.

Table 50. Bore hole exit water temperature at different values of inlet velocity for k = 0.52 W/m-K, D_i = 0.2 m, and L = 150 m (U-tube).

V_{in} (m/s)	$\dot{m}$ (kg/s)	T_{exit} (K)
0.01258	0.394026719	302.098
0.00621	0.194507625	300.620
0.003145	0.09850668	297.407
0.001398	0.043780503	292.879

The last three set of values from Table 50 were used to derive an equation (Eq. (4-11)) for bore hole exit water temperature as a function of inlet velocity. Since Eq. (4-11) was used to determine V_{in} for which T_{exit} was equal to 295 K, and since 295 K was in between 300.620 K and 292.879 K, the first set of values for T_{exit} and V_{in} (i.e., 302.098, 0.01258) was not used in deriving

Eq. (4-11). (Also, if the first set of values were included, the trend line would not accurately fit all of the four sets of values.)

$$T_{exit} = \left(328.78\ \frac{s^{0.0175}\ K}{m^{0.0175}}\right)\ (V_{in})^{0.0175} \qquad (4\text{-}11)$$

Equation (4-11) was used to interpolate for the inlet velocity at which the bore hole exit water temperature would be equal to 295 K. It was found that, for 0.002039474 m/s, the bore hole exit temperature at the outlet, at time 10368000 s, was equal to 295 K. For k = 0.52 W/m-K and L = 150 m (U-tube), a mass flow rate (Eq. (4-9)) of 0.063879749 kg/s (density of water was found at T_{in} = 305.1 K, ρ_w = 997 kg/m^3) would be required to maintain the exit water temperature at the outlet less than or equal to 295 K.

The bore hole exit water temperature for 0.063879749 kg/s would remain below 295 K for all of the simulated times. These low temperatures during the initial time periods would have a positive effect on the power plant cycle thermal efficiency. Discussion of the effects of these low temperatures on the thermal efficiency of the power plant during the initial time periods can be found in Section 4.4.11. Number of bore holes required for each case is discussed in Section 4.4.10.

4.4.7.2 Run 4-2 with V_{in} = 0.00621 m/s, t = 10368000 s, L = 150 m, and k = 2.4 W/m-K

Run 4-2 was conducted on the cylindrical model of the earth with U-tube at V_{in} = 0.00621 m/s, L = 150 m, D_i = 0.2 m, D_o = 12 m, k = 2.4 W/m-K, and t = 10368000 s. All results extracted using CFX-Post for this run are discussed in the following pages. Table 51 shows the input values of inlet velocity, inlet temperature and other parameters used for the water domain of Run 4-2.

Table 51. Input values given at the inlet boundary of the water domain for Run 4-2.

Boundary – Inlet	
Type	INLET
Location	F20.15
Heat Transfer	Static Temperature
T_{in}	3.051 x 10^2 K
V_{in}	6.210 x 10^{-3} m/s
Turbulence (I)	Medium Intensity and Eddy Viscosity Ratio (5 %)
Wall Roughness (e)	0 m
Opening Temperature (T_{op})	285 K

Since the thermal conductivity of the earth ranges from 0.52 W/m-K to over 5 W/m-K (Section 2.4.2), therefore, for Run 4-2, the thermal conductivity of the earth was changed to 2.4 W/m-K, while keeping the inlet velocity and other input parameters the same as those of Run 4-1.

With the common input values of Table 47 and the input values given for the water domain at the inlet (see Table 51), a run was conducted. Figure 72 shows the temperature distribution of the earth domain at two different locations along the depth of the bore hole for t = 10368000 s and k = 2.4 W/m-K. Note that at d = 150 m and r = 0.3 m, earth temperatures on both downcomer and riser sides are approximatley equal.

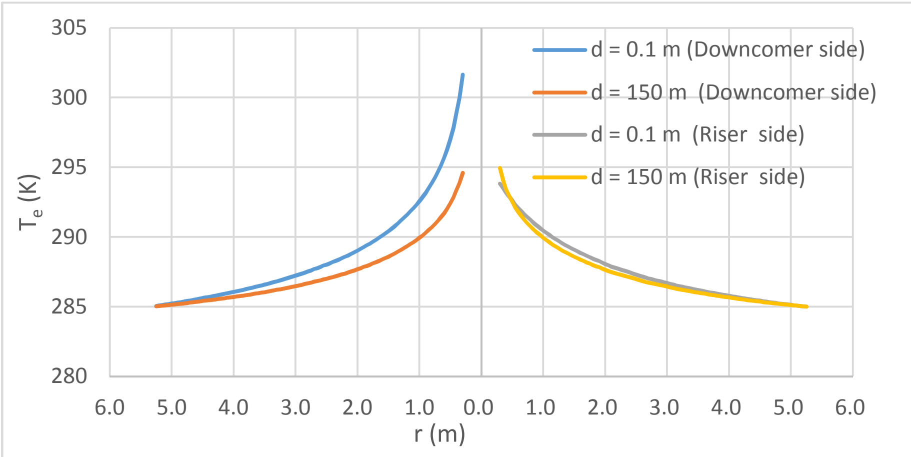

Figure 72. Earth temperature vs. radius at different depths along the bore hole for V_{in} = 0.00621 m/s, t =10368000 s, and k = 2.4 W/m-K (U-tube, L = 150 m).

The initial earth temperature remained unchanged at a radius approximately greater than 5 m at the surface and the greatest depth along the bore hole (see Fig. 72). Also, Fig. 73 shows that the earth temperature changes are smooth (consistent) both radially and along the depth of the bore hole indicating that the earth temperature distribution results shown in Fig. 72 are representative of the results all along the bore hole. Therefore, a distance of 10 m (2 x 5 m) can be used as the minimum spacing that would be needed between the bore holes if the inputs for Run 4-2 were used.

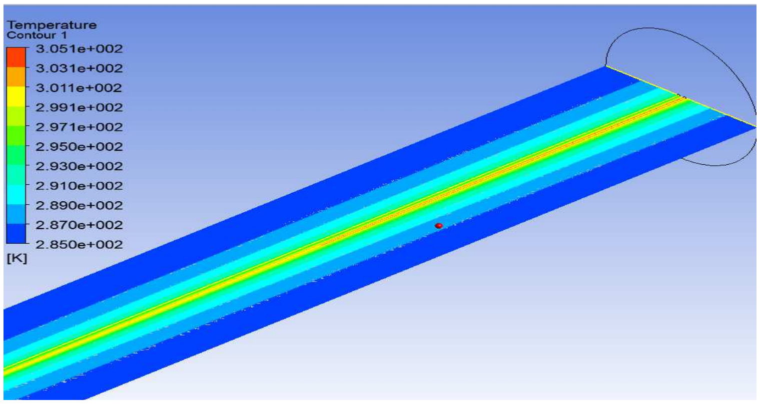

Figure 73. Temperature contours at the uppermost section of the vertical plane through both domains for t = 10368000 s, V_{in} = 0.00621 m/s, and k = 2.4 W/m-K (U-tube, L = 150 m).

As can seen from Fig. 74, the area averaged bore hole exit water temperature at the end of the riser was 294.407 K, which was lower than the target temperature of 295 K. Also, water in the riser increases in temperature from approximately d = 35 m to 0 m (see Fig. 74), which is not desirable and means that heat is being transferred from the earth to the water (reversed direction). This case of reversed heat transfer should be used in future studies to help determine the length of the bore hole required so that water temperature is always higher than earth temperature.

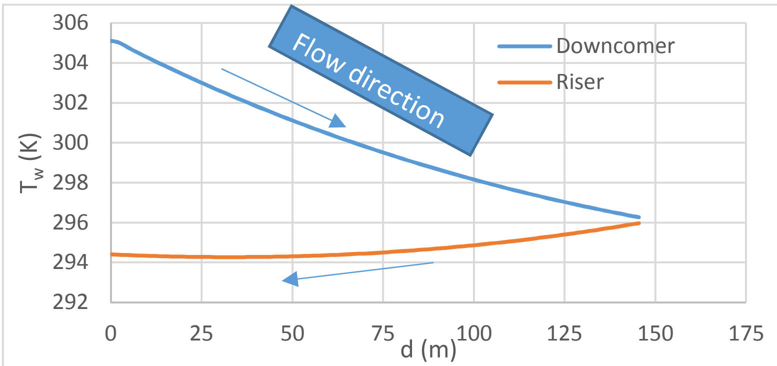

Figure 74. Water temperature at different depths along the bore hole for t = 10368000 s, V_{in} = 0.00621 m/s, and k = 2.4 W/m-K (U-tube, L = 150 m).

Figure 75 shows the area averaged bore hole exit water temperature plotted versus time. The water temperature at the bore hole exit was less than 295 K for all simulation times. A few more runs were conducted at different inlet velocities, while keeping the thermal conductivity of the earth the same and equal to 2.4 W/m-K. These extra runs were conducted in order to determine the exact inlet water velocity required to reach the target bore hole exit water temperature of 295 K.

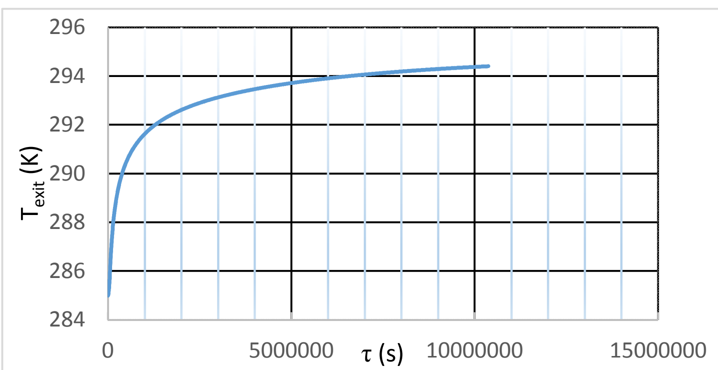

Figure 75. Bore hole exit water temperature vs. time for k = 2.4 W/m-K and V_{in} = 0.00621 m/s (U-tube, L = 150 m).

Table 52 shows the bore hole exit water temperature for different inlet velocities with k = 2.4 W/m-K and the bore hole depth equal to 150 m.

Table 52. Bore hole exit water temperature at different values of inlet velocity for k = 2.4 W/m-K, D_i = 0.2 m, and L = 150 m (U-tube).

V_{in} (m/s)	$\dot{m}$ (kg/s)	T_{exit} (K)
0.00621	0.194507625	294.407
0.006989	0.218907213	295.026
0.0077625	0.243134531	295.590

Values from Table 52 were used to derive an equation for the bore hole exit water temperature as a function of inlet velocity.

$$T_{exit}\,[\mathrm{K}] = (-4.794 \times 10^4\ \tfrac{\mathrm{s^2\,K}}{\mathrm{m^2}})\ V_{in}^2 + (1436.476\ \tfrac{\mathrm{s\,K}}{\mathrm{m}})\ V_{in} + (287.32\ \mathrm{K}) \qquad (4\text{-}12)$$

Equation (4-12) was used to interpolate for the inlet velocity at which the bore hole exit water temperature would be equal to 295 K. It was determined that, for V_{in} = 0.006977 m/s, the bore hole exit water temperature at the end of the riser would be equal to 295 K. For k = 2.4 W/m-K and L = 150 m (U-tube), a mass flow rate (Eq. (4-9)) of 0.218531353 kg/s (density of water was found at T_{in} = 305.1 K, ρ_w = 997 kg/m^3) would be required to maintain the bore hole exit water temperature at 295 K. The bore hole exit water temperature at 0.218531353 kg/s would remain below 295 K for all but the maximum simulation time. These low temperatures during the initial time periods would have a positive effect on the cycle thermal efficiency of the power plant (see Section 4.4.11). Number of bore holes required is discussed in Section 4.4.10.

4.4.7.3 Run 4-3 with V_{in} = 0.00621 m/s, t = 10368000 s, L = 150 m, and k = 4 W/m-K

Run 4-3 was conducted on the cylindrical model of the earth with U-tube at V_{in} = 0.00621 m/s, D_i = 0.2 m, D_o = 12 m, k = 4 W/m-K, and t = 10368000 s (4 months). All results extracted using CFX-Post for this run are discussed in the following pages. Table 53 shows the input values of inlet velocity, inlet temperature and other parameters used for the water domain of Run 4-3.

Table 53. Input values given at the inlet boundary of the water domain for Run 4-3.

Boundary – Inlet	
Type	INLET
Location	F20.15
Heat Transfer	Static Temperature
T_{in}	3.051 x 10^2 K
V_{in}	6.2100 x 10^{-3} m/s
Turbulence (I)	Medium Intensity and Eddy Viscosity Ratio (5 %)
Wall Roughness (e)	0 m
Opening Temperature (T_{op})	285 K

As discussed in Section 2.4.2, the thermal conductivity of the earth ranges from 0.52 W/m-K to over 5 W/m-K. For Run 4-3, the thermal conductivity of the earth was changed to 4 W/m-K while keeping the inlet velocity and other input parameters the same as those of Run 4-1. With the common input values of Table 47 and the Table 53 input values given for the water domain at the inlet, a run was conducted. Figure 76 shows the temperature distribution of the earth domain at two different locations along the depth of the bore hole for t = 10368000 s and k = 4 W/m-K. Also, Fig. 77 shows that the earth temperature changes are smooth (consistent) both radially and along the depth of the bore hole indicating that the earth temperature distribution results shown in Fig. 76 produced using ANSYS-CFX are representative of the results all along the bore hole.

Earth temperatures at d = 150 m and r = 0.3 m on both the downcomer and the riser sides should be approximately the same. They are close for Fig. 70, but they are not close for cases shown in Figs. 70 and 76. This difference was due to an error made in extracting the data from ANSYS-CFX. Using ANSYS-CFX, extracting temperature distribution data at any given depth and radius requires a geometrical entity (line, point, etc.) defined at that location. For the cases shown in Figs. 70 and 76, the geometrical entities defined (drawn) were a little off in their position and size, leading to this difference. This issue could not be addressed while reviewing and correcting this thesis, because ANSYS-CFX was not accessible.

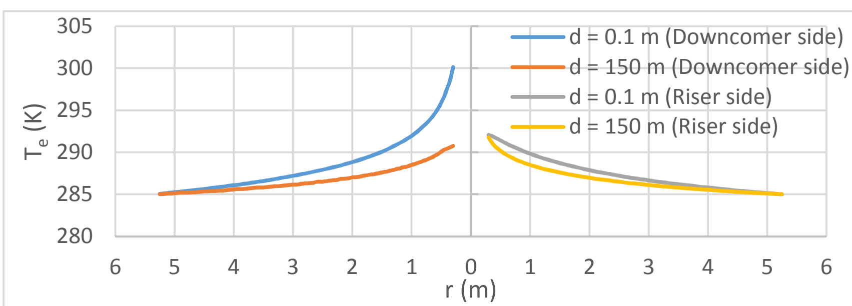

Figure 76. Earth temperature vs. radius at different depths along the bore hole for t = 10368000 s, V_{in} = 0.00621 m/s, and k = 4 W/m-K (U-tube, L = 150 m).

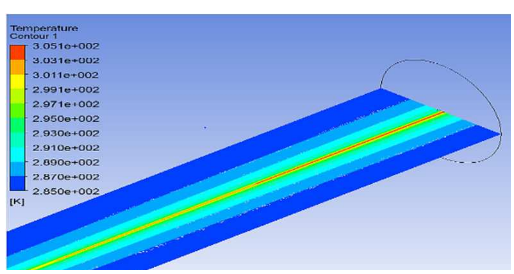

Figure 77. Temperature contours in the uppermost section of the vertical plane through both domains for t = 10368000 s, V_{in} = 0.00621 m/s, and k = 4 W/m-K (U-tube, L = 150 m).

When the thermal conductivity of the earth was changed to 4 W/m-K, initial earth temperature remained unchanged at radii greater than approximately 5 m for t = 10368000 s, at the surface and greatest depths along the bore hole (see Fig. 76).

Water temperature at the bore hole exit was 292.253 K (see Fig. 78). Also, water in the riser starts to increase in temperature from approximately d = 50 m to d = 0 m (see Fig. 78), which is not desirable. This rise in water temperature should be used in future studies when examining the length of the bore hole required so that water temperature is always higher than the earth temperature.

A few more runs were conducted at different inlet water velocities, while keeping the thermal conductivity of the earth equal to 4 W/m-K. This was done in order to determine the inlet velocity at which the bore hole exit water temperature was always below or equal to 295 K. Figure 79 shows the bore hole exit water temperature plotted versus time for t = 10368000 s, L = 150 m and k = 4 W/m-K.

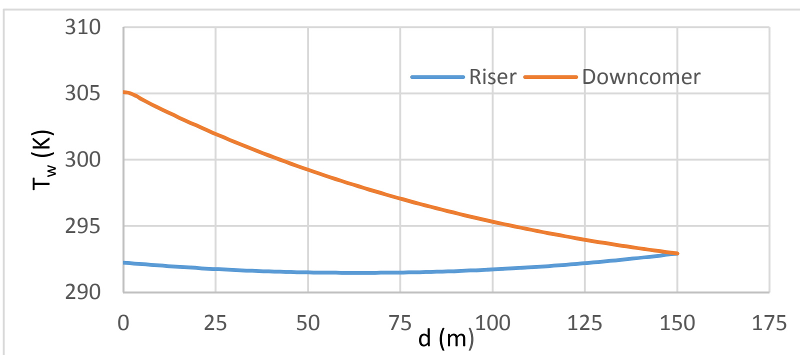

Figure 78. Water temperature at different depths along the bore hole for t = 10368000 s, V_{in} = 0.00621 m/s, and k = 4 W/m-K (U-tube, L = 150 m).

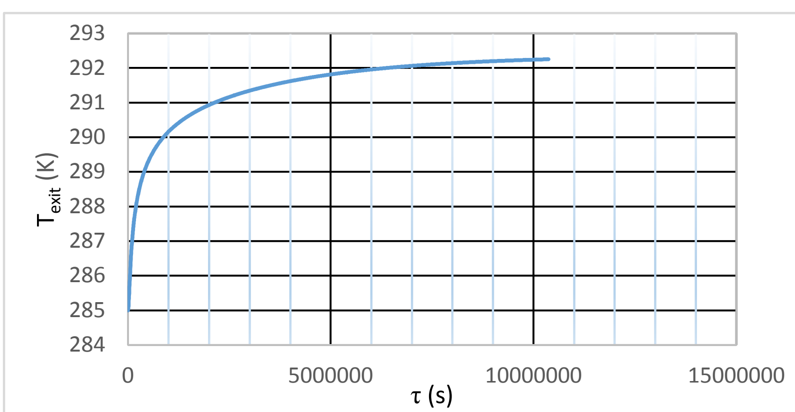

Figure 79. Bore hole exit water temperature vs. time for k = 4 W/m-K and V_{in} = 0.00621 m/s (U-tube, L = 150 m).

Table 54 shows the bore hole exit water temperatures for different inlet velocities with k = 4 W/m-K and bore hole depth equal to 150 m.

Table 54. Bore hole exit water temperature at different values of inlet velocity for k = 4 W/m-K, D_i = 0.2 m, and L = 150 m (U-tube).

V_{in} (m/s)	$\dot{m}$ (kg/s)	T_{exit} (K)
0.00621	0.194507625	292.253
0.0077625	0.243134531	293.254
0.0104833	0.328354555	294.763
0.01258	0.394026719	295.957

Values from Table 54 were used to derive an equation for bore hole exit water temperature as a function of inlet velocity.

$$T_{exit} = (-6.6585557 \text{ x } 10^3 \frac{s^2\ K}{m^2})\ V_{in}^2 + (7.0045 \text{ x } 10^2 \frac{s\ K}{m})\ V_{in} + (288.17\ K) \qquad (4\text{-}13)$$

Equation (4-13) was used to interpolate for the inlet velocity at which the exit temperature of the water would be equal to 295 K. It was found that, for V_{in} = 0.010875 m/s, the bore hole exit water temperature at the end of the riser would be equal to 295 K. For k = 4 W/m-K and L = 150 m (U-tube), a mass flow rate (Eq. (4-9)) of 0.34062822 kg/s (density of water was found at T_{in} = 305.1 K, ρ_w = 997 kg/m^3) would be required to maintain the bore hole exit water temperature at 295 K. The bore hole exit water temperature would be less than 295 K for all of the simulation times. These low temperatures during the initial time periods would have a positive effect on the cycle thermal efficiency of the power plant (see Section 4.4.11). Number of bore holes required is discussed in Section 4.4.10.

4.4.7.4 Runs with k = 5 W/m-K, t = 10368000 s, and L = 150 m at Different Inlet Velocities

To determine the exact inlet velocity required to reach a bore hole exit water temperature of 295 K for maximum simulation time, four runs were conducted with D_i = 0.2 m, D_o = 12 m, k = 5 W/m-K, and t = 10368000 s (4 months) at different inlet velocities (Table 55).

Table 55. Bore hole exit water temperature at different values of inlet velocity for k = 5 W/m-K, D_i = 0.2 m, and L = 150 m (U-tube).

V_{in} (m/s)	$\dot{m}$ (kg/s)	T_{exit} (K)
0.00621	0.194507625	291.428
0.00898571	0.281447522	292.950
0.01258	0.394026719	294.616
0.014615176	0.457771848	295.400

Values from Table 55 can be used to derive an equation for bore hole exit water temperature as a function of inlet velocity.

$$T_{exit}\,[K] = (-1.35496 \text{ x } 10^4 \frac{s^2\,K}{m^2})\, V_{in}^{\;2} + (754.89\, \frac{s\,K}{m})\, V_{in} + (287.262\text{ K}) \tag{4-14}$$

Equation (4-14) was used to interpolate for the inlet velocity at which the bore hole exit water temperature for maximum simulation time is equal to 295 K. It was found that for V_{in} = 0.013542 m/s, the bore hole exit water temperature at the outlet for t = 10368000 s was equal to 295 K. For k = 5 W/m-K and L = 150 m U-tube, a mass flow rate (Eq. (4-9)) of 0.424168616 kg/s (density of water was found at T_{in} = 305.1 K, ρ_w = 997 kg/m^3) would be required to maintain the bore hole exit water temperature at the outlet equal to 295 K. Number of bore holes required for each case is discussed in Section 4.4.10.

4.4.7.5 Inlet Velocity of Water Required to Reach 295 K at the Bore Hole Exit for Different Thermal Conductivities of the Earth (U-tube, L = 150 m)

Table 56 shows the inlet velocities of water required to reach the bore hole exit target temperature of 295 K, at t = 103680000 s, for different values of earth thermal conductivity when the depth of the bore hole is 150 m.

Table 56. Inlet velocities of water for different thermal conductivities of earth to reach 295 K at the bore hole exit for D_i = 0.2 m and L = 150 m (U-tube).

k (W/m-K)	0.52	2.4	4	5
V_{in} (m/s)	0.002039474	0.006977	0.010875	0.013542

Values from Table 56 were used to derive an equation for the inlet velocity as a function of thermal conductivity of the earth to determine the inlet velocity required to reach bore hole exit water temperature of 295 K for different thermal conductivities of the earth.

$$V_{in} = (0.002543\, \frac{m^2\,K}{Ws})\, k + (0.0007922\, \frac{m}{s}) \tag{4-15}$$

For D_i = 0.2 m and L = 150 m (U-tube), Eq. (4-15) can be used to interpolate for the inlet velocity required to reach the target bore hole exit water temperature of 295 K at different thermal conductivities of the earth ranging from 0.52 W/m-K to 5 W/m-K. For instance, when k = 3 W/m-K and L = 150 m, a water inlet velocity of 0.0084212 m/s would be required to maintain the bore hole exit water temperature below or equal to 295 K at all of the intermediate times, with the maximum time being 10368000 s.

4.4.8 ANSYS-CFX Runs of Cylindrical Model with U-tube When L = 100 m and D_i = 0.2 m

After conducting multiple runs on the cylindrical model with L = 150 m (U-tube), it was decided to run a few more cases by changing the depth of the bore hole to 100 m for different inlet parameters. These runs were conducted in order to check the effect of bore hole depth on the total number of bore holes required. All of the runs conducted on the cylindrical model with U-tube (L = 100 m) used D_i = 0.2 m, D_o = 12 m, ρ = 2050 kg/m^3, C_p = 1840 J/kg-K, T_{in} = 305.1 K, T_{op} = 285 K, wall roughness (e) = 0 m, and turbulence (I) = medium intensity (5 %). Although some of the results, including radial temperature distributions and temperature of water at different depths, are not discussed in detail here, bore hole exit water temperature at different inlet velocities for different earth thermal conductivities are discussed in this section. First, four runs were conducted at four different thermal conductivities of the earth, while keeping the inlet velocity of water constant and equal to 0.00621 m/s for a total time equal to 1038000 s (4 months) with time steps given by Eq. (4-4). Table 57 shows the area averaged bore hole exit water temperatures for different thermal conductivities of the earth when inlet velocity equals 0.00621 m/s.

Table 57. Bore hole exit water temperature for different thermal conductivities of earth for V_{in} = 0.00621 m/s and L = 100 m (U-tube).

k (W/m-K)	0.52	2.4	4	5
T_{exit} (K)	301.930	296.573	294.129	293.069

Values from Table 57 were used to derive an equation to determinine T_{exit} for any value of thermal conductivity of the earth ranging from 0.52 W/m-K to 5 W/m-K, when the inlet velocity is 0.00621 m/s and L = 100 m.

$$T_{exit} = (0.317367\frac{m^2K^3}{W^2})\,(k^2) - (3.7088\frac{K^2\,m}{W})\,k + (303.746\ K) \qquad (4\text{-}16)$$

For instance, for k = 3 W/m-K, V_{in} = 0.00621 m/s, and L = 100 m, the bore hole exit water temperature would be 295.4759 K. In Sections 4.4.8.1 through 4.4.8.4, results of three or four runs (with different inlet velocities) are presented for each of the four earth thermal conductivity values listed in Table 57. These results helped in determining the flow rate required to reach 295 K at the bore hole exit, and helped to determine installation costs for different k values when L = 100 m (Section 4.4.10).

4.4.8.1 Results from Runs Conducted with k = 0.52 W/m-K at Different Inlet Velocities (U-tube, L = 100 m)

Table 58 shows the results from the runs conducted on the U-tube model (L = 100 m, D_i = 0.2 m, D_o = 12 m, and T_{in} = 305.1 K), at different inlet water velocities keeping the thermal conductivity of the earth constant, and equal to 0.52 W/m-K. Since Eq. (4-17) was used to determine V_{in} for which T_{exit} would be equal to 295 K, and 295 K was in between 299.425 K and 294.458 K, the first set of values for T_{exit} and V_{in}, (i.e., 301.93, 0.00621) was not used in deriving Eq. (4-17). (Also, if the first set of values were included, the trend line would not accurately fit all of the four sets of values.)

$$T_{exit} = (-3.677019 \times 10^5 \frac{s^2\ K}{m^2})\ (V_{in})^2 + (4.22169 \times 10^3\ \frac{s\ K}{m})\ V_{in} + (289.881\ K) \qquad (4\text{-}17)$$

Table 58. Bore hole exit water temperature at different values of inlet velocity for k = 0.52 W/m-K, D_i = 0.2 m, and L = 100 m (U-tube).

k = 0.52 W/m-K	
T_{exit} (K)	V_{in} (m/s)
301.930	0.00621
299.425	0.003145
296.502	0.001791
294.458	0.001258

Equation (4-17) was used to interpolate for the inlet velocity at which the bore hole exit water temperature was equal to 295 K at the maximum simulation time. It was determined that, for V_{in} = 0.001378 m/s, the bore hole exit water temperature, at time 10368000 s, was equal to 295 K. For k = 0.52 W/m-K and L = 100 m (U-tube), a mass flow rate (Eq. (4-9)) of 0.04315859 kg/s (density of water was found at T_{in} = 305.1 K, ρ_w = 997 kg/m^3) would be required to maintain the bore hole exit water temperature less than or equal to 295 K at all of the intermediate times up to maximum simulation time. The number of bore holes required is summarized in Section 4.4.10.

4.4.8.2 Results from Runs Conducted with k = 2.4 W/m-K at Different Inlet Velocities (U-tube, L = 100 m)

Table 59 shows the results from the runs conducted on the U-tube model (L = 100 m, D_i = 0.2 m, and D_o = 12 m), at different inlet water velocities keeping the thermal conductivity of the earth constant, and equal to 2.4 W/m-K. Values from Table 59 were used to develop an equation for the bore hole exit water temperature versus the water inlet velocity (for t = 10368000 s).

$$T_{exit}\,[K] = (1.044127x\ 10^{3}\,\frac{s\,K}{m})\,(V_{in}) + (290.1084878\ K) \tag{4-18}$$

Table 59. Bore hole exit water temperature at different values of inlet velocity for k = 2.4 W/m-K, D_i = 0.2 m, and L = 100 m (U-tube).

k = 2.4 W/m-K	
T_{exit} (K)	V_{in} (m/s)
296.573	0.00621
295.221	0.004838
294.445	0.004193

Equation (4-18) was used to interpolate for the inlet velocity at which the bore hole exit water temperature was equal to 295 K for maximum simulation time. It was found that, for V_{in} = 0.00468337 m/s, the bore hole exit water temperature, at time 10368000 s was equal to 295 K. For k = 2.4 W/m-K, and L = 100 m (U-tube), a mass flow rate (Eq. (4-9)) of 0.146691011 kg/s (density of water was found at T_{in} = 305.1 K, ρ_w = 997 kg/m^3) would be required to maintain the bore hole exit water temperature less than or equal to 295 K at all of the intermediate times up to maximum simulation time. The number of bore holes for each individual case is shown in Section 4.4.10.

4.4.8.3 Results from Runs Conducted with k = 4 W/m-K at Different Inlet Velocities (U- tube, L = 100 m)

Table 60 shows the results from the runs conducted on the U-tube model (L = 100 m, D_i = 0.2 m, and D_o = 12 m), at different inlet water velocities keeping the thermal conductivity of the earth constant, and equal to 4 W/m-K. Values from Table 60 were used to develop an equation for the bore hole exit water temperature versus the water inlet velocity (for t = 10368000 s).

$$T_{exit}\,[K] = (7.568807\ x\ 10^{2}\ \frac{s\,K}{m})\,(V_{in}) + (289.4403\ K) \tag{4-19}$$

Table 60. Bore hole exit water temperature at different values of inlet velocity for k = 4 W/m-K, D_i = 0.2 m, and L = 100 m (U-tube).

k = 4 W/m-K	
T_{exit} (K)	V_{in} (m/s)
294.129	0.00621
295.381	0.0078625
294.752	0.00698889

Equation (4-19) was used to interpolate for the inlet velocity at which the bore hole exit water temperature was equal to 295 K for maximum simulation time. It was found that, for V_{in} = 0.00734548 m/s, the bore hole exit water temperature, at time 10368000 s, was equal to 295 K. For k = 4 W/m-K and L = 100 m, a mass flow rate (Eq. (4-9), ρ_w = 997 kg/m^3) of 0.2300729 kg/s would be required to maintain the bore hole exit water temperature less than or equal to 295 K at all of the intermediate times. Number of bore holes required is shown in Section 4.4.10.

4.4.8.4 Results from Runs Conducted with k = 5 W/m-K at Different Inlet Velocities (U- tube, L = 100 m)

Table 61 shows the results from the runs conducted on the U-tube model (L = 100 m, D_i = 0.2 m, and D_o = 12 m) at different inlet water velocities keeping the earth's thermal conductivity constant and equal to 5 W/m-K. Values from Table 61 were used to develop an equation for the bore hole exit water temperature versus the water inlet velocity (for t = 10368000 s).

$$T_{exit}\,[\mathrm{K}] = (6.32186 \times 10^{2}\,\tfrac{\mathrm{s\,K}}{\mathrm{m}})\ (V_{in}) + (289.2017)\ \mathrm{K} \qquad (4\text{-}20)$$

Table 61. Bore hole exit water temperature at different values of inlet velocity for k = 5 W/m-K, D_i = 0.2 m, and L = 100 m (U-tube).

k = 5 W/m-K	
T_{exit} (K)	V_{in} (m/s)
293.069	0.00621
294.268	0.0078625
295.792	0.010483

Equation (4-20) was used to interpolate for the inlet velocity at which the bore hole exit water temperature was equal to 295 K. For V_{in} = 0.00917169 m/s, the bore hole exit water temperature, at time 10368000 s, was equal to 295 K. For k = 5 W/m-K and L = 100 m U-tube, a mass flow rate (Eq. (4-9), ρ_w = 997 kg/m^3) of 0.2872727 kg/s would be required to maintain the bore hole exit water temperature at the outlet less than or equal to 295 K for all of the intermediate times. The number of bore holes required for each case is summarized in Section 4.4.10.

4.4.8.5 Inlet Velocity of Water Required to Reach 295 K at the Bore Hole Exit for Different Thermal Conductivities of the Earth (U-tube, L = 100 m)

Table 62 summarizes the inlet velocities of water (from Sections 4.4.8.1-4.4.8.4) required to reach the target bore hole exit water temperature of 295 K, at 103680000 s, for different values of earth thermal conductivity when the depth of the bore hole is 100 m.

Table 62. Inlet velocities of the water for different thermal conductivities of earth to reach 295 K at the bore hole exit for D_i = 0.2 m and L = 100 m (U-tube).

k (W/m-K)	0.52	2.4	4	5
V_{in} (m/s)	0.001378	0.00468337	0.00734548	0.00917169

Values from Table 62 were used to derive an equation for water inlet velocity as a function of thermal conductivity of the earth.

$$V_{in}\,[m/s] = \left(0.00173023\,\frac{m^2\,K}{Ws}\right) k + \left(0.00048852\,\frac{m}{s}\right) \qquad (4\text{-}21)$$

For D_i = 0.2 m and L = 100 m (U-tube), Eq. (4-21) can be used to interpolate for the water inlet velocity required to reach the target bore hole exit water temperature of 295 K at different earth thermal conductivities. For instance, for k = 3 W/m-K and L = 100 m, a water inlet velocity of 0.00567921 m/s would be required to maintain the bore hole exit water temperature equal to 295 K.

Figure 80 shows the thermal conductivity of the earth plotted, versus water inlet velocity required to reach 295 K at the bore hole exit, for two different depths of the bore hole. As can be seen from Fig. 80, for any k from 0.52 W/m-K to 5 W/m-K, a lower inlet velocity is required to achieve the target bore hole exit water temperature of 295 K when L = 100 m as compared to that for L = 150 m. Therefore, a bore hole of greater depth is suggested. On the other hand, the cost to drill the bore hole should also be considered (see Section 4.4.9).

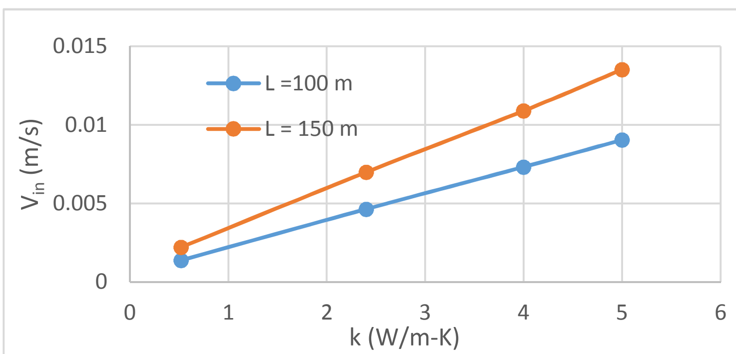

Figure 80. Inlet velocity of the water required to reach the target 295 K at the bore hole exit vs. thermal conductivity of the earth for two different depths of the bore hole.

4.4.9 Cost to Install the Ground Loop Cooling System

The cost of installing a ground loop cooling system involves various parameters such as land acquisition, HDPE tubes, drilling bore holes, and pumps. Assuming that the ground loop cooling system would be installed in Kansas, an acre of non-irrigated land would cost \$1200-\$4000/acre [25]. From all of the results produced by ANYS-CFX, the Finite Difference method, and the closed form solution, it is clear that a minimum spacing of 20 m (2 x 10 m) would be needed between the bore holes. Therefore, a minimum of 8325.44 acres (84230 bore holes) (k = 5

W/m-K, L = 150 m, spacing = 20 m) to a maximum of 81823.58 acres (827824 bore holes) (k = 0.52 W/m-K, L = 100 m, spacing = 20 m) of land would be required to install the ground loop cooling system. Therefore, each bore hole would require a maximum of 400 m^2 (0.0988422 acre) of land. So, the land cost would range from \$118.66 to \$395.37/bore hole (based on land cost).

Assuming all of the bore holes that should be drilled are 150 m deep, and 0.6 m in diameter (two 0.2 m diameter tubes with 0.2 m spacing between the tubes), drilling would cost \$360-410 /meter, which includes the U-tubes with U-bends, grout, sand, and water to fill the bore hole [26]. Therefore, to drill a 150 m deep bore hole would cost approximately \$54000-\$61500 [26]. Excluding the pump power required and the cost of the HDPE tubing for completely installing a bore hole, it would cost approximately \$54310-\$61810/bore hole (cost to drill per bore hole [\$54000-\$61500] + average land cost per bore hole [\$310.5]). The costs previously described are approximate and may vary depending on the location (freight considerations), drilling conditions, and the contractor. Based on the volume of the project, minimal mobility fees, and soil conditions, the bore hole cost may have a 25% variance [26].

4.4.10 Summary of All Results from the Cylindrical Model with U-Tube

A typical fossil-fueled 1000 MW thermal power plant operating at full capacity with η = 40% would reject about 1500 MW at full load, which requires 35727.73 kg/s of circulating cooling water, based on a 10 ^oC difference in temperatures from the inlet to the outlet of the cooling system (with $C_{p\ (water)}$ = 4198.42 J/kg-K). ρ_w = 997 kg/m^3 was used to convert gal/min to kg/s in Table 63 [6]. Table 63 shows cooling water flow required and evaporation rate from wet cooling towers serving a 1000 MW plant for two different cycle thermal efficiencies.

Table 63. Circulating cooling water flow required and evaporation from wet cooling towers serving a typical 1000 MW plant (reproduced from Ref. 6).

		Circulating Water Flow ($\dot{M}$)			Evaporation Rate		
η	$\dot{Q}_r$ (MW)	gal/min	kg/s	Climate	gal/min	kg/s	m^3/s
0.33	2000	757333.3	47636.97	Hot	10000	629.01	0.63
				Cold	8000	503.21	0.5
0.4	1500	568000.0	35727.73	Hot	7500	471.76	0.47
				Cold	6000	377.41	0.38

A ground loop cooling system substituting for this wet cooling system would require 35727.73/$\dot{m}$ bore holes Eq. (4-8) (where $\dot{m}$ is the mass flow rate of water through each tube required to reach 295 K at the bore hole exit, Eq. (4-9). The number bore holes required for different earth thermal conductivities, depths of the bore hole and water inlet velocities was calculated using the mass flow rate required to reach the different bore hole exit water temperatures for each individual case (Sections 4.4.7.1-4.4.8.4). The costs from Section 4.4.9 were used to find the total cost.

Table 64 summarizes of all of the results from the runs conducted using the cylindrical model with a U-tube and L = 100 m. Since this thesis is aimed at substituting for a wet cooling system operating over a range of 10 ^{o}C, the cost to install and the number of bore holes required for different thermal conductivities of the earth will only be discussed for the case where T_{exit} = 295 K. For k = 0.52 W/m-K and L = 100 m, 827824 bore holes are required, which would cost 34,111.82 million USD. For increased earth thermal conductivity, the number of bore holes required decreases, because, lower water temperatures at the bore hole exit can be achieved at higher mass flow rates. For k = 2.4 W/m-K and L = 100 m, 243558 bore holes are required, which would cost 10,036.18 million USD.

Table 64. Summary of results from the runs conducted using the cylindrical model for L = 100 m (U-tube).

L = 100 m					
k (W/m-K)	V_{in} (m/s)	$\dot{m}$ (kg/s)	T_{exit} (K)	B_{num}	Cost to install (million USD)
0.52	0.00621	0.1945076	301.930	183683	$7,568.95
0.52	0.003145	0.0985067	299.425	362693	$14,945.36
0.52	0.001791	0.0560971	296.502	636891	$26,244.10
0.52	0.001258	0.0394027	294.458	906733	$37,363.38
0.52	0.001378	0.04315859	295.00	827824	$34,111.82
2.4	0.00621	0.1945076	296.573	183683	$7,568.95
2.4	0.004838	0.1515343	295.221	235773	$9,715.41
2.4	0.004193	0.1313318	294.445	272042	$11,209.91
2.4	0.00468337	0.146691011	295.00	243558	$10,036.18
4	0.00621	0.1945076	294.129	183683	$7,568.95
4	0.0078625	0.2462667	295.381	145077	$5,978.14
4	0.00698889	0.2189038	294.752	163212	$6,725.41
4	0.00734548	0.2300729	295.00	155289	$6,398.92
5	0.00621	0.1945076	293.069	183683	$7,568.95
5	0.0078625	0.2462667	294.268	145077	$5,978.14
5	0.010483	0.3283452	295.792	108811	$4,483.75
5	0.00917169	0.2872727	295.00	124369	$5,124.81

Figure 81 shows the number of bore holes required to maintain the cycle thermal efficiency at four different earth thermal conductivities, when L = 100 m and D_i = 0.2 m (U-tube).

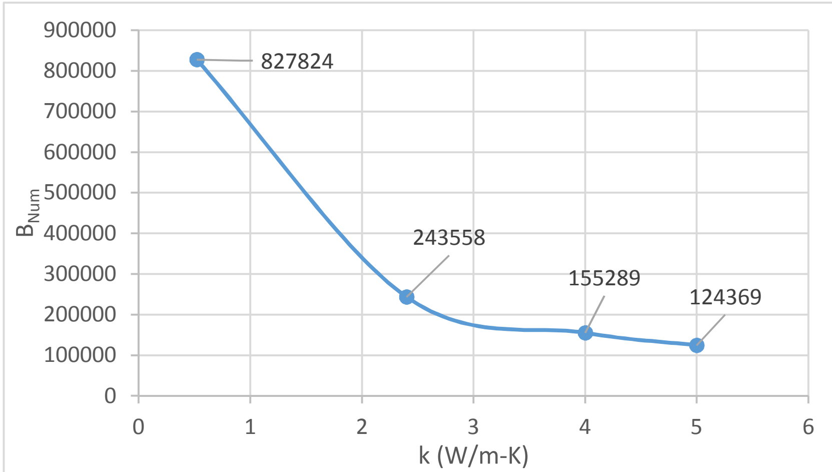

Figure 81. Number of bore holes required to substitute for a wet cooling system serving a 1000 MW power plant vs. thermal conductivity of the earth for L = 100 m (U-tube).

As can be seen from Fig. 81, the number bore holes required decreases with increasing thermal conductivity of the earth. This is due to better heat transfer in the earth domain. In addition, for higher earth thermal conductivity, the cost to install the ground loop cooling system will decrease. For instance, when the thermal conductivity of the earth is increased from 0.52 W/m-K to 5 W/m-K, the total cost to install the ground loop cooling system decreases by 28,987.01 million USD (see Table 64).

Table 65 summarizes all of the results from the runs conducted with the cylindrical model of a U-tube and L = 150 m. For k = 0.52 W/m-K and L = 150 m, 559296 bore holes are required, which would cost 34,570.03 million USD as compared to 34,111.82 million USD for L = 100 m. So increasing the bore hole depth from 100 m to 150 m (while keeping all of the other inputs constant) increases the total cost to install by 458.21 million USD. On the other hand, for higher earth thermal conductivity, the cost to install decreases. Comparing the cost to install the ground loop cooling system for two different bore hole depths, L = 150 m and L = 100 m, while keeping earth thermal conductivity constant, indicates that, for all of the values of earth thermal conductivity, the difference between the costs to install is within the range of 0.02 to 1000 million USD. This effect of bore hole depth on the cost to install can be taken into consideration during further development of the project by finding the optimum depth that minimizes the cost to install the ground loop cooling system.

Table 65. Summary of results from the runs conducted using the cylindrical model for L = 150 m (U-tube).

L = 150 m					
k (W/m-K)	V_{in} (m/s)	$\dot{m}$ (kg/s)	T_{exit} (K)	B_{num}	Cost to install (million USD)
0.52	0.00621	0.194507625	300.620	183683	$11,353.41
0.52	0.01258	0.394026719	302.098	90673	$5,604.51
0.52	0.003145	0.09850668	297.407	362693	$22,418.02
0.52	0.001398	0.043780503	292.879	816065	$50,440.83
0.52	0.002039474	0.063879749	295.00	559296	$34,570.03
2.4	0.00621	0.194507625	294.407	183683	$11,353.41
2.4	0.006989	0.218907213	295.026	163209	$10,087.95
2.4	0.0077625	0.243134531	295.590	146946	$9,082.73
2.4	0.006977	0.218531353	295.00	163490	$10,105.30
4	0.00621	0.194507625	292.253	183683	$11,353.41
4	0.0077625	0.243134531	293.254	146946	$9,082.73
4	0.0104833	0.328354555	294.763	108808	$6,725.43
4	0.01258	0.394026719	295.957	90673	$5,604.51
4	0.010875	0.34062822	295.00	104888	$6,483.09
5	0.00621	0.194507625	291.428	183683	$11,353.41
5	0.00898571	0.281447522	292.950	126943	$7,846.31
5	0.01258	0.394026719	294.616	90673	$5,604.51
5	0.014615176	0.457771848	295.400	78047	$4,824.07
5	0.013542	0.424168616	295.00	84230	$5,206.24

Figure 82 shows the number bore holes required for L = 150 m while varying earth thermal conductivity. For higher earth thermal conductivity (k = 5 W/m-K), the cost to install the ground loop cooling system decreases by approximately 29,363.79 million USD when compared to that

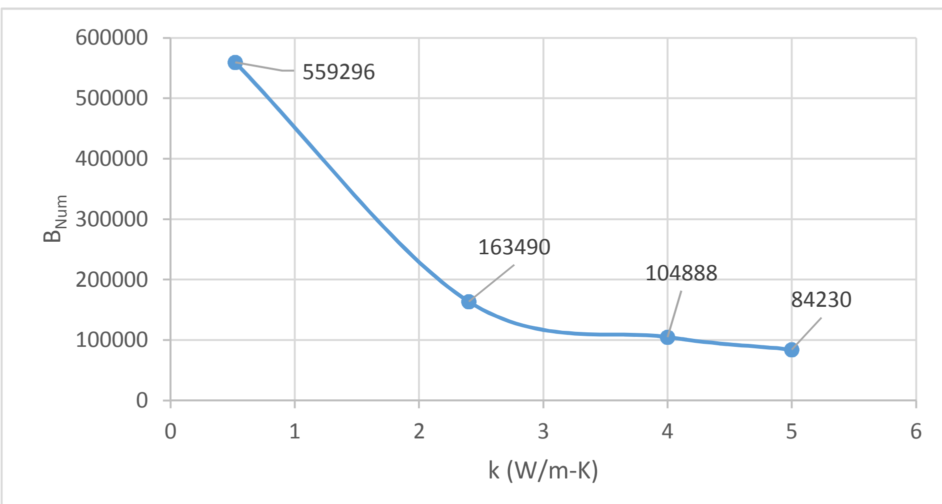

Figure 82. Number of bore holes required to substitute for a wet cooling system serving a 1000 MW power plant vs. thermal conductivity of the earth for L = 150 m (U-tube)

of k = 0.52 W/m-K. The total cost to install a ground loop cooling system ranges from 34,570.03 million USD for k = 0.52 W/m-K to 5,206.24 million USD for k = 5 W/m-K USD (see Table 65).

These costs, when compared to a wet cooling system (~ 39 million USD) for the same 1000 MW thermal power plant, are between approximately 864:1 (k = 0.52 W/m-K) and 133:1 (k = 5 W/m-K). Therefore, it is clear from these results that total cost to install a ground loop cooling system is not yet reasonable and still needs to be investigated for potential reduction.

4.4.11 Thermal Efficiency of the Power Plant

In all of the cases solved, water exits bore hole at a temperature lower than 295 K during the initial times and increases with increasing time. When trying to achieve a bore hole exit temperature of 295 K at the maximum time (i.e., 10368000 s or four months), the bore hole exit water temperature during the initial time periods is less than 295 K. Since the Carnot cycle thermal efficiency (Eq. (2-1)) increases with decreasing T_c (cold reservoir temperature), the cycle efficiency of the power plant will be potentially larger initially, then decrease with increasing time. This higher initial cycle efficiency of the plant is desirable. An approximately constant thermal efficiency could be achieved by making the water inlet velocity a time dependent variable, so that bore hole exit water temperature remained nearly constant.

4.4.12 Extracting Thermal Energy from the Earth

After using ground loop cooling as a substitute for wet cooling for four summer months of the year, it is important to extract the heat energy that has been rejected to the earth. This needs to be done in order to reuse the earth for the next cycle (next year). The winter season is the best time to extract this heat from the earth domain. Therefore, three different runs were conducted at different inlet temperatures of water while keeping the inlet water velocity constant and equal to 0.00621 m/s. It was determined that all of the energy that was rejected to the earth can be extracted. The time to extract the stored energy was determined for different inlet water temperatures [T_{in} = 285 K, 283 K, and 275 K]. For T_{in} = 283 K, it would take approximately three months to extract all of the energy that is rejected to the earth from cooling the warm cooling water during the four summer months. The results obtained from these three runs are presented and discussed in Appendix G. This extracted energy can be used in base warming (low level warming) of residential or commercial buildings or also could be used in melting the snow during the winter.

CHAPTER 5

CONCLUSIONS AND RECOMMENDATIONS

5.1 Conclusions

The primary objective of this thesis was to design a ground loop cooling system as a substitute for the wet cooling system of a thermal power plant. In order to design a ground loop cooling system, it was important to determine the number of bore holes required and the spacing required between the bore holes. A ground loop cooling system has been modeled to substitute for a wet cooling system of a 1000 MW thermal power plant operating at full load with 40% efficiency. The modelling of the ground loop cooling system was performed for different inputs such as earth thermal conductivity, bore hole depth, inlet water velocity, and inner diameter of the tube. It was determined that installing a ground loop cooling system is currently too high in cost (see Tables 64 and 65).

It was found that, to provide cooling for a 40% efficient 1000 MW power plant operating at full load, it would take a minimum of 84230 bore holes (0.6 m diameter) at a total installation cost of 5,206.24 million USD for earth thermal conductivity of 5 W/m-K and bore hole depth of 150 m (see Table 65). For that same plant, it would take a maximum of 827824 bore holes at a total installation cost of 34,111.82 million USD for earth thermal conductivity of 0.52 W/m-K and bore hole depth of 100 m (see Table 64). The cost to install a ground loop cooling system primarily depends on bore hole drilling expenses.

The capital cost to install traditional cooling systems for the same 1000 MW power plant ranges from 19 million USD for once-through cooling systems to 182 million USD for dry cooling systems [27]. Although a ground loop cooling system reduces water consumption of thermal power plants, the installation cost as compared to that of wet cooling systems is very high, and is between approximately 864:1 (k = 0.52 W/m-K) and 133:1 (k = 5 W/m-K). Considering the scarcity of fresh water and large amounts of water consumption for cooling in thermal power plants, future studies are needed to explore methods for reducing the installation cost of the ground loop cooling systems. Future studies need to examine enhancement of heat transfer from the cooling water to the earth in order to reduce the number of bore holes required. Some recommendations for future work are discussed in Section 5.2.

5.2 Recommendations for Future Work

As discussed in Section 4.4.9, bore hole drilling expenses significantly affect the total cost of installing a ground loop cooling system. Therefore, it is important to reduce the number of bore holes required or reduce the cost per bore hole. Some recommendations are:

- As can be seen from Tables 64 and 65, at higher L values, the cost to install the bore holes (for T_{exit} = 295 K) increases; therefore, future studies could investigate changing the bore hole depth to analyze cost sensitivity.
- For all of the runs conducted using a cylindrical model with U-tube, inner diameter was kept constant and equal to 0.2 m. Thus, future studies should examine decreasing the tube diameter. Since the cost to drill a bore hole is determined by the diameter and depth of the bore hole, at smaller diameters, the total cost to drill decreases. For instance, it would cost approximately 1/3 to drill a bore hole of 0.16 m diameter compared to 0.6 m diameter. On the other hand, decreasing the diameter will decrease the mass flow rate per bore hole, which in turn increases the number of bore holes required. Therefore, cost sensitivity to the number of bore holes required for different diameters can be studied.
- Since the bore hole exit water temperature increases with time, future studies could make the inlet velocity a time-dependent variable, so that the exit water temperature could remain almost constant. Doing so, the number of bore holes required during the initial time periods could be reduced. However, the number of bore holes needed during the later time periods will increase to that shown in Tables 64 and 65, because the mass flow rate of water has to be reduced in order to reach the target bore hole exit water temperature.
- Studies could be done by decreasing the 0.2 m spacing that between the tubes. Decreasing the spacing between the tubes would decrease the total diameter of the bore hole (which is 0.6 m for all of the cases studied in this thesis). This in turn would decrease the total cost of installation, because it costs less to drill a smaller diameter bore hole.
- As can be seen from Figs. 74 and 78, for Runs 4-2 and 4-3 with a U-tube (Sections 4.4.7), water temperature at the top section of the riser increases due to heat transfer from the higher surrounding earth temperature, which is not desirable. Therefore, future studies can be done to help determine the length of the bore hole such that the water is always at a higher temperature than the earth temperature.

REFERENCES

1. A. Sieminski. International Energy Outlook 2016, U.S. Energy Information Administration, May 2016 [cited 07/2016]; available from: http://www.eia.gov/pressroom/presentations/sieminski_05112016.pdf
2. J. Maulbetsch and B. Barker. "Water Use for Electric Power Generation," EPRI, Palo Alto, CA, 2008 [cited 11/2015]; available from: http://ucowr.org/files/Achieved_Journal_Issues/v143An_Electric_Power_Industry_Perspective.pdf
3. B. Sean. "Advanced Cooling Technologies for Water Savings at Coal-Fired Power Plants," Cornerstone, 2014, 2(1) [cited 09/2015]; available from: http://cornerstonemag.net/advanced-cooling-technologies-for-water-savings-at-coal-fired-power-plants/
4. M. A. Maupin, J. F. Kenny, S. S. Hutson, J. K. Lovelace, N. L. Barber and K. S. Linsey. "Estimated Use of Water in the United States in 2010," 2014, U.S. Geological Survey Circular 1045. p. 56 [cited 11/2015]; available from: https://pubs.usgs.gov/circ/1405/pdf/circ1405.pdf
5. "Theory of Thermal Power Station" [cited 09/2016]; available from: http://www.electrical4u.com/thermal-power-generation-plant-or-thermal-power-station/
6. M. M. El-Wakil. <u>Power Plant Technology</u>. New York, McGraw Hill, 1984
7. J. Fisher, A. Huber-Lee, A. Lewis, J. Macknick, N. Madden, J. Rogers and S. Tellinghuisen. "Freshwater Use by U.S. Power Plants: Electricity's Thirst for a Precious Resource," a report of the Energy and Water in a Warming World initiative, Cambridge, MA, Union of Concerned Scientists, November, 2011 [cited 03/2016]; available from: http://www.ucsusa.org/sites/default/files/legacy/assets/documents/clean_energy/ew3/ew3-freshwater-use-by-us-power-plants.pdf
8. A. Williams and R. Stancich. "When It Comes to Cooling Options, Must Developers Face a Trade-Off Between Financial and Environmental Costs," Concentrating Solar Panels Today. 2010 [cited 04/2015]; available from: http://analysis.newenergyupdate.com/csp-today/technology/cooling-cost-efficiency-vs-water-usage
9. R. A. Paddock and J. D. Ditmars. "An Assessment of the Once-Through Cooling

Alternative for Central Steam-Electric Generating Stations," US Department of Energy, Argonne National Laboratory, Energy and Environmental Systems Division, December 1978 [cited 11/2015]; available from: http://www.iaea.org/inis/collection/NCLCollectionStore/_Public/11/517/11517186.pdf

10. U.S. Energy Information Administration, "Annual Electric Generator Report. 2013" [cited 08/2015]; available from: http://www.iaea.org/inis/collection/NCLCollectionStore/_Public/11/517/11517186.pdf

11. J. Fernandes, N. Flynn, S. Gibbes, M. Griffis, T. Isshiki, S. Killian, L. Palombi, N. Rujanavech, S. Tomsky, and M. Tondro. "Renewable Energy in the California Desert Mechanisms for Evaluating Solar Development on Public Lands," School of Natural Resources and Environment, University of Michigan, April 2010 [cited 06/2015]; available from: http://erb.umich.edu/Research/InstituteReports/09-10/renewable-energy-in-CA-desert.pdf

12. A. D. Martin. "Water for Thermal Power Plants: Understanding a Piece of the Water Energy Nexus," Global Water Forum, June 22, 2015 [cited 09/2016]; available from: http://www.globalwaterforum.org/2015/06/22/water-for-thermal-power-plants-understanding-a-piece-of-the-water-energy-nexus/

13. W. Mills, A. Gabriel, and D. Gabriel. "Viability and Impacts of Implementing Various Power Plant Cooling Technologies in Texas," Water Conservation and Technology Center, Texas A&M University System, August 2012 [cited 09/2016]; available from: http://twri.tamu.edu/media/370735/goes%20with%20water%20value%20in%20power%20generation1_final%20report.pdf

14. J. F. Kenny, N. L. Barber, S. S. Hutson, K. S. Linsey, J. K. Lovelace, and M. A. Maupin. "Estimated Use of Water in the United States in 2005," U.S. Geological Survey Circular 1344, 52 p [cited 02/2016]; available from: https://pubs.usgs.gov/circ/1344/pdf/c1344.pdf

15. G. Reysa. "Ground Temperatures as a Function of Location, Season, and Depth," 2005 [cited 01/2016]; available from: http://www.builditsolar.com/Projects/Cooling/EarthTemperatures.htm

16. A. Mustafa. "Experimental Investigation of the Performance of a Ground Source Heat Pump System for Buildings Heating and Cooling," Innovative Mathematics, Statistics & Energy Policies, January-March, 2016 [cited 11/2016]; available from:

http://seahipaj.org/journals-ci/mar-2016/IJIMSEP/full/IJIMSEP-M-2-2016.pdf

17. “Temperature and Thermal Properties (Basic),” British Geological Survey, 2011 [cited 09/2016]; available from: https://shop.bgs.ac.uk/GeoReports/examples/modules/C012.pdf
18. Software by Environmental Systems Research Institute, ArcGIS® and ArcMap™ [cited 08/2016]; available from: http://www.arcgis.com/home/webmap/viewer.html?webmap=7498b9f186bc4a2a9fee6c85d863f3b6
19. T. L. Bergman, F. P. Incropera, D. P. Dewitt, and A. S. Lavine. Fundamentals of Heat and Mass Transfer, 7 ed, 2011, John Wiley and Sons, United States of America
20. M. N. Ozisik. Boundary Value Problems of Heat Conduction. 2013, Mineola, NY: Dover
21. Wolfram Alpha [cited 11/2015]; available from http://www.wolframalpha.com/input/?i=2%2B2
22. R. J. LeVeque. Finite Difference Methods for Ordinary and Partial Differential Equations: Steady-State and Time-Dependent Problems, 2007, SIAM
23. CFD online [cited 08/2016]; available from: http://www.cfdonline.com/Wiki/Ansys_FAQ
24. F. S. V. Hurtado, C. R. Maliska, A. F. C. da Silva, and J. Cordazo. “A Quadrilateral Element-Based Finite-Volume Formulation for the Simulation of Complex Reservoirs,” Latin American & Caribbean Petroleum Engineering Conference, Society of Petroleum Engineers, 2007 [cited 07/2016]; available from: http://www.sinmec.ufsc.br/site/arquivos/b-byincwwxaj_spe107444.pdf
25. M. Hart. “Kansas Farm Land Prices Fall in June,” The Topeka Capital Journal, June 27, 2015 [cited 11/2016]; available from: http://cjonline.com/news-business-state/2015-06-27/kansas-farm-land-prices-fall-june
26. R. Heskett, Sales Manager, Email Communication, September 2016, CETCO
27. B. Lamya. “A Comparative Study of Cooling System Parameters in US Thermoelectric Power Plants,” Virginia Polytechnic Institute and State University, 2010 [cited 05/2016]; available from: https://theses.lib.vt.edu/theses/available/etd-09102010-173859/unrestricted/Badr_LA_T_2010.pdf

Appendix A. Calculations for β_m Values

Appendix A deals with calculations of the β_m values using Wolfram Alpha and MS Excel.The first 8 β_m values were calculated using Wolfram Alpha [21]. Figure A-1 shows how

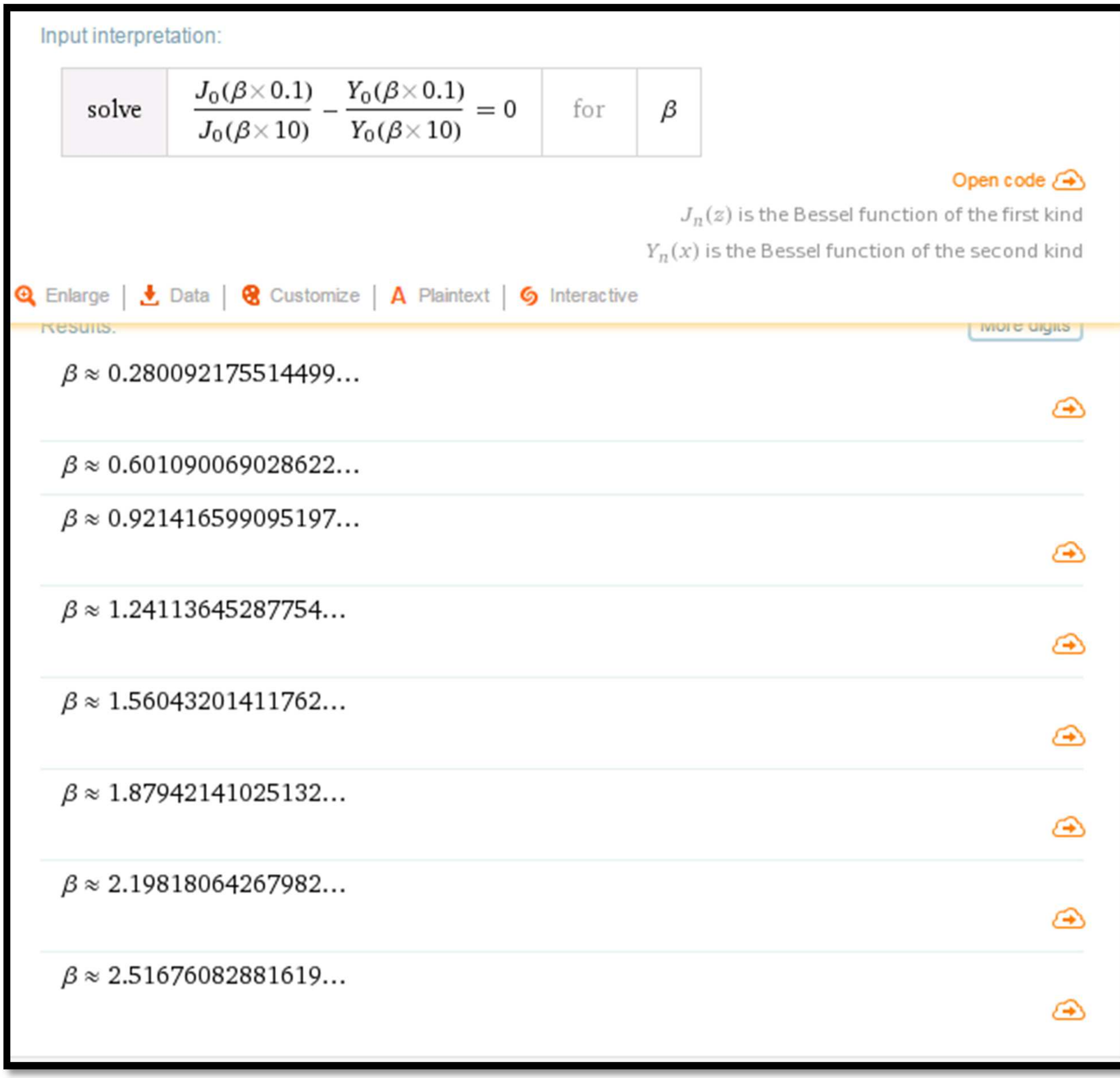

Figure A-1. Calculation of the first 8 zeros of Eq. (3-10) using Wolfram Alpha.

Wolfram Alpha was used to calculate the first 8 β_m values. Units of the β_m values are 1/m.

The other 90 values of β_m were calculated using Microsoft Excel. Table A-1 shows the results of the spreadsheet used to calculate the other 90 values of β_m (starting from m = 9) alongside the first 8 β_m values (calculated using Wolfram Alpha).

Table A-1. Calculated β_m values using MS Excel.

	A	B	C	D	E
m			β_{m+1}- β_m (1/m)	β_m (1/m)	Eq. (3-10) with β_m
1	r_i (m)	0.1 (Cell B1)	0.320998	0.280092	-7.58 x 10^{-13}
2	r_o (m)	10 (Cell B2)	0.320327	0.601090	2.05E-15
3	β_m (guess) (1/m)	Eq. (3-10)	0.319720	0.921417	-1.12E-15
4	12.36748890	-2.22E-04	0.319296	1.241136	-5.42E-14
5	12.36748800	3.72E-05	0.318989	1.560432	-2.53E-13
6	12.36748810	8.42E-06	0.318759	1.879421	-2.58E-14
7	12.36748813	-1.44E-10	0.318580	2.198181	8.31E-15
8	12.36748813	-1.24E-13	0.318437	2.516761	6.27E-14
9	12.36748813	6.93E-13	0.318320	2.835198	9.07E-11
10	12.3674881	-1.2E-13	0.318223	3.153518	1.34E-14
11			0.318141	3.471741	3.76E-12
12			0.318070	3.789881	1.12E-11
13			0.318010	4.107952	-9.64E-15
14			0.317957	4.425961	3.52E-15
15			0.317910	4.743918	1.67E-14
16			0.317869	5.061828	2.70E-14
17			0.317832	5.379698	5.89E-12
18			0.317800	5.697530	2.37E-14
19			0.317770	6.015330	1.02E-10
20			0.317743	6.333100	1.61E-14
21			0.317719	6.650843	6.24E-14
22			0.317697	6.968563	1.45E-14
23			0.317677	7.286260	3.04E-14
24			0.317659	7.603937	1.04E-13
25			0.317642	7.921596	5.16E-12
26			0.317626	8.239237	2.83E-14
27			0.317611	8.556863	9.53E-12
28			0.317598	8.874474	1.85E-12
29			0.317586	9.192072	1.28E-13
30			0.317574	9.509658	7.03E-13
31			0.317563	9.827232	4.81E-14
32			0.317553	10.144795	2.70E-14
33			0.317544	10.462348	-1.91E-14
34			0.317535	10.779892	-5.45E-14
35			0.317527	11.097427	1.89E-14
36			0.317519	11.414953	-4.57E-14
37			0.317511	11.732472	1.75E-14
38			0.317505	12.049984	-4.56E-15
39			0.314498	12.367488	9.37E-13

m	C	D	E
40	0.317492	12.684986	3.56E-13
41	0.317486	13.002478	7.17E-14
42	0.317481	13.319964	-6.73E-15
43	0.317475	13.637445	5.78E-14
44	0.317470	13.954920	1.03E-14
45	0.317466	14.272390	-4.35E-15
46	0.317461	14.589856	2.52E-14
47	0.317457	14.907317	3.26E-15
48	0.317453	15.224775	2.19E-14
49	0.317449	15.542228	1.81E-15
50	0.317445	15.859677	1.18E-14
51	0.317442	16.177122	5.62E-14
52	0.317439	16.494564	-4.97E-14
53	0.317435	16.812003	-1.23E-14
54	0.317432	17.129438	5.02E-14
55	0.317430	17.446871	-1.79E-11
56	0.317427	17.764300	-2.52E-15
57	0.317424	18.081727	1.28E-14
58	0.317421	18.399151	6.14E-14
59	0.317419	18.716572	-1.31E-12
60	0.317417	19.033991	2.14E-14
61	0.317414	19.351408	1.69E-14
62	0.317412	19.668823	3.80E-14
63	0.317410	19.986235	2.52E-14
64	0.317408	20.303645	4.24E-14
65	0.317406	20.621053	-9.90E-14
66	0.317404	20.938459	-5.39E-14
67	0.317403	21.255863	-1.54E-13
68	0.317401	21.573266	-2.86E-14
69	0.317399	21.890667	-3.64E-14
70	0.317398	22.208066	-8.34E-13
71	0.317396	22.525463	1.71E-13
72	0.317394	22.842859	-1.43E-13
73	0.317393	23.160254	3.03E-13
74	0.317392	23.477647	3.59E-13
75	0.317390	23.795038	-5.65E-12
76	0.317389	24.112429	-1.39E-12
77	0.317388	24.429818	-5.59E-13
78	0.317386	24.747205	-5.17E-11

m	C	D	E
79	0.317385	25.064592	-4.77E-13
80	0.317384	25.381977	-9.17E-14
81	0.317383	25.699361	-3.21E-11
82	0.317382	26.016745	-1.94E-13
83	0.317381	26.334127	-2.91E-11
84	0.317380	26.651507	-3.71E-12
85	0.317379	26.968887	-1.34E-11
86	0.317378	27.286266	1.79E-14
87	0.317377	27.603644	8.91E-14
88	0.317376	27.921022	1.77E-14
89	0.317375	28.238398	-2.16E-14
90	0.317375	28.555773	-3.11E-14
91	0.317374	28.873148	9.65E-15
92	0.317373	29.190521	-2.63E-14
93	0.317372	29.507894	-6.17E-14
94	0.317371	29.825266	-7.33E-15
95	0.317371	30.142638	-2.75E-14
96	0.3173700	30.460008	-1.14E-14
97	0.317369	30.777378	1.13E-14
98	N/A	31.094746	2.14E-13

Table A-1 shows the first 8 values of β_m calculated using Wolfram Alpha, and shows calculations performed with MS Excel to find the next 90 values of β_m. The Eq. (3-10) solution with Excel does not exactly equal zero, and column E shows how close that value is to zero when β_m is substituted into the equation. Cells B1and B2 are the inner radius and outer radius of the earth, respectively, for which the temperature distribution is to be determined. In order to determine the next β_m value, guesses were made for that next β_m value in cells A4, A5, and A6. These guesses were made using the existing β_m values calculated [21]. For each β_m value computed, guesses were made, based on the current number of known β_m values. For instance, shown in cells A4-A10 are the values used in determining the 39th β_m value. The previous 38 β_m values were used to guess the β_m values which were input into cells A4, A5, and A6. With these guesses in cells A4-A6 and the equations shown on the following page for cells A7-A10, values were computed for cells A7-A10. Cells B7-B10 (Eq. (3-10)) were computed using the corresponding calculated β_m values (cells A7-A10) from column A. Once one of cells B7-B10 was on the order of 10^{-10} or less, the corresponding row value from column A was placed in column D, which displays the final β_m values. Next, for the 40th β_m value, the process was started over by guessing the values for cells A4-A6.

Cell A7 = IF(B6*B5<0, (A6*ABS(B5/(B5-B6))+A5*ABS(B6/(B5-B6))), (A6*ABS(B4/(B6-B4))+A4*ABS(B6/(B6-B4)))

Cell A8 = IF(B7*B6<0, (A7*ABS(B6/(B6-B7))+A6*ABS(B7/(B6-B7))),IF(B7*B5<0,(A7*ABS(B5/(B7-B5))+A5*ABS(B7/(B7-B5))), (A7*ABS(B4/(B7-B4))+A4*ABS(B7/(B7-B4)))))

Cell A9 = IF(B8*B7<0, (A8*ABS(B7/(B7-B8))+A7*ABS(B8/(B7-B8))),IF(B8*B6<0,(A8*ABS(B6/(B8-B6))+A6*ABS(B8/(B8-B6))), IF(B8*B5<0,(A8*ABS(B5/(B8-B5))+A5*ABS(B8/(B8-B5))), (A8*ABS(B4/(B8-B4))+A4*ABS(B8/(B8-B4))))))

Cell A10 = IF(B9*B8<0,(A9*ABS(B8/(B8-B9))+A8*ABS(B9/(B8-B9))),IF(B9*B7<0,(A9*ABS(B7/(B9-B7))+A7*ABS(B9/(B9-B7))), IF(B9*B6<0,(A9*ABS(B6/(B9-B6))+A6*ABS(B9/(B9-B6))),IF(B9*B5<0,(A9*ABS(B5/(B9-B5))+A5*ABS(B9/(B9-B5))), (A9*A4*ABS(B4/(B9-B4))+A4*ABS(B9/(B9-B4)))))))

Figure A-2 shows the difference between two consecutive terms ($\Delta T_{e,\,m}(r, \tau)$) of the summation series (Eq. (B-3)) plotted versus m of β_m values for r = 2 m, k = 4 W/m-K, D_i = 0.2 m, and t = 10368000 s. It can be seen that, after approximately 60 terms, the difference between two consecutive terms was not significant and was on the order of ± 0.04 K.

$$\Delta T_{e,\,m}(r, \tau) = T_{e,\,m+1}(r, \tau) - T_{e,\,m}(r, \tau) \qquad \text{(A-1)}$$

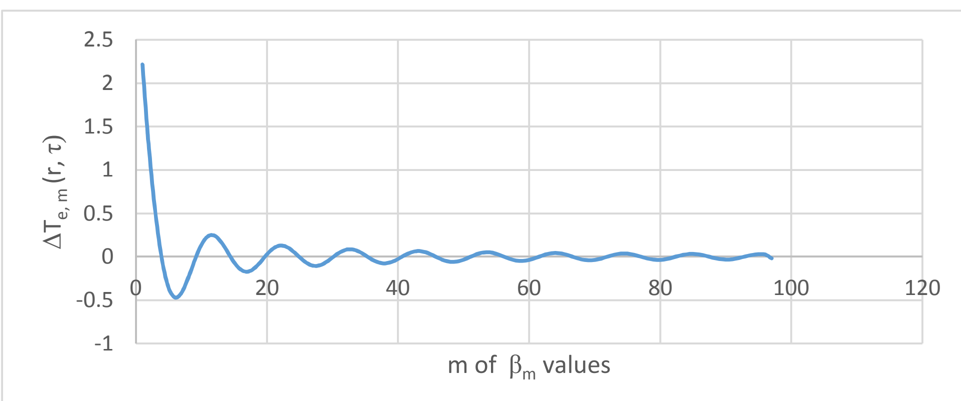

Figure A-2. Difference between two consecutive terms of the summation series vs. m of β_m values at r = 2 m for k = 4 W/m-K, D_i = 0.2 m, and t = 10368000 s.

The 98 values of β_m that were computed using Wolfram Alpha (m = 1 to 8) and Microsoft Excel (m = 9 to 98) are shown in Table A-2.

Table A-2. First 98 eigenvalues of Eq. (3-10).

m	β_m (1/m)	m	β_m (1/m)	m	β_m (1/m)	m	β_m (1/m)
1	0.280092175	29	9.192072474	57	18.08172694	85	26.96888742
2	0.601090069	30	9.509658038	58	18.39915098	86	27.28626639
3	0.921416599	31	9.827232018	59	18.71657245	87	27.60364442
4	1.241136453	32	10.1447952	60	19.03399147	88	27.92102153
5	1.560432014	33	10.4623483	61	19.35140813	89	28.23839775
6	1.87942141	34	10.77989198	62	19.66882252	90	28.55577311
7	2.198180642	35	11.09742682	63	19.98623473	91	28.87314762
8	2.516760829	36	11.41495337	64	20.30364486	92	29.19052132
9	2.835197876	37	11.73247214	65	20.62105297	93	29.50789422
10	3.153517955	38	12.04998359	66	20.93845914	94	29.82526636
11	3.471740724	39	12.36748813	67	21.25586345	95	30.14263775
12	3.789881335	40	12.68498616	68	21.57326597	96	30.4600084
13	4.107951709	41	13.00247805	69	21.89066676	97	30.77737835
14	4.4259614	42	13.31996412	70	22.20806589	98	31.0094746
15	4.743918184	43	13.6374447	71	22.5254634		
16	5.06182847	44	13.95492006	72	22.84285937		
17	5.379697606	45	14.27239048	73	23.16025384		
18	5.697530101	46	14.58985621	74	23.47764686		
19	6.015329787	47	14.90731749	75	23.79503849		
20	6.333099952	48	15.22477452	76	24.11242877		
21	6.650843435	49	15.54222752	77	24.42981774		
22	6.968562704	50	15.85967668	78	24.74720546		
23	7.286259915	51	16.17712217	79	25.06459196		
24	7.603936968	52	16.49456417	80	25.38197727		
25	7.921595539	53	16.81200283	81	25.69936145		
26	8.239237116	54	17.1294383	82	26.01674451		
27	8.556863027	55	17.44687072	83	26.33412651		
28	8.874474457	56	17.76430022	84	26.65150747		

Appendix B. Calculations for One-Dimensional Temperature Using Closed Form Solution

Appendix B shows the calculations for the earth temperature distribution for a sample case with inputs from Table B-1 using the closed form solution. All calculations were performed using MS Excel, and the equations are given below.

Table B-1. Input values used in calculating the temperature distribution using the closed form solution with MS Excel.

k (W/m-K)	0.5	r (m)	1
ρ (kg/m^3)	2050	r_i (m)	0.1
C_p (J/kg-K)	1840	r_o (m)	10
t (s)	10368000	α (m^2/s)	1.33E-07

First, Eqs. (3-1)-(3-10) were simplified, because, subtracting 285 K from each of the initial and boundary conditions will make $T_e(r_o = 10\text{ m}, \tau>0)$ and $T_e(0.1\text{ m} \leq r \leq 10\text{ m}, \tau = 0)$ equal to zero. Also, $A(\beta_m, \tau)$ is independent of τ (Eq. (B-2)), because, $T_e(r_i, \tau)$ of Eq. (B-2) is constant and equal to 20.1 K (Eq. (B-1A)). Therefore, the integral in Eq. (B-1) can be simplified by just integrating $e^{\alpha\beta_m^2\tau'}$

$$T_e(r,\tau) = \sum_{m=1}^{\infty} e^{-\alpha\beta_m^2\tau} K_o(\beta_m, r)\left[\int_{\tau'=0}^{\tau} e^{\alpha\beta_m^2\tau'} A(\beta_m, \tau')d\tau'\right] \text{ (K)} \qquad \text{(B-1)}$$

which gives Eq. (B-3).

Subtracting 285 K from each boundary and initial condition (Eqs. (3-2)-(3-4)), gives

$$T_e(r_i = 0.1\text{ m}, \tau>0) = 305.1\text{ K} - 285\text{ K} = 20.1\text{ K} \qquad \text{(B-1A)}$$

$$T_e(r_o = 10\text{ m}, \tau>0) = 285\text{ K} - 285\text{ K} = 0\text{ K} \qquad \text{(B-1B)}$$

$$T_e(0.1\text{ m} \leq r \leq 10\text{ m}, \tau = 0) = 285\text{ K} - 285\text{ K} = 0\text{ K} \qquad \text{(B-1C)}$$

With the simplified boundary and initial conditions, Eq. (3-6) reduces to

$$A(\beta_m, \tau) = \alpha\left[r_i \frac{dK_o(\beta_m, r = r_i)}{dr} (T_e(r_i, \tau))\right] \qquad \text{(B-2)}$$

Table B-1 values and Eq. (B-2) were substituted into Eq. (B-1); and the resulting equation (Eq. (B-3)) was solved in an MS Excel spreadsheet

$$T_e(r,\tau) = \sum_{m=1}^{\infty} K_o(\beta_m, r)\left[\left(\frac{1-e^{-\alpha\beta_m^2\tau}}{\beta_m^2}\right) r_i \frac{dK_o(\beta_m, r = r_i)}{dr} T_e(r_i, \tau)\right] = \sum_{m=1}^{\infty} T_{e,m}(r,\tau) \qquad \text{(B-3)}$$

where $K_o(\beta_m,r)$ is defined by Eq. (3-7), $R_o(\beta_m,r)$ is defined by Eq. (3-8), N is defined by Eq. (3-9), and

$$\frac{dK_o(\beta_m, r = r_i)}{dr} = \frac{\beta_m}{\sqrt{N}}\left[-\frac{J_1(r_i\beta_m)}{J_0(r_o\beta_m)} + \frac{Y_1(r_i\beta_m)}{Y_0(r_o\beta_m)}\right] \ (1/m^2) \qquad \text{(B-4)}$$

Table B-2 shows the spreadsheet's results. The 98th value from the column labelled $T_e(r,\tau)$-285 was added to 285 K, in order to determine the earth temperature at that location (r) and time (τ). These calculations were then used to determine the minimum spacing required between the bore holes for different times (τ) and radii (r). Radius (r) and time (t) values from Table B-1 (values from Table B-1 were used as inputs for Table B-2 calculations) were changed to different values in order to determine the earth temperature at those radii and times.

Table B-2. Spreadsheet results showing the closed form solution for one-dimensional transient temperature distribution using Table B-1 inputs and r = 1 m and t = 10368000 s.

m	β_m (1/m)	$R_o(\beta_m,r)$ (-)	$K_o(\beta_m,r)$ (1/m)	N (m^2)	$\exp(-\alpha\beta_m^2\tau)$ (-)	$\frac{dK_o(\beta_m, r=r_i)}{dr}$ ($1/m^2$)	$T_{e,m}(r,\tau)$ (K)	$T_e(r,\tau)$-285 (K)
1	0.2801	-3.327	-0.170	382.23	8.98E-01	-0.7476	0.33	0.33
2	0.6011	4.861	0.289	283.03	6.09E-01	1.3230	0.83	1.17
3	0.9214	-5.821	-0.374	242.10	3.11E-01	-1.8439	1.12	2.29
4	1.2411	6.316	0.426	219.93	1.20E-01	2.3394	1.14	3.43
5	1.5604	-6.367	-0.442	207.14	3.52E-02	-2.8201	0.99	4.43
6	1.8794	5.988	0.423	200.18	7.79E-03	3.2913	0.79	5.21
7	2.1982	-5.205	-0.370	197.40	1.31E-03	-3.7558	0.58	5.79
8	2.5168	4.055	0.288	198.02	1.66E-04	4.2156	0.39	6.18
9	2.8352	-2.598	-0.183	201.68	1.59E-05	-4.6718	0.21	6.39
10	3.1535	0.910	0.063	208.32	1.16E-06	5.1253	0.07	6.46
11	3.4717	0.918	0.062	218.12	6.40E-08	-5.5768	-0.06	6.40
12	3.7899	-2.780	-0.183	231.45	2.67E-09	6.0267	-0.15	6.24
13	4.1080	4.563	0.289	248.95	8.47E-11	-6.4753	-0.22	6.02
14	4.4260	-6.149	-0.373	271.55	2.03E-12	6.9229	-0.27	5.76
15	4.7439	7.417	0.428	300.65	3.70E-14	-7.3697	-0.28	5.47
16	5.0618	-8.252	-0.449	338.28	5.09E-16	7.8159	-0.28	5.20
17	5.3797	8.546	0.434	387.44	5.32E-18	-8.2617	-0.25	4.95
18	5.6975	-8.198	-0.385	452.74	4.21E-20	8.7070	-0.21	4.74
19	6.0153	7.117	0.306	541.46	2.53E-22	-9.1521	-0.16	4.59
20	6.3331	-5.214	-0.202	665.62	1.15E-24	9.5969	-0.10	4.49
21	6.6508	2.391	0.082	846.16	3.97E-27	-10.0416	-0.04	4.45

m	β_m (1/m)	$R_o(\beta_m,r)$ (-)	$K_o(\beta_m,r)$ (1/m)	N (m^2)	$\exp(-\alpha\beta_m^2\tau)$ (-)	$\frac{dK_o(\beta_m, r = r_i)}{dr}$ ($1/m^2$)	$T_{e,m}(r,\tau)$ (K)	$T_e(r,\tau)$-285 (K)
22	6.9686	1.485	0.044	1122.31	1.04E-29	10.4861	0.02	4.47
23	7.2863	-6.642	-0.167	1574.57	2.05E-32	-10.9306	0.07	4.54
24	7.6039	13.551	0.277	2390.18	3.08E-35	11.3750	0.11	4.65
25	7.9216	-23.346	-0.365	4092.00	3.51E-38	-11.8194	0.14	4.79
26	8.2392	39.378	0.424	8638.82	3.03E-41	12.2638	0.15	4.94
27	8.5569	-76.602	-0.449	29159.09	1.98E-44	-12.7082	0.16	5.10
28	8.8745	462.467	0.438	1116336.9	9.84E-48	13.1526	0.15	5.25
29	9.1921	99.250	0.392	64157.10	3.70E-51	13.5971	0.13	5.37
30	9.5097	-35.730	-0.315	12896.98	1.05E-54	-14.0417	0.10	5.47
31	9.8272	15.599	0.212	5402.68	2.28E-58	14.4863	0.06	5.53
32	10.1448	-5.064	-0.093	2977.81	3.74E-62	-14.9310	0.03	5.56
33	10.4623	-1.486	-0.034	1899.16	4.64E-66	15.3758	-0.01	5.55
34	10.7799	5.766	0.158	1327.21	4.37E-70	-15.8207	-0.04	5.51
35	11.0974	-8.481	-0.270	987.99	3.12E-74	16.2657	-0.07	5.44
36	11.4150	9.986	0.360	770.59	1.69E-78	-16.7107	-0.09	5.34
37	11.7325	-10.505	-0.421	623.13	6.93E-83	17.1558	-0.11	5.24
38	12.0500	10.207	0.448	518.72	2.16E-87	-17.6011	-0.11	5.13
39	12.3675	-9.244	-0.440	442.31	5.09E-92	18.0464	-0.10	5.03
40	12.6850	7.761	0.396	384.91	9.09E-97	-18.4918	-0.09	4.93
41	13.0025	-5.906	-0.320	340.92	1.23E-101	18.9374	-0.07	4.86
42	13.3200	3.825	0.218	306.69	1.27E-106	-19.3830	-0.05	4.81
43	13.6374	-1.663	-0.099	279.76	9.88E-112	19.8287	-0.02	4.79
44	13.9549	-0.443	-0.028	258.44	5.84E-117	-20.2745	0.01	4.80
45	14.2724	2.368	0.152	241.53	2.62E-122	20.7204	0.03	4.83
46	14.5899	-4.002	-0.265	228.17	8.88E-128	-21.1664	0.05	4.88
47	14.9073	5.257	0.356	217.76	2.29E-133	21.6125	0.07	4.95
48	15.2248	-6.067	-0.419	209.84	4.47E-139	-22.0586	0.08	5.03
49	15.5422	6.397	0.448	204.10	6.61E-145	22.5049	0.08	5.12
50	15.8597	-6.236	-0.441	200.30	7.42E-151	-22.9513	0.08	5.20
51	16.1771	5.605	0.398	198.30	6.31E-157	23.3977	0.07	5.27
52	16.4946	-4.550	-0.323	198.03	4.07E-163	-23.8442	0.06	5.33
53	16.8120	3.144	0.223	199.48	1.99E-169	24.2908	0.04	5.36
54	17.1294	-1.480	-0.104	202.69	7.39E-176	-24.7375	0.02	5.38
55	17.4469	-0.333	-0.023	207.76	2.08E-182	25.1843	0.00	5.38
56	17.7643	2.174	0.148	214.88	4.43E-189	-25.6311	-0.02	5.35
57	18.0817	-3.917	-0.262	224.32	7.16E-196	26.0780	-0.04	5.31
58	18.3992	5.439	0.354	236.44	8.78E-203	-26.5250	-0.06	5.26
59	18.7166	-6.623	-0.417	251.75	8.16E-210	26.9721	-0.06	5.19
60	19.0340	7.365	0.447	270.96	5.75E-217	-27.4192	-0.07	5.12

m	β_m (1/m)	$R_o(\beta_m,r)$ (-)	$K_o(\beta_m,r)$ (1/m)	N (m^2)	$\exp(-\alpha\beta_m^2\tau)$ (-)	$\frac{dK_o(\beta_m, r=r_i)}{dr}$ (1/m^2)	$T_{e,m}(r,\tau)$ (K)	$T_e(r,\tau)$-285 (K)
61	19.3514	-7.581	-0.441	295.05	3.07E-224	27.8665	-0.07	5.06
62	19.6688	7.210	0.400	325.34	1.24E-231	-28.3137	-0.06	5.00
63	19.9862	-6.214	-0.326	363.77	3.82E-239	28.7611	-0.05	4.95
64	20.3036	4.586	0.226	413.10	8.89E-247	-29.2085	-0.03	4.92
65	20.6211	-2.344	-0.107	477.45	1.57E-254	29.6560	-0.02	4.90
66	20.9385	-0.470	-0.020	563.16	2.10E-262	-30.1035	0.00	4.91
67	21.2559	3.789	0.145	680.40	2.13E-270	30.5511	0.02	4.93
68	21.5733	-7.534	-0.259	846.24	1.64E-278	-30.9988	0.03	4.96
69	21.8907	11.623	0.352	1091.22	9.56E-287	31.4465	0.05	5.01
70	22.2081	-15.985	-0.416	1474.33	4.23E-295	-31.8943	0.05	5.06
71	22.5255	20.598	0.447	2122.08	1.42E-303	32.3421	0.06	5.12
72	22.8429	-25.568	-0.442	3347.66	0.00E+00	-32.7900	0.06	5.18
73	23.1603	31.354	0.401	6114.45	0.00E+00	33.2380	0.05	5.23
74	23.4776	-39.755	-0.328	14720.05	0.00E+00	-33.6860	0.04	5.27
75	23.7950	62.209	0.228	74641.18	0.00E+00	34.1040	0.03	5.29
76	24.1124	118.161	0.110	1161655.6	0.00E+00	34.5517	0.01	5.31
77	24.4298	3.139	0.017	32936.59	0.00E+00	-34.9994	0.00	5.30
78	24.7472	-14.187	-0.143	9866.14	0.00E+00	35.4472	-0.02	5.29
79	25.0646	17.614	0.257	4703.29	0.00E+00	-35.8951	-0.03	5.26
80	25.3820	-18.394	-0.350	2760.55	0.00E+00	36.3430	-0.04	5.22
81	25.6994	17.736	0.415	1825.76	0.00E+00	-36.7909	-0.05	5.17
82	26.0167	-16.135	-0.447	1305.64	0.00E+00	37.2389	-0.05	5.12
83	26.3341	13.883	0.442	987.00	0.00E+00	-37.6870	-0.05	5.07
84	26.6515	-11.201	-0.402	777.98	0.00E+00	38.1351	-0.04	5.03
85	26.9689	8.277	0.329	633.72	0.00E+00	-38.5832	-0.04	5.00
86	27.2863	-5.283	-0.229	530.19	0.00E+00	39.0313	-0.02	4.97
87	27.6036	2.376	0.112	453.58	0.00E+00	-39.4795	-0.01	4.96
88	27.9210	0.305	0.015	395.50	0.00E+00	39.9278	0.00	4.96
89	28.2384	-2.641	-0.141	350.64	0.00E+00	-40.3760	0.01	4.98
90	28.5558	4.535	0.255	315.47	0.00E+00	40.8244	0.03	5.00
91	28.8731	-5.918	-0.349	287.60	0.00E+00	-41.2727	0.03	5.04
92	29.1905	6.751	0.414	265.37	0.00E+00	41.7211	0.04	5.08
93	29.5079	-7.023	-0.446	247.59	0.00E+00	-42.1695	0.04	5.12
94	29.8253	6.756	0.442	233.41	0.00E+00	42.6180	0.04	5.16
95	30.1426	-5.997	-0.402	222.18	0.00E+00	-43.0664	0.04	5.20
96	30.4600	4.820	0.330	213.47	0.00E+00	43.5150	0.03	5.23
97	30.7774	-3.321	-0.231	206.94	0.00E+00	-43.9635	0.02	5.25
98	31.7295	-1.966	-0.140	198.36	0.00E+00	45.3094	-0.01	5.24

Appendix C. Comparing Temperature Distributions from Closed Form Solution for D_i = 0.1 m and 0.2 m

Appendix C deals with the results obtained from the closed form solution (Appendix B) for temperature distribution when using D_i = 0.1 m, D_o = 20 m. In addition, to examine the effect of inner diameter of the tube on the temperature distribution, these results are compared to the results obtained when D_i = 0.2 m.

Table C-1 shows the one-dimensional temperatures above 285 K (ΔT_e) for different times and radii when using k = 0.5 W/m-K, ρ = 2050 kg/m^3, and C_p = 1840 J/kg-K, where $\Delta T_e = T_e(r,\tau)$ - 285 [K]. As can be seen from Table C-1, for the given boundary and initial conditions (Eqs. (B-1A)-(B-1C)), initial earth temperature remained unchanged within an error of approximately 0.01 K, for radii greater than approximately 5 m for all of the times studied. Therefore, a distance of 10 m (2 x 5 m) can be used as the minimum spacing needed between the bore holes when the thermal conductivity of the earth is assumed to be 0.5 W/m-K and D_i = 0.1 m.

Table C-1. Temperature rise (ΔT_e) distribution for k = 0.5 W/m-K at different times for D_i = 0.1 m (closed form).

r (m)	ΔT_e (K) at t = 2592000 s	ΔT_e (K) at t = 5184000 s	ΔT_e (K) at t = 7776000 s	ΔT_e (K) at t = 10368000 s
1	2.19	3.68	4.55	5.14
2	0.12	0.61	1.12	1.56
3	0.00	0.06	0.21	0.39
4	0.00	0.00	0.02	0.07
5	0.00	0.00	0.00	0.01
6	0.00	0.00	0.00	0.00
7	0.00	0.00	0.00	0.00
8	0.00	0.00	0.00	0.00
9	0.00	0.00	0.00	0.00
10	0.00	0.00	0.00	0.00

Table C-2 shows the one-dimensional temperatures above 285 K (ΔT_e) for different times and radii when using D_i = 0.1 m, D_o = 20 m, k = 2 W/m-K, ρ = 2050 kg/m^3, and C_p = 1840 J/kg-K, where $\Delta T_e = T_e(r,\tau)$ - 285 [K]. As can be seen from Table C-2, for the given boundary and initial conditions (Eqs. (B-1A)-(B-1C)), the initial earth temperature remained unchanged within an error of 0.02 K, for radius greater than approximately 9 m for all of the times studied. Therefore, a distance of 18 m (2 x 9 m) can be used as the minimum spacing that is needed between the bore holes when the thermal conductivity of the earth is assumed to be 2 W/m-K and D_i = 0.1 m. Also, note that ΔT_e values at all radii when k = 0.5 W/m-K, t = 10368000 s (Table C-1), are exactly the same as those for k = 2 W/m-K, t = 2592000 s (Table C-2). This is because $T_e(r,\tau)$ depends on α and τ, as only the product of the two (Eq. (B-3)). Therefore, when τ is halved and α is doubled, the value of $T_e(r,\tau)$ will be exactly the same.

Table C-2. Temperature rise (ΔT_e) distribution for k = 2 W/m-K at different times for D_i = 0.1 m (closed form)

r (m)	ΔT_e (K) at t = 2592000 s	ΔT_e (K) at t = 5184000 s	ΔT_e (K) at t = 7776000 s	ΔT_e (K) at t = 10368000 s
1	5.14	6.48	7.18	7.65
2	1.56	2.78	3.54	4.06
3	0.39	1.16	1.77	2.24
4	0.07	0.44	0.84	1.20
5	0.01	0.14	0.37	0.61
6	0.00	0.04	0.15	0.29
7	0.00	0.01	0.05	0.13
8	0.00	0.00	0.02	0.02
9	0.00	0.00	0.00	0.02
10	0.00	0.00	0.00	0.00

Table C-3 shows the one-dimensional temperatures above 285 K (ΔT_e) for different times and radii when using D_i = 0.1 m, D_o = 20 m, k = 4 W/m-K, ρ = 2050 kg/m^3, and C_p = 1840 J/kg-K, where $\Delta T_e = T_e(r,\tau) - 285$ [K]. As can be seen from Table C-3, for the given boundary and initial conditions (Eqs. (B-1A)-(B-1C)), the initial earth temperature remained unchanged within an error of 0.13 K, at radius greater than approximately 9 m for all of the times studied. Therefore, a distance of 18 m (2 x 9 m) can be used as the minimum spacing that is needed between the bore holes when the thermal conductivity of the earth is assumed to be 4 W/m-K and D_i = 0.1 m. Also, note that ΔT_e values at all radii when k = 2 W/m-K, t = 5184000 s and 10368000 s (Table C-2), are exactly the same as those for k = 4 W/m-K, t = 2592000 s and 5184000 s (Table C-3), respectively. This is because $T_e(r,\tau)$ depends on α and τ, as only the product of the two (Eq. (B-3)). Therefore, when τ is halved and α is doubled, the value of $T_e(r,\tau)$ will be exactly the same.

Table C-3. Temperature rise (ΔT_e) distribution for k = 4 W/m-K at different times for D_i = 0.1 m (closed form).

r (m)	ΔT_e (K) at t = 2592000 s	ΔT_e (K) at t = 5184000 s	ΔT_e (K) at t = 7776000 s	ΔT_e (K) at t = 10368000 s
1.00	6.48	7.65	8.26	8.66
2.00	2.78	4.06	4.78	5.27
3.00	1.16	2.24	2.92	3.41
4.00	0.44	1.20	1.78	2.23
5.00	0.14	0.61	1.06	1.44
6.00	0.04	0.29	0.61	0.91
7.00	0.01	0.13	0.34	0.55
8.00	0.00	0.05	0.17	0.30
9.00	0.00	0.02	0.07	0.13
10.00	0.00	0.00	0.00	0.00

Tables C-4 to C-6 show the differences between temperatures (DT_e) from the closed form solution for D_i = 0.2 m (Tables 8-10) versus 0.1 m (Tables C-1 to C-3).

$$DT_e\ (K) = T_{e\ (closed\ form,\ D_i\ =\ 0.2\ m)} - T_{e\ (closed\ form,\ D_i\ =\ 0.1\ m)} \quad (C\text{-}1)$$

As can be seen from Tables C-4 to C-6, when the inner diameter was changed from 0.2 m to 0.1 m, the difference between temperatures at any thermal conductivity for a given a radius and time is the same; and, at most radii and times, the difference ranged from magnitudes of 0.01 K to 0.10 K. Taking into consideration these small changes in temperature, all of the runs conducted for the cylindrical model of the earth with a U-tube were performed with an inner diameter equal to 0.2 m.

The inner diameter of the tube was chosen to be 0.2 m and not 0.1 m because, with decreasing inner diameter of the tube, the mass flow rate of warm cooling water through each bore hole decreases (for the same inlet velocity of water), which in turn leads to an increase in the total number of bore holes required. Since the results suggest that the temperature distribution in the earth domain remains approximately the same when decreasing inner diameter from D_i = 0.2 m to D_i = 0.1 m, D_i = 0.2 m was used for all of the runs conducted for the cylindrical model of the earth with a U-tube. However, the results studied in this thesis do not provide enough evidence to choose an optimum value for the inner diameter of the tube. Future studies are needed, which vary the inner diameter in order to produce the results needed to determine the diameters for which the cost of installation decreases compared to that of D_i = 0.2 m.

Table C-4. Difference between temperatures from closed form solution at D_i = 0.2 m and 0.1 m for k = 0.5 W/m-K and different times and radii.

r (m)	DT_e at t = 2592000 s	DT_e (K) at t = 5184000 s	DT_e (K) at t = 7776000 s	DT_e (K) at t = 10368000 s
1	0.09	0.10	0.10	0.10
2	0.01	0.01	0.01	0.01
3	-0.01	-0.01	-0.01	-0.01
4	-0.02	-0.02	-0.02	-0.02
5	-0.02	-0.02	-0.02	-0.02
6	-0.02	-0.02	-0.02	-0.02
7	-0.02	-0.02	-0.02	-0.02
8	-0.01	-0.01	-0.01	-0.01
9	-0.01	-0.01	-0.01	-0.01
10	0.00	0.00	0.00	0.00

Table C-5. Difference between temperatures from closed from solution at D_i = 0.2 m and 0.1 m for k = 2 W/m-K and different times and radii.

r (m)	DT_e at t = 2592000 s	DT_e (K) at t = 5184000 s	DT_e (K) at t = 7776000 s	DT_e (K) at t = 10368000 s
1	0.10	0.10	0.10	0.10
2	0.01	0.01	0.01	0.01
3	-0.01	-0.01	-0.01	-0.01
4	-0.02	-0.02	-0.02	-0.02
5	-0.02	-0.02	-0.02	-0.02
6	-0.02	-0.02	-0.02	-0.02
7	-0.02	-0.02	-0.02	-0.02
8	-0.01	-0.01	-0.01	0.02
9	-0.01	-0.01	-0.01	-0.01
10	0.00	0.00	0.00	0.00

Table C-6. Difference between temperatures from closed form solution at D_i = 0.2 m and 0.1 m for k = 4 W/m-K and different times and radii.

r (m)	DT_e at t = 2592000 s	DT_e (K) at t = 5184000 s	DT_e (K) at t = 7776000 s	DT_e (K) at t = 10368000 s
1	0.10	0.10	0.10	0.10
2	0.01	0.01	0.01	0.01
3	-0.01	-0.01	-0.01	-0.01
4	-0.02	-0.02	-0.02	-0.02
5	-0.02	-0.02	-0.02	-0.02
6	-0.02	-0.02	-0.02	-0.02
7	-0.02	-0.02	-0.02	-0.02
8	-0.01	-0.01	-0.01	-0.01
9	-0.01	-0.01	-0.01	-0.01

It can be seen from Tables C-4 to C-6 that the change in the inner diameter from 0.2 m to 0.1 m does not have an appreciable effect on the earth temperatures calculated. However, the small temperature changes, on the order of 0.10 K, can be examined for future development of the project. Since it costs approximately 1/3 to drill a 0.16 m diameter bore hole as compared to drilling a 0.6 m diameter bore hole, therefore, studies could be done to determine the effect of bore hole diameter on the earth temperature distribution and bore hole exit water temperature in order to reduce the installation cost.

Appendix D. Comparing Temperature Distribution Results from Finite Difference Method and ANSYS-CFX

Appendix D shows the difference between radial earth temperatures obtained using ANSYS-CFX and the Finite Difference method.

Since all of the ANSYS-CFX runs on the 3.6^o wedge (D_i = 0.2 m) were performed using k = 0.52 W/m-K, Finite Difference results were also produced using k = 0.52 W/m-K (not shown in this thesis) and were compared. Table D-1 shows the differences, DT_e, between radial earth temperatures obtained using ANSYS-CFX (Run 8, Section 4.4.3.7) at d = 0.1 m and the Finite Difference method (D_i = 0.2 m, k = 0.52 W/m-K) at four different times.

$$DT_e = T_{e\ (ANSYS\text{-}CFX)} - T_{e\ (Finite\ Difference\ method)} \qquad \text{(D-1)}$$

Table D-1. Difference between ANSYS-CFX and Finite Difference method temperatures for D_i = 0.2 m, k = 0.52 W/m-K, and different times and radii.

r [m]	DT_e (K) at t = 2592000 s	DT_e (K) at t = 5184000 s	DT_e (K) at t = 7776000 s	DT_e (K) at t = 10368000 s
0.1	0.00	0.00	0.00	0.00
0.3	0.57	0.54	0.52	0.51
0.5	0.58	0.59	0.57	0.57
0.8	0.41	0.35	0.31	0.29
1.0	0.23	0.17	0.14	0.11
1.2	0.17	0.08	0.05	0.02
1.4	0.16	0.06	0.01	0.02
1.7	0.30	0.28	0.27	0.25
1.9	0.26	0.24	0.21	0.19
2.1	0.26	0.21	0.18	0.15

Using the results from this Appendix, it was concluded that the earth temperature distribution results obtained using the Finite Difference method are approximately equal to (within a maximum error of 0.6 K) the results from ANSYS-CFX. Therefore, the earth temperature distribution results produced using the Finite Difference method can be used in determining the minimum spacing that is required between the bore holes. The differences between the temperatures calculated by ANSYS CFX and Finite Difference methods are reasonable, but it is unknown as to whether these differences increase, decrease or remain the same as k increases.

Therefore, incorporating a safety factor of 2, by increasing the spacing to approximately 16 m or 18 m, can address this issue. Also, it can be observed that the temperature differences are not always decreasing as radius increases. For instance, DT_e for t = 2592000 s decreases from 0.57 K (r = 0.3 m) to 0.16 K (r = 1.4 m) and then increases to 0.26 K (r = 2.1 m). This is because the ANSYS-CFX mesh size was not constant, neither along the depth nor along the radius. The mesh size was increased, in order to reduce the computer simulation times. Reduction in the number of elements was possible, because the temperature changes at larger radii and depths were not as large as those at smaller radii and depths. Therefore, decreasing the number of elements at larger radii (greater than r = ~ 1.5 m) and depths (greater than d = ~ 20 m), as compared to smaller radii and depths, did not affect the results significantly (by much). On the other hand, radius steps for the Finite Difference method were constant.

Appendix E. Steps Performed in SolidWorks to Create the Three-Dimensional Models of the Earth and Water Domains

Appendix E shows the steps performed in SolidWorks to create the three-dimensional models of the earth and water domains.

First, SolidWorks was started and “New” from the tool bar was selected to “Create a New Part”. Units were set to MKS by going to “Options” → “Units” and selecting “MKS”.

Steps Involved in Creating a Three-Dimensional 3.6° Wedge for Initial Runs

1. The front plane was selected to draw a sketch. As shown in Fig. E-1, a two-dimensional rectangle was drawn about the origin with dimensions of r_i = 0.1 m and L = 500 m. The values of r_i, r_o and L were changed for different runs, depending upon the flow rate and thermal conductivity (k) of the earth in order to reduce the simulation time.

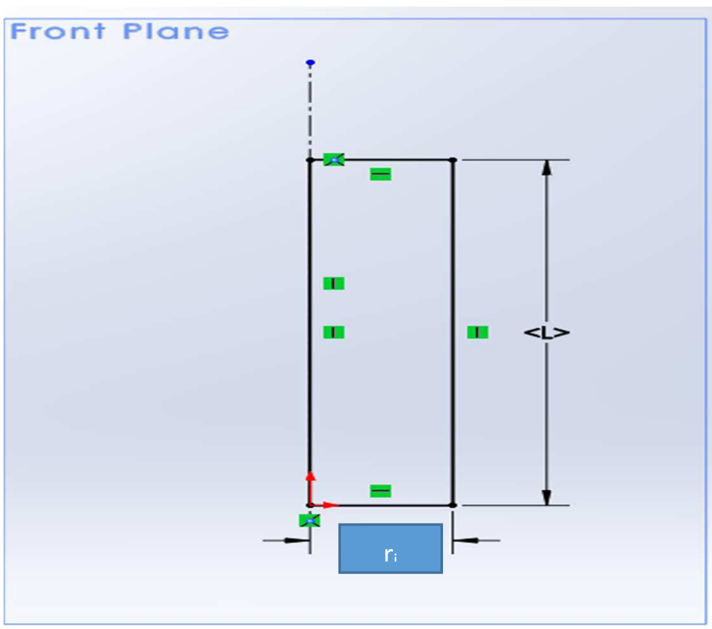

Figure E-1. Two-dimensional drawing of the 3.6° wedge model of the water domain in the front plane (vertical plane).

2. The two-dimensional drawing was converted into a three-dimensional wedge by selecting the “Revolve Boss/Base” option from the “Features” tab. Figure E-2 shows the inputs, including “Axis of Revolution”, “Direction”, and “Angle”, given to the “Revolve Boss/Base” feature and the three-dimensional image of the water model. The axis of revolution was chosen as the vertical line passing through the origin, and a 3.6° angle was given for “Angle to Revolve”.

The green check mark was clicked to accept the inputs and complete the three-dimensional model of the water domain.

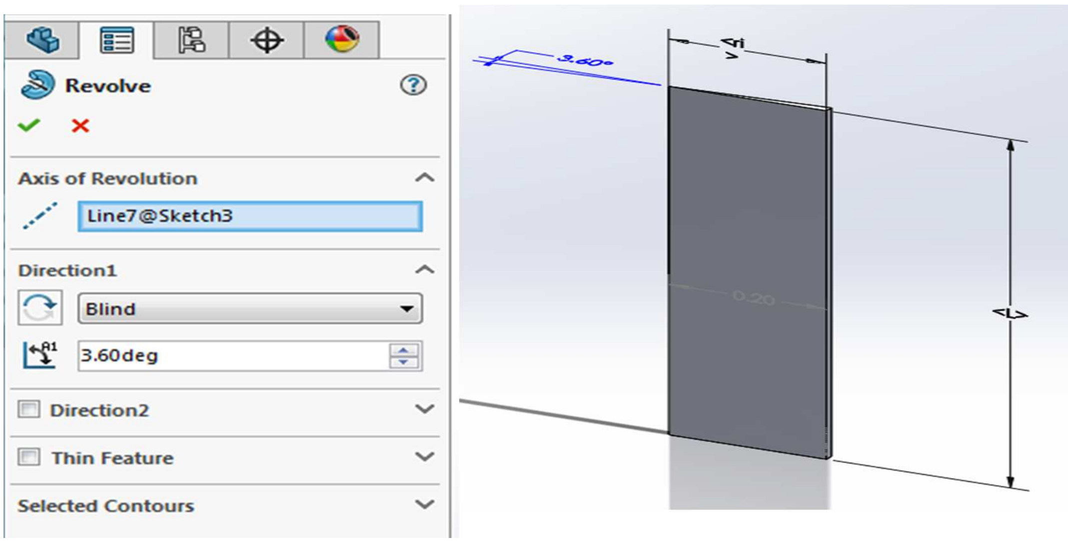

Figure E-2. Creating a three-dimensional wedge model of the water domain from the two-dimensional sketch using the "Revolve" feature.

3. For creating a three-dimensional model of the earth domain, a rectangle was created with the origin located at a distance of r_i from the inside edge of the rectangle (edge of the rectangle closer to the origin). The three-dimensional model of the earth domain was then created using the same steps carried out in creating the 3.6^o wedge model of the water domain (Steps 1 and 2). Figure E-3 shows both the two-dimensional and the three-dimensional models of the water domain created.

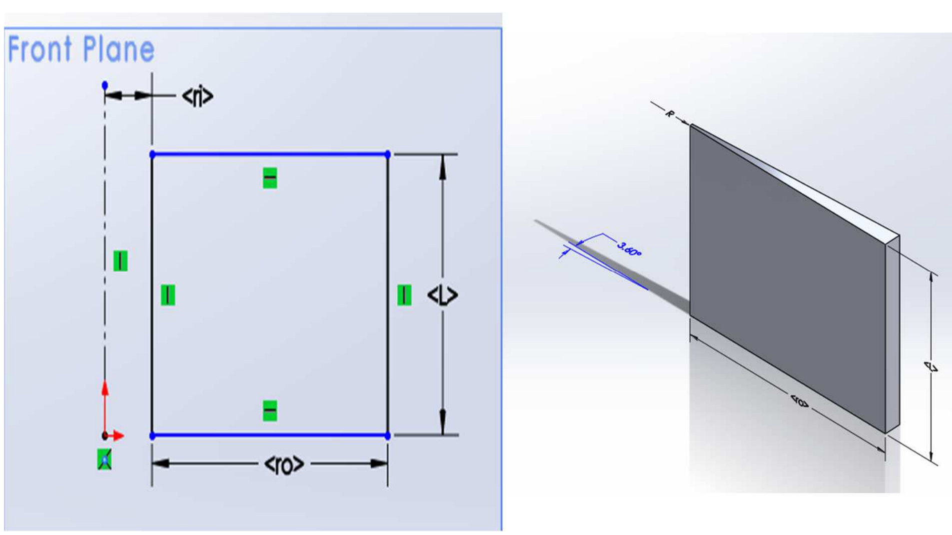

Figure E-3. Creating a three-dimensional wedge model of the earth domain in SolidWorks.

4. Both three-dimensional models were then saved and were imported into the “Assembly” feature of SolidWorks and were connected to form a single part using “Coincident” and “Parallel” mates. The assembly was then saved in “parasolid x_t*” format to be imported into ANSYS-CFX for performing simulations.

Steps Involved in Creating a Complete Three-Dimensional Model of the Earth and Water Domains.

A complete 360^o three-dimensional model of the earth and water domains is different from the 3.6^o wedge model in terms of the U-bend for the complete 360^o model as opposed to one straight tube without any bends for the 3.6^o wedge model. Therefore, the steps involved in creating the two models are different. The steps involved in creating the complete 360^o three-dimensional model of the earth and water domains are discussed in the following pages.

1. First, the top plane was selected to draw a sketch. As shown in Fig E-4, a circle of diameter r_i was drawn.

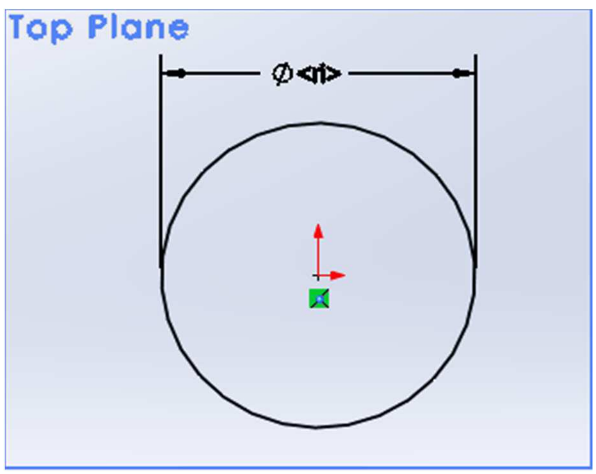

Figure E-4. Two-dimensional sketch of the tube in the top plane.

2. Exiting from the previous sketch, the front plane was then chosen to sketch the path for the U-tube. A line was started from the center of the circle drawn previously in the top plane and was then continued to form a U-shape when in the front plane. Dimensions for L (depth of the bore hole) and the distance between the tubes were given (see Fig. E-5). Figure E-5 shows how the sketch of the path for the U-tube was drawn in the front plane.

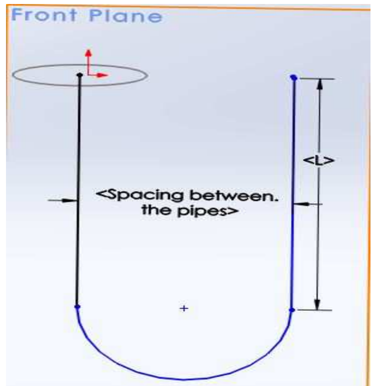

Figure E-5. Two-dimensional sketch of the U-tube path in the front plane (vertical plane)

3. Exiting the previous sketch, the "Sweep" boss feature was selected from the "Features" tab to sweep the circle along the U-shape created in the front plane to form a U-shaped three-dimensional water model. The circle drawn in the top plane was given as an input to the sketch profile, the U-shape created in the front plane was given as an input to the sketch path, and the green check mark was clicked to complete and create the three-dimensional water domain. Figure E-6 shows the inputs (sketch profile and path) that were given to the "Sweep" feature. The part was then saved as water.SLDPRT.

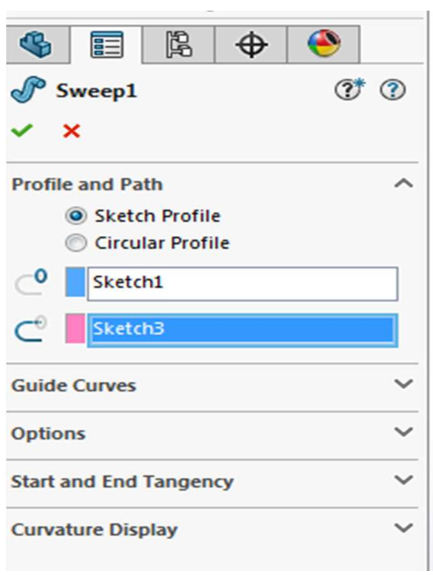

Figure E-6. "Sweep" feature to create the three-dimensional model of the U-tube.

4. To create the earth domain, a two-dimensional sketch was made in the top plane. Figure E-7 shows how the two-dimensional sketch of the earth domain was made in the top plane.

Dimensions such as r_o, r_i, and the distance between the tubes were given for the sketch to match the previous two-dimensional sketch drawn for the water domain (Steps 1 and 2).

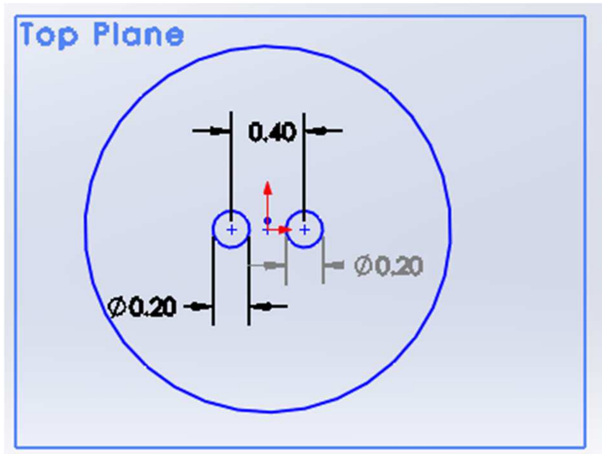

Figure E-7. Two-dimensional sketch of the earth domain in the top plane.

5. The sketch was then “Extruded” to length ”L” for creating a three-dimensional model of the earth domain. Figure E-8 shows the three-dimensional model of the earth domain and the inputs including direction and length that were given to the “Boss-Extrude” feature. The values of L and r_i must be equal to the values of L and r_i given in creating the water domain. After giving the inputs (Steps 2 and 3), the green check mark was clicked to complete and create the three-dimensional model of the earth domain. The part was then saved as earth.SLDPRT.

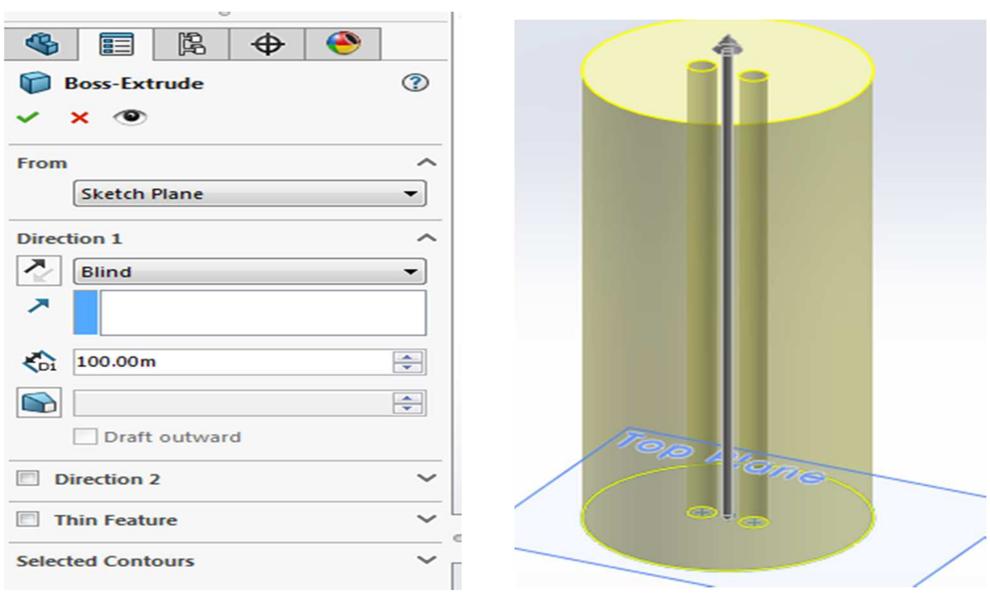

Figure E-8. Three-dimensional model of the earth domain.

6. Both the water and earth domains, which were saved as .SLDPRT were imported into the “Assembly” feature of the SolidWorks. The imported files were then connected using different SolidWorks mates such as “Coincident” and “Concentric”. The assembly file was then saved as one single body in “parasolid x_t*” format to be imported into ANSYS-CFX to perform simulations.

Appendix F. Comparing Temperature Distribution Results from Finite Difference Method using Δτ = 18000 s versus Δτ = 600 s

Appendix F shows the difference between radial earth temperatures obtained using the Finite Difference method with time steps of $\Delta\tau$ = 18000 s and $\Delta\tau$ = 600 s.

As discussed in Section 4.2, the Finite Difference problem was solved using different values of Δr and $\Delta\tau$, while satisfying the stability criterion (Eq. (3-11)). This was done in order to check for the consistency of the results. It was determined that, for k = 2 W/m-K, when Δr = 1 m and $\Delta\tau$ = 18000 s were reduced to Δr = 0.1 m and $\Delta\tau$ = 600 s, there were earth temperature differences from approximately 1.691 K (max) at r = 1.1 m, t = 10368000 s to approximately 0.001 K (min) at r = 9.1 m, t = 5184000 s. For k = 2 W/m-K, when Δr = 0.1 m and $\Delta\tau$ = 600 s were changed to Δr = 0.05 m and $\Delta\tau$ = 300 s, there were earth temperature differences of approximately 0.081 K (max) at r = 0.5 m, t = 2592000 s, and 0.001 K (min) at r = 5 W/m-K, t = 5184000 s (comparison results are not presented in this thesis). Considering these small changes in the earth temperatures calculated, Δr = 0.05 m and $\Delta\tau$ = 300 s were used to perform all of the calculations.

Table F-1 show the difference between Finite Difference method temperatures when $\Delta\tau$ = 600 s and $\Delta\tau$ = 18000 s for D_i = 0.2 m, k = 2 W/m-K and different times (t) and radii (r).

$$DT_e = T_{e\,(\text{Finite Difference method},\ \Delta\tau = 18000\ s)} - T_{e\,(\text{Finite Difference method},\ \Delta\tau = 600\ s)} \tag{F-1}$$

Table F-1. Difference between Finite Difference method temperatures when $\Delta\tau$ = 600 s and $\Delta\tau$ = 18000 s for D_i = 0.2 m, k = 2 W/m-K, and different times and radii.

r (m)	DT_e (K) at t = 259200 s	DT_e (K) at t = 5184000 s	DT_e (K) at t = 7776000 s	DT_e (K) at t = 10368000 s
1.1	1.423	1.584	1.661	1.691
2.1	0.569	0.796	0.943	1.025
3.1	0.213	0.380	0.519	0.611
4.1	0.071	0.173	0.276	0.354
5.1	0.019	0.074	0.140	0.199
6.1	0.004	0.030	0.067	0.108
7.1	0.001	0.011	0.031	0.055
8.1	0.000	0.003	0.013	0.027
9.1	0.000	0.001	0.004	0.012
10	0.000	0.000	0.000	0.000

Appendix G. Extracting Energy from the Earth Domain

Appendix G deals with the results obtained from the runs conducted to examine the time required to extract the stored thermal energy [by the ground source system] from the earth domain.

For the runs conducted to extract thermal energy, the result file from Run 4-3 (Section 4.4.7.3) was given as an input in the CFX Solution Manager. This result file acted as an initial condition for the earth domain. Inlet water velocity for the water domain was given as 0.00621 m/s, which was the same as the inlet velocity of water from Run 4-3; and the water temperature at the inlet, was changed to 285 K, 283 K, and 275 K, respectively, for three different runs conducted.

Figure G-1 shows the energy stored in the earth domain at different times for a total time of 20736000 s (8 months).

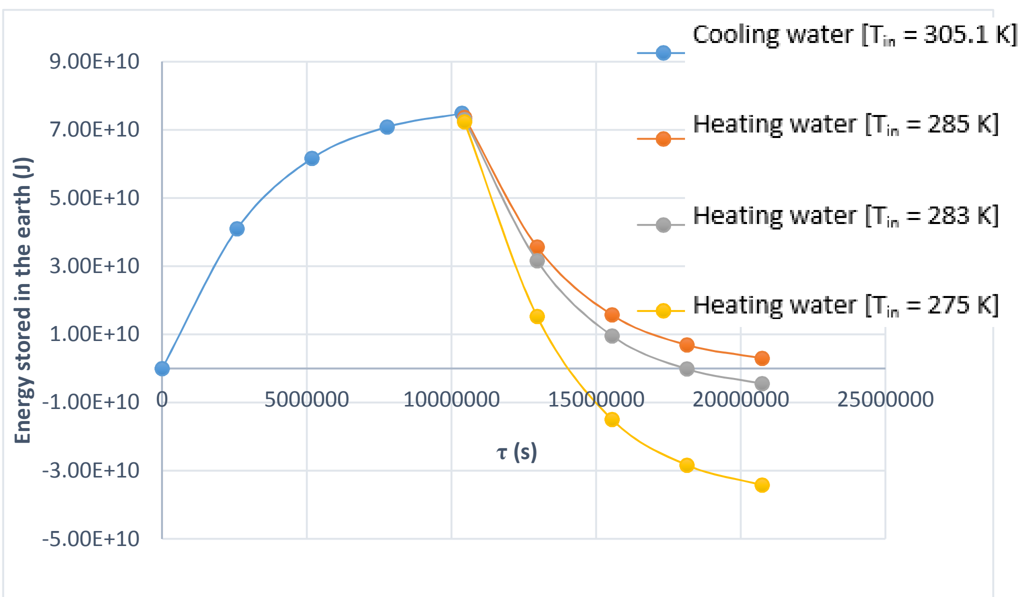

Figure G-1. Energy stored in the earth domain at different times for a maximum time of 20736000 s at different inlet water temperatures with V_{in} = 0.00621 m/s.

As can be seen from Fig. G-1, thermal energy stored in the earth domain starts increasing with increasing time when T_{in} = 305.1 K. This is due to the heat transfer from the warm cooling water exiting the condenser to enter the earth domain, which is initially at 285 K (see Section 4.4.7.3). The total thermal energy stored in the earth domain at a time of 10368000 s can be extracted by pumping lower temperature water into the ground source cooling system. The total time required to extract the thermal energy stored in the earth (which has been rejected to the earth domain by warm cooling water during the initial 10368000 s) depends on the water temperature at the inlet for the next 10368000 s or more. As can be seen from Fig. G-1, for T_{in} = 275 K and T_{in} = 283 K, the total energy that has been rejected to the earth (from warm cooling water) can be extracted in the given time of 4 months (10368000 s). On the other hand, for inlet water temperature of T_{in} = 285 K, all of the energy that was rejected to the earth could not be extracted in the given time of 4 months (10368000 s), and will require more time to extract all of the energy. The negative values for the energy stored in the earth in Fig G-1 represent the additional energy that would be extracted by the ground source system beyond the energy that was rejected to the earth domain during the initial 10368000 s. It is clear from the runs conducted that all of the energy that is rejected to the earth by the power plant can be extracted. However, although the total energy extracted from the earth is large, it is low temperature energy and cannot be applied to heating situations requiring significant temperature differences. Therefore, this extracted energy might be used in base (low level) warming of residential or commercial buildings or also could be used for melting snow during the winter.

Appendix H. CFX Command Language

This appendix shows the CFX command language for an example case with k = 0.52 W/m-K, L = 500 m, D_i = 0.2 m, V_{in} = 0.015525 m/s (3.6^o wedge).

CFX Command Language for Run

```
LIBRARY:
  CEL:
    EXPRESSIONS:
      dt = 0.1[s]+(1-e^((-0.00005[s^-1])*t))*3599.9[s]
    END
  END
  MATERIAL: Earth
    Material Group = User
    Option = Pure Substance
    Thermodynamic State = Solid
    PROPERTIES:
      Option = General Material
      EQUATION OF STATE:
        Density = 2050 [kg m^-3]
        Molar Mass = 1.0 [kg kmol^-1]
        Option = Value
      END
      SPECIFIC HEAT CAPACITY:
        Option = Value
        Specific Heat Capacity = 1840 [J kg^-1 K^-1]
      END
      THERMAL CONDUCTIVITY:
        Option = Value
        Thermal Conductivity = 0.52 [W m^-1 K^-1]
      END
    END
  END
  MATERIAL: Water
    Material Description = Water (liquid)
    Material Group = Water Data, Constant Property Liquids
    Option = Pure Substance
    Thermodynamic State = Liquid
    PROPERTIES:
      Option = General Material
      EQUATION OF STATE:
        Density = 997.0 [kg m^-3]
        Molar Mass = 18.02 [kg kmol^-1]
        Option = Value
      END
      SPECIFIC HEAT CAPACITY:
        Option = Value
        Specific Heat Capacity = 4181.7 [J kg^-1 K^-1]
        Specific Heat Type = Constant Pressure
      END
      REFERENCE STATE:
        Option = Specified Point
        Reference Pressure = 1 [atm]
        Reference Specific Enthalpy = 0.0 [J/kg]
```

```
        Reference Specific Entropy = 0.0 [J/kg/K]
        Reference Temperature = 25 [C]
      END
      DYNAMIC VISCOSITY:
        Dynamic Viscosity = 8.899E-4 [kg m^-1 s^-1]
        Option = Value
      END
      THERMAL CONDUCTIVITY:
        Option = Value
        Thermal Conductivity = 0.6069 [W m^-1 K^-1]
      END
      ABSORPTION COEFFICIENT:
        Absorption Coefficient = 1.0 [m^-1]
        Option = Value
      END
      SCATTERING COEFFICIENT:
        Option = Value
        Scattering Coefficient = 0.0 [m^-1]
      END
      REFRACTIVE INDEX:
        Option = Value
        Refractive Index = 1.0 [m m^-1]
      END
      THERMAL EXPANSIVITY:
        Option = Value
        Thermal Expansivity = 2.57E-04 [K^-1]
      END
    END
  END
END
FLOW: Flow Analysis 1
  SOLUTION UNITS:
    Angle Units = [rad]
    Length Units = [m]
    Mass Units = [kg]
    Solid Angle Units = [sr]
    Temperature Units = [K]
    Time Units = [s]
  END
  ANALYSIS TYPE:
    Option = Transient
    EXTERNAL SOLVER COUPLING:
      Option = None
    END
    INITIAL TIME:
      Option = Automatic with Value
      Time = 0 [s]
    END
    TIME DURATION:
      Option = Total Time
      Total Time = 2592000 [s]
    END
    TIME STEPS:
      Option = Timesteps
      Timesteps = dt
    END
  END
```

```
DOMAIN: Earth
  Coord Frame = Coord 0
  Domain Type = Solid
  Location = B26
  BOUNDARY: Default Fluid Solid Interface Side 1
    Boundary Type = INTERFACE
    Location = F32.26
    BOUNDARY CONDITIONS:
      HEAT TRANSFER:
        Option = Conservative Interface Flux
      END
    END
  END
  BOUNDARY: Earth Default
    Boundary Type = WALL
    Location = F30.26,F31.26
    BOUNDARY CONDITIONS:
      HEAT TRANSFER:
        Option = Adiabatic
      END
    END
  END
  BOUNDARY: Sym walls
    Boundary Type = SYMMETRY
    Location = F28.26,F29.26
  END
  BOUNDARY: wall temp
    Boundary Type = WALL
    Location = F27.26
    BOUNDARY CONDITIONS:
      HEAT TRANSFER:
        Fixed Temperature = 285 [K]
        Option = Fixed Temperature
      END
  END
  END
  DOMAIN MODELS:
    DOMAIN MOTION:
      Option = Stationary
    END
    MESH DEFORMATION:
      Option = None
    END
  END
  INITIALISATION:
    Option = Automatic
    INITIAL CONDITIONS:
      TEMPERATURE:
        Option = Automatic with Value
        Temperature = 285 [K]
      END
    END
  END
  SOLID DEFINITION: Solid 1
    Material = Earth
    Option = Material Library
    MORPHOLOGY:
```

```
        Option = Continuous Solid
      END
    END
    SOLID MODELS:
      HEAT TRANSFER MODEL:
        Option = Thermal Energy
      END
      THERMAL RADIATION MODEL:
        Option = None
      END
    END
  END
  DOMAIN: water
    Coord Frame = Coord 0
    Domain Type = Fluid
    Location = B21
    BOUNDARY: Default Fluid Solid Interface Side 2
      Boundary Type = INTERFACE
      Location = F32.21
      BOUNDARY CONDITIONS:
        HEAT TRANSFER:
          Option = Conservative Interface Flux
        END
        MASS AND MOMENTUM:
          Option = No Slip Wall
        END
        WALL ROUGHNESS:
          Option = Smooth Wall
        END
      END
    END
    BOUNDARY: Inlet
      Boundary Type = INLET
      Location = F23.21
      BOUNDARY CONDITIONS:
        FLOW REGIME:
          Option = Subsonic
        END
        HEAT TRANSFER:
          Option = Static Temperature
          Static Temperature = 368 [K]
        END
        MASS AND MOMENTUM:
          Normal Speed = 0.015525 [m s^-1]
          Option = Normal Speed
        END
        TURBULENCE:
          Option = Medium Intensity and Eddy Viscosity Ratio
        END
      END
    END
    BOUNDARY: Outlet
      Boundary Type = OPENING
      Location = F22.21
      BOUNDARY CONDITIONS:
        FLOW DIRECTION:
          Option = Normal to Boundary Condition
```

```
    END
    FLOW REGIME:
      Option = Subsonic
    END
    HEAT TRANSFER:
      Opening Temperature = 285 [K]
      Option = Opening Temperature
    END
    MASS AND MOMENTUM:
      Option = Opening Pressure and Direction
      Relative Pressure = 0.5
    END
    TURBULENCE:
      Option = Medium Intensity and Eddy Viscosity Ratio
    END
  END
END
BOUNDARY: water sym
  Boundary Type = SYMMETRY
  Location = F24.21,F25.21
END
DOMAIN MODELS:
  BUOYANCY MODEL:
    Option = Non Buoyant
  END
  DOMAIN MOTION:
    Option = Stationary
  END
  MESH DEFORMATION:
    Option = None
  END
  REFERENCE PRESSURE:
    Reference Pressure = 1 [atm]
  END
END
FLUID DEFINITION: Fluid 1
  Material = Water
  Option = Material Library
  MORPHOLOGY:
    Option = Continuous Fluid
  END
END
FLUID MODELS:
  COMBUSTION MODEL:
    Option = None
  END
  HEAT TRANSFER MODEL:
    Option = Thermal Energy
  END
  THERMAL RADIATION MODEL:
    Option = None
  END
  TURBULENCE MODEL:
    Option = SST
  END
  TURBULENT WALL FUNCTIONS:
    Option = Automatic
```

```
    END
  END
  INITIALISATION:
    Option = Automatic
    INITIAL CONDITIONS:
      Velocity Type = Cartesian
      CARTESIAN VELOCITY COMPONENTS:
        Option = Automatic with Value
        U = 0 [m s^-1]
        V = 0 [m s^-1]
        W = 0 [m s^-1]
      END
      STATIC PRESSURE:
        Option = Automatic with Value
        Relative Pressure = 0.5
      END
      TEMPERATURE:
        Option = Automatic with Value
        Temperature = 285 [K]
      END
      TURBULENCE INITIAL CONDITIONS:
        Option = Medium Intensity and Eddy Viscosity Ratio
      END
    END
  END
END
DOMAIN INTERFACE: Default Fluid Solid Interface
  Boundary List1 = Default Fluid Solid Interface Side 1
  Boundary List2 = Default Fluid Solid Interface Side 2
  Interface Type = Fluid Solid
  INTERFACE MODELS:
    Option = General Connection
    FRAME CHANGE:
      Option = None
    END
    PITCH CHANGE:
      Option = None
    END
  END
  MESH CONNECTION:
    Option = Automatic
  END
END
OUTPUT CONTROL:
  RESULTS:
    File Compression Level = Default
    Option = Standard
  END
  TRANSIENT RESULTS: Transient Results 1
    File Compression Level = Default
    Option = Standard
    OUTPUT FREQUENCY:
      Option = Every Timestep
    END
  END
END
SOLVER CONTROL:
```

```
    Turbulence Numerics = First Order
    ADVECTION SCHEME:
      Option = High Resolution
    END
    CONVERGENCE CONTROL:
      Maximum Number of Coefficient Loops = 10
      Minimum Number of Coefficient Loops = 1
      Timescale Control = Coefficient Loops
    END
    CONVERGENCE CRITERIA:
      Residual Target = 0.000001
      Residual Type = RMS
    END
    TRANSIENT SCHEME:
      Option = Second Order Backward Euler
      TIMESTEP INITIALISATION:
        Option = Automatic
      END
    END
  END
END
COMMAND FILE:
  Version = 15.0
  Results Version = 15.0.7
END
SIMULATION CONTROL:
  EXECUTION CONTROL:
    EXECUTABLE SELECTION:
      Double Precision = On
    END
    INTERPOLATOR STEP CONTROL:
      Runtime Priority = Standard
      DOMAIN SEARCH CONTROL:
        Bounding Box Tolerance = 0.01
      END
      INTERPOLATION MODEL CONTROL:
        Enforce Strict Name Mapping for Phases = Off
        Mesh Deformation Option = Automatic
        Particle Relocalisation Tolerance = 0.01
      END
      MEMORY CONTROL:
        Memory Allocation Factor = 1.0
      END
    END
    PARALLEL HOST LIBRARY:
      HOST DEFINITION: engdwybbg1
        Remote Host Name = ENG-DWYBBG1
        Host Architecture String = winnt-amd64
        Installation Root = C:\Program Files\ANSYS Inc\v%v\CFX
      END
    END
    PARTITIONER STEP CONTROL:
      Multidomain Option = Independent Partitioning
      Runtime Priority = Standard
      EXECUTABLE SELECTION:
        Use Large Problem Partitioner = Off
      END
```

```
      MEMORY CONTROL:
        Memory Allocation Factor = 1.0
      END
      PARTITIONING TYPE:
        MeTiS Type = k-way
        Option = MeTiS
        Partition Size Rule = Automatic
      END
    END
    RUN DEFINITION:
      Run Mode = Full
      Solver Input File = Fluid Flow CFX.def
    END
    SOLVER STEP CONTROL:
      Runtime Priority = High
      MEMORY CONTROL:
        Memory Allocation Factor = 1.0
      END
      PARALLEL ENVIRONMENT:
        Number of Processes = 1
        Start Method = Serial
      END
    END
  END
END
```

```
+--------------------------------------------------------------------+
|                                                                    |
|                     ANSYS(R) CFX(R) Solver 15.0.7                  |
|                                                                    |
| Version 2014.04.10-23.00-131675     Thu Apr 10 23:42:43 GMTDT 2014 |
|                                                                    |
|                         Executable Attributes                      |
|                                                                    |
|          double-64bit-int32-supfort-optimised-noprof-lcomp         |
|                                                                    |
| (C) 2014 ANSYS, Inc.                                               |
|                                                                    |
| All rights reserved. Unauthorized use, distribution or duplication |
| is prohibited. This product is subject to U.S. laws governing      |
| export and re-export. For full Legal Notice, see documentation.    |
+--------------------------------------------------------------------+
```

```
+--------------------------------------------------------------------+
|                    Job Information at Start of Run                 |
+--------------------------------------------------------------------+

Run mode:       serial run
```

Host	Mesh Part	PID	Job Started DD/MM/YY	Job Started hh:mm:ss
ENG-DWYBBG1	1	4688	14/07/16	13:04:02

Mesh Statistics

Domain Name	Orthog. Angle Minimum [deg]	Exp. Factor Maximum	Aspect Ratio Maximum
water	7.2 !	3 OK	968 OK
Earth	2.7 !	1 OK	221 OK
Global	2.7 !	3 OK	968 OK

Domain Name	Orthog. Angle %!	%ok	%OK	Exp. Factor %!	%ok	%OK	Aspect Ratio %!	%ok	%OK
water	1	3	96	0	0	100	0	0	100
Earth	74	24	2	0	0	100	0	0	100
Global	36	13	51	0	0	100	0	0	100

```
Domain Name : water

    Total Number of Nodes                                =      280112

    Total Number of Elements                             =      205000
        Total Number of Prisms                           =        7500
        Total Number of Hexahedrons                      =      197500

    Total Number of Faces                                =      152664

Domain Name : Earth

    Total Number of Nodes                                =      255102

    Total Number of Elements                             =      125000
        Total Number of Hexahedrons                      =      125000

    Total Number of Faces                                =      255100

Global Statistics :

    Global Number of Nodes                               =      535214

    Global Number of Elements                            =      330000
        Total Number of Prisms                           =        7500
        Total Number of Hexahedrons                      =      322500

    Global Number of Faces                               =      407764

Domain Interface Name : Default Fluid Solid Interface
```

```
    Discretization type                                    =        GGI
    Intersection type                                      = Topological

+--------------------------------------------------------------------+
|                     Average Scale Information                      |
+--------------------------------------------------------------------+

Domain Name : water
    Global Length                                           = 5.3944E-01
    Minimum Extent                                          = 6.2791E-03
    Maximum Extent                                          = 5.0000E+02
    Density                                                 = 9.9700E+02
    Dynamic Viscosity                                       = 8.8990E-04
    Velocity                                                = 0.0000E+00
    Thermal Conductivity                                    = 6.0690E-01
    Specific Heat Capacity at Constant Pressure             = 4.1817E+03
    Prandtl Number                                          = 6.1316E+00

Domain Name : Earth
    Global Length                                           = 1.1622E+01
    Minimum Extent                                          = 6.2791E-01
    Maximum Extent                                          = 5.0000E+02
    Density                                                 = 2.0500E+03
    Thermal Conductivity                                    = 5.2000E-01
    Specific Heat Capacity at Constant Pressure             = 1.8400E+03
    Thermal Diffusivity                                     = 1.3786E-07
    Average Diffusion Timescale                             = 9.7971E+08
    Minimum Diffusion Timescale                             = 2.8599E+06
    Maximum Diffusion Timescale                             = 1.8135E+12

+--------------------------------------------------------------------+
|                Checking for Isolated Fluid Regions                 |
+--------------------------------------------------------------------+

No isolated fluid regions were found.

+--------------------------------------------------------------------+
|              The Equations Solved in This Calculation              |
+--------------------------------------------------------------------+

 Equations are given two labels: the individual name and a combined name used
for combining residuals together.  Residuals for multi domain problems are
combined provided the domains are connected together and have the same domain
type (solid or fluid/porous).  If there are multiple groups of the same
domain type, then the group residual is identified by the name of the first
domain in the connected group.

 The individual and combined equation names are given below.

 Subsystem : Wall Scale

 Wallscale-water                           --> Wallscale

 Subsystem : Momentum and Mass

   U-Mom-water                               --> U-Mom
   V-Mom-water                               --> V-Mom
```

```
  W-Mom-water                             --> W-Mom
  P-Mass-water                            --> P-Mass

Subsystem : Heat Transfer

  H-Energy-water                          --> H-Energy
  T-Energy-Earth                          --> T-Energy

Subsystem : TurbKE and TurbFreq

  K-TurbKE-water                          --> K-TurbKE
  O-TurbFreq-water                        --> O-TurbFreq
```